Dear Editor Andrea Di Muro

Manuscript **Lahar events in the last 2,000 years from Vesuvius eruptions. Part 1: Distribution and impact on densely-inhabited territory estimated from field data analysis**

Many thank for your revision which improved and clarified some points of the the manuscript. In red our answer

It follows the reply to the comments one-by-one:

I'm happy to join the reviewers in stressing the importance of the work your team has performed and the high quality of the dataset you have integrated to build a very exhaustive study of lahar processes in the Vesuvius area. The review process has permitted to effectively integrate the suggestions and remarks of the three reviewers and I consider the paper can be accepted for publication. In order to produce a final version best conveying the important messages of your paper to a broad audience, I would like to suggest you to consider here below some minor modifications and suggestions.

A rapid submission of a final version integrating these suggestions will thus permit the review process of the three companion papers to be finalized basically synchronously.

Many thanks for your consideration. We have followed the suggestions below.

Line 100: "Mobility" would imply long range transport capability, but in the sentence here it is unclear whether you are instead stressing that lahar triggering can occur also in distal areas (xx km from the summit Vesuvius crater); if this is correct, this term should be modified to express you are showing a large trigger area can be affected and not that flows have a large transport distance.

Thanks. We have clarified this point (LINES 98-102).

Line 108: unclear sentence; what does that mean "repeated lahar..episodes...stroke..its human settlements...evidencing attempts of resettlement"?

Thanks. We have clarified this sentence (LINE 110).

Line 640 “Both Acerra and Nola localities”; this is one of the many examples scattered in the whole paper and already pointed by the reviewers, where the sites are quoted but with no reference to a map, or (most important) explicit quotation of distance with respect to the volcano summit or to the location with respect to the primary deposits etc etc are reported; Reference sites are also described in detail in the appendix, but no distance is reported with respect to Vesuvius or other information able to help the reader to quickly locate the sites. This kind of sentences implies the reader has a good knowledge of the study area, but make the reading difficult for researchers knowing little about the Vesuvius area and related eruptions and request a frequent check in maps to locate the quoted sites; in order to improve the readability of the whole text, please integrate these basic information 2orcesi s the whole paper, in order to help the reader to immediately locate the quoted areas/cities (“how far from Vesuvius is a given distal area”?) and thus better follow the line of reasoning presented in the text.

Thanks. We have specified the distance between Acerra and Nola from their source areas (Somma-Vesuvius and Apennines, respectively) throughout the text.

Also, we have slightly modified all maps throughout the text in order to show the main toponyms, in particular the recurrent ones that we use for results presentation and discussion.

Fig. 17 Do the velocity values reported in the figure correspond to syn-eruptives or post-eruptive units? Do you find a correlation between deposit thickness and calculated velocity?

Thanks. The velocity and pressure values correspond both to the syn- and post-eruptive lahar units, which we have specified immediately after Fig. 16 and also before Fig. 17. This is specified now also in Fig. A1 caption (LINE 739, LINES 1025-1026).

There is no correlation between deposit thickness and calculated velocity; the correlation is between clast dimension and calculated velocity (Eq. A3).

Line 861 : please delete the brackets enclosing the temperature value.

Thanks. We have done it (LINE 885).

>>Both Pollena and 1631 distribution maps suggest that for a given location, the thickness of post eruptive lahars is larger than that of syn-eruptive; if this is correct, this information could be better stressed, discussed and interpreted, a link with grain size

could be made more explicit, if existing, and ,most important, the implications in terms of trigger processes and hazard included in the paper.

Thanks. We have double checked this point, both in the database and in Figs. 8-11, and actually the thickness of the post-eruptive lahar units is not larger than the one of the syn-eruptive units. An issue might have arisen from Fig. 9, which has the colour bar scale different from the one of Fig. 8; we can improve this in the final editing of the paper.

>>Magnetization study suggest that some units had emplacement temperatures above 100°C; the implication of that in terms of occurrence of vapour phase, sedimentary structures and transport properties should be discussed. Does that imply the fluid phase was multiphase? How is that included in the physical modelling?

Thanks. We have added the following paragraph in the discussion section to link this point on temperature with the modelling presented in the companion paper of de'Michieli Vitturi et al. (this issue):

The companion paper of de'Michieli Vitturi et al. (this issue) 3orcesi s3e salso the nexus between water temperature, flow viscosity, and their consequential impact on fluid dynamics. Specifically, when the dominance of frictional 3orcesi s attributable to the yield slope term, the initial divergence between high- and low-temperature scenarios appears negligible. However, discernible dissimilarity appears over time for the inundation area of the colder flow case (i.e., 27 °C) with respect to the warmer counterpart (i.e., 100 °C), the latter case being close to the 120 °C one reported from paleomagnetism. Remarkably, the temperature-induced variations assume a pivotal role in shaping the dynamic characteristics of the hotter flow. The diminished viscosity associated with elevated temperatures not only amplifies fluid mobility but also prompts a notable acceleration in sediment settling velocity. This, in turn, initiates a debulking mechanism, thereby intensifying overall flow mobility. Consequently, this intricate interplay contributes to a reduced footprint of deposited material from the flow, altering the spatial distribution of sediments. However, the overall impact on the inundation area is typically quite reduced, being typically less than 10-20% even considering a thickness threshold of 1 mm (see de'Michieli Vitturi et al., this issue) (LINES 888-901).

Line 222 In spite of being Sarno one of the most affected municipalities, no reference to 1998 Sarno lahar events in terms of triggering, dynamics, sources, impact areas and deposit facies is offered in this paper. As this is one of the most recent and significant (including in terms of victims) events affecting the studied area, it is surprising the lack of explicit reference and comparison in the paper.

Thanks. We have specified on this point at the end of Section 3.1 (LINES 235-243).

Looking forward receiving the final version of this important research paper.

Many thanks again.

Mauro and co-authors

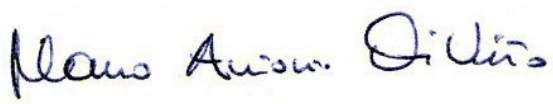

Lahar events in the last 2,000 years from Vesuvius eruptions. Part 1: Distribution and impact on denselyinhabited territory estimated from field data analysis

Mauro A. Di Vito (1,*), Ilaria Rucco (2), Sandro de Vita (1), Domenico M. Doronzo (1), Marina Bisson (3), Mattia de' Michieli Vitturi (3), Mauro Rosi (4), Laura Sandri (5), Giovanni Zanchetta (4), Elena Zanella (6), Antonio Costa (5)

(1) Istituto Nazionale di Geofisica e Vulcanologia - Sezione di Napoli Osservatorio Vesuviano, Napoli, Italy

(2) Heriot-Watt University, School of Engineering and Physical Sciences, Edinburgh, United Kingdom

(3) Istituto Nazionale di Geofisica e Vulcanologia - Sezione di Pisa, Pisa Italy

(4) Università di Pisa, Dipartimento di Scienze della Terra, Pisa, Italy

(5) Istituto Nazionale di Geofisica e Vulcanologia - Sezione di Bologna, Bologna, Italy

(6) Università di Torino, Dipartimento di Scienze della Terra, Torino, Italy

*Corresponding author: Mauro A. Di Vito (mauro.divito@ingv.it)

Abstract

Lahars represent some of the most dangerous phenomena in volcanic areas for their destructive power, causing dramatic changes in the landscape with no premonitory signs and impacting on population and infrastructures. In this regard, the Campanian Plain turns out to be very prone to the development of these phenomena, since the slopes of the Somma-Vesuvius and Campi Flegrei volcanoes, along with the Apennine reliefs are mantled by pyroclastic deposits that can be easily remobilized, especially after intense and/or prolonged rainfall.

This study focuses on the analysis of the pyroclastic fall and flow deposits and of the syn- and post-eruptive lahar deposits related to two sub-Plinian eruptions of Vesuvius, 472 CE (Pollena) and 1631. To begin with, historical and field data from the existing literature and from hundreds of outcrops were collected and organized into a database, which was integrated with several new pieces of data.

In particular, stratigraphic, sedimentological (facies analysis and laboratory) and archaeological analyses were carried out, in addition to rock magnetic investigations and impact parameter calculations. The new data are also referred to the finding of ash beds in more distal areas, which were included into new isopach maps for the two sub-Plinian eruptions.

The results show that for both the eruptions the distribution of the primary deposits is wider than previously known. A consequence of these results is that a wider areal impact should be expected in terms of civil protection, as the sub-Plinian scenario is the reference one for a future large eruption of Vesuvius. Such distribution of the pyroclastic deposits directly affects the one of the lahar deposits, also because a significant remobilization took place during and after the studied eruptions, which involved the distal phreatomagmatic ash. From these integrated analyses, it was possible to constrain the timing of the deposition and the kind of deposits remobilized (pyroclastic fall vs. flow), as well as was possible to calculate the velocities and dynamic pressures of the lahars, and ultimately infer the lahar transport and emplacement mechanisms.

The multidisciplinary approach adopted in this work shows how it is crucial to assess the impact of lahars in densely populated areas even at distances of several to tens of km from active volcanoes. This especially applies to large parts of the densely populated areas around Somma-Vesuvius up to the nearby Apennine valleys.

Keywords: Somma-Vesuvius; Apennine valleys; pyroclastic deposits; lahars; areal distribution; local impact.

1. Introduction

The movement of volcaniclastic mass flows, and the consequent damage along the flanks of active volcanoes and perivolcanic plains, represent a constant threat to inhabited areas and populations (e.g., Waitt et al., 1983; Lowe et al., 1986; Pierson, 1985; Newhall and Punongbayan, 1996). Such systems

are variably-fluidized, gravity-driven flows that consist of a mixture of pyroclastic sediment and water. They can be triggered by various mechanisms, among which the most common are intense or prolonged atmospheric precipitations (Arguden and Rodolfo, 1990; Rodolfo and Arguden, 1991; Pareschi et al., 2000; Rodolfo, 2000; Scott et al., 2001; Vallance and Iverson, 2015). Such precipitations or water runoff, especially during and/or after the eruptions, can cause the remobilization of pyroclastic deposits evolving into water-saturated multiphase systems called lahars (e.g., White et al., 1997; Sheridan et al., 1999; Scott et al., 2001; Baumann et al., 2020). The last century was affected by a significant number of highly-impacting lahar events associated to well-studied explosive volcanic eruptions worldwide, such as for example at Colima (Mexico) in 1913 (Rodriguez-Sedano et al., 2022), Nevado del Ruiz (Colombia) in 1985 (Voight, 1990), Ruapehu (New Zealand) in 2007 (Lube et al., 2012), and Merapi (Indonesia) in 2011 (Jenkins et al., 2015).

According to Rodolfo (2000), Sulpizio et al. (2006), and Vallance and Iverson (2015), volcaniclastic mass flows can be generated at variably-long time intervals, spanning from eruptive to post-eruptive phases of tens to hundreds of years. In case these flows are directly related to volcanic eruptions, that is occurring during or shortly after the eruptive event, lahars are defined as syn-eruptive, and can represent an important multihazard factor in the short-to-middle term for perivolcanic areas (Rodolfo, 2000; Sulpizio et al., 2006). Instead, in case they are unrelated to any eruption dynamics, that is occurring during long periods of volcanic quiescence, they are defined as post-eruptive (Vallance and Iverson, 2015), and can represent a long-term hazard factor (e.g., Siebe et al., 1999; Pareschi et al., 2002; Zanchetta et al., 2004a, 2004b; Sulpizio et al., 2006). Usually, post-eruptive lahars are not accounted for the assessment of volcanic hazard, although their study is important for hydrogeological hazard assessment and long-term territorial planning.

In this sense, that is from the hazard assessment point of view, one of the priorities concerns the assessment of those areas potentially exposed to such a threat, taking into account the temporal recurrences of the phenomena (over days to months after an eruption, or years to decades after) and physical features of the volcaniclastic mass flows (volume, thickness, velocity, dynamic pressure,

74 concentration, and invasion areas). We stress the fact that the definition of syn-eruptive lahars
75 (Sulpizio et al., 2006; Vallance and Iverson, 2015) adopted in the present work is important when
76 accounting for the multihazard of explosive eruptions, which in areas like Vesuvius and surroundings
77 should not be neglected for its assessment and mapping purposes (de'Michieli Vitturi et al., this issue;
78 Sandri et al., this issue). The methodology used in this work is geological (see Section 3.2), and the
79 syn-eruptive definition of lahars is necessary to avoid underestimations of the volcanic hazard from
80 sub-Plinian eruptions at Vesuvius.
81 A lot of the existing literature analyzed the hazard related with volcaniclastic mass flows on the flanks
82 of active volcanoes, through the reconstruction of historical and prehistoric events (e.g., Scott, 1989;
83 Scott et al., 1995; Vallance and Scott, 1997; Zaragoza et al., 2020), by using empirical relationships
84 or physical models (e.g., Macedonio and Pareschi, 1992; Costa, 1997; Iverson et al., 2000; Walsh et
85 al., 2020). However, the areas affected by these phenomena can be extended well beyond the
86 boundaries of the volcanic complex, also including the surrounding plains and the downwind-lying
87 mountainous areas, which are subjected to tephra fallout sometimes even at great distances from the
88 volcano (e.g., Siebe et al., 1999; Pareschi et al., 2000, 2002; Zanchetta et al., 2004a, 2004b; Di
89 Crescenzo and Santo, 2005). In these areas, volcaniclastic mass flows may cause victims and
90 damages, even where considered safe or scarcely affected by other volcanic hazards.
91 In this paper, we present the results of a multidisciplinary study, including geomorphological,
92 stratigraphic, sedimentological and rock magnetic investigations, as well as impact parameter
93 calculations by reverse engineering from the deposits. These investigations followed several
94 surveying campaigns carried out in natural exposures, archaeological excavations, and trenches dug
95 specifically for this purpose in the plain surrounding the Vesuvius edifice and along the Apennine
96 valleys (Fig. 1). One of the goals of this study is to show the presence of lahar deposits even in areas
97 several km far from the source areas of the Apennine hills and Somma-Vesuvius edifice,
98 demonstrating the high mobility of these flows. Indeed, these two areas acted as source areas because
99 they were largely affected by deposition of primary pyroclastic deposits from Plinian and sub-Plinian

100 Somma-Vesuvius eruptions. The study of the past lahar deposits has been useful for the understanding
101 of the feeding drainage basins, their extent and facies variations with distance from the source area,
102 and the associated impact on landscape. As already pointed out by Di Vito et al. (2013, 2019), in the
103 past 4.5 ka repeated lahar and flooding episodes related to the main eruptions of Somma-Vesuvius
104 and Campi Flegrei volcanoes strongly stroke the Campanian Plain and its human settlements,
105 influencing their partial or total abandonment. In particular, for the areas around Vesuvius, these
106 phenomena included: i) large volume and high energy lahars, originated from the volcanic edifice,
107 which affected the volcanic apron; ii) large flooding phenomena, i.e. overflowing of water affecting
108 the Campanian plain; iii) lahars originated from the perivolcanic mountains that affected the
109 Apennine valleys, and invaded the areas of the plain at their mouths. All of these phenomena differed
110 to each other in terms of amount and grain-size of the involved sediment. The data and pieces of
111 information described here were the basis for validating a new model for lahar transport (de' Michieli
112 Vitturi et al., this issue), which was applied for assessing the related hazard at Vesuvius and
113 Campanian Plain (Sandri et al., this issue).

114 The structure of the work consists of an integrated geological, geomorphological, stratigraphic and
115 sedimentological study, a paleomagnetic and sediment-mechanic impact assessment calculation, and
116 a comprehensive discussion on the lahar problem in the Campanian Plain.

117

118 **2. Geological setting**

119 The study area is part of the Campanian Plain, which includes the lowlands surrounding Mount
120 Vesuvius volcano and the nearby Apennine ridges and valleys (Fig. 1). The orography of the area is
121 characterized by three WNW-ESE trending mountain ridges that border eastward the plain, with an
122 elevation ranging from 500 to 1600 m a.s.l., and slope angles from 30 to 60°. From north to south,
123 the Avella-Partenio, Lauro-Visciano and Sarno-Quindici mountain ridges are separated by two
124 depressions: the Avella-Baiano Valley, in which the alluvial plain of the Clanio river occurs, and the

Lauro valley. Both are narrow valleys that widen toward north-west, among the cities of Cicciano, Nola and Palma Campania (Fig. 1). The reliefs are characterized by a high drainage density, associated with a poorly developed and torrential hydrographic network, which over time has favored the incision and dismantling of the pyroclastic cover on the ridges, and the development of numerous detrital conoids that connect with the main valley floor (Di Vito et al., 1998).

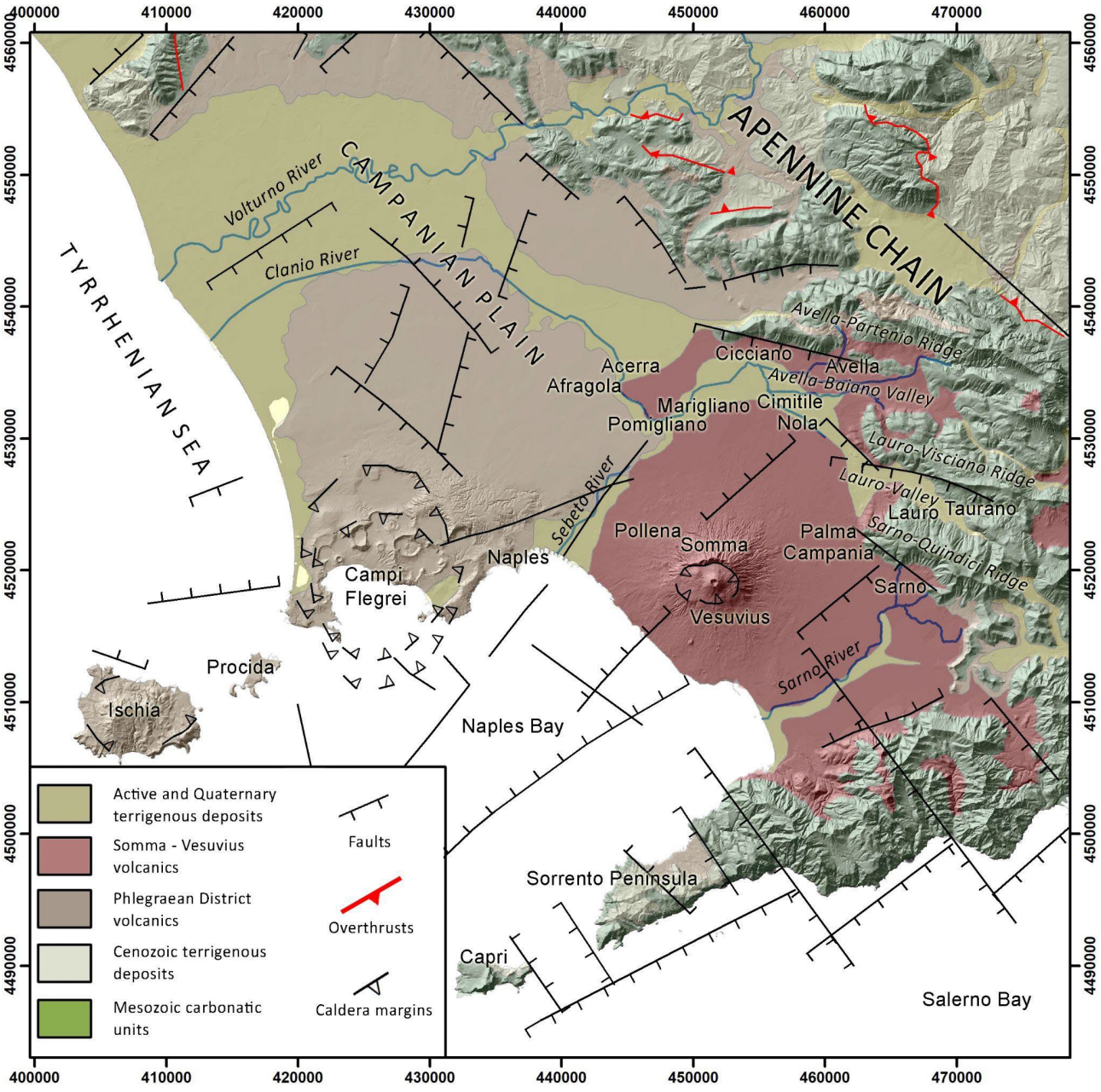

Fig. 1. Geological and structural sketch of the Campania Region on a Shaded Relief derived from TINITALY DEM. The coordinates are expressed in WGS 84 UTM N33 (modified after Orsi et al., 1996).

Vesuvius, or more properly Mt. Somma-Vesuvius, is a composite central volcano less than 39,000 years old, composed of the remnant of the oldest Mt. Somma edifice, dismantled by repeated episodes of caldera collapse, and the more recent Mt. Vesuvius, grown inside it. Its volcanic history is characterized by an initial phase, dominated by low-energy effusive and explosive eruptions, which ended at around 22,000 years ago. Since then, the volcano generated four Plinian eruptions with VEI 5-6, each preceded by long periods of quiescence and all accompanied by a summit caldera collapse (Somma caldera; Cioni et al., 1999). The last Plinian eruption occurred in 79 CE and once again modified the Somma caldera, inside which the recent cone has subsequently grown due to an alternation of periods of open conduit, persistent Strombolian and effusive activity, and long periods of quiescence with obstructed conduit, interrupted by high-energy sub-Plinian eruptions. In historical times, the other more energetic events were the sub-Plinian 'Pollena' (472 CE) and 1631 eruptions (Santacroce et al., 2008). The last eruption occurred in 1944 and caused the return to obstructed conduit conditions, which characterize the current quiescent phase of the volcano. The rocks composition varies from slightly silica-undersaturated (K-basalt to K-trachyte) to highly silica-undersaturated (K-tephrite to K-phonolite). The Somma-Vesuvius complex is characterized by a well-developed radial drainage network, which feeds an extensive volcaniclastic apron that morphologically connects the edifice with the surrounding plain (Santacroce et al., 2003). It represents the active southern termination of the Plio-Quaternary volcanic chain that borders the eastern Tyrrhenian margin (Peccerillo, 2003). Volcanism in this margin is related to the extensional tectonic phases that accompanied the anticlockwise rotation of the Italian peninsula, during the complex interaction between the Africa and Eurasian plates, which generated the Apennine thrust-and-fold belt (Ippolito et al., 1973; D'Argenio et al., 1973; Finetti and Morelli, 1974; Bartole, 1984; Piochi et al., 2004; Patacca and Scandone, 2007; Vitale and Ciarcia, 2018). The extension along the Tyrrhenian margin of the Apennine chain was accommodated by the activation of NW-SE normal faults and NE-SW normal to strike-slip transfer fault systems, which dismembered the chain in horst and graben structures, and allowed magmas to reach the surface and feed the volcanism (Mariani and

160 Prato, 1988; Faccenna et al., 1994; Acocella and Funiciello, 2006). The Campanian Plain is one of
161 these grabens that hosts the Neapolitan volcanic area. It is a NW-SE elongated structural depression,
162 filled by a thick sequence of marine and continental sedimentary deposits, and volcanic-volcaniclastic
163 successions that compensated its subsidence, leading to a complete emersion at around 39 ka
164 (Brocchini et al., 2001; De Vivo et al., 2001; Santangelo et al., 2017). This graben is bordered toward
165 NW, NE and SE by the Meso-Cenozoic carbonate and terrigenous successions of the Apennine chain,
166 and is subdivided in minor NE-SW oriented horst-and-graben structures (Carrara et al., 1973; Finetti
167 and Morelli, 1974; Fedi and Rapolla, 1987; Brancaccio et al., 1991). Neapolitan volcanoes lie on
168 these second-order structural highs (Marotta et al., 2022 and reference therein), and the products of
169 their most powerful eruptions blanketed the Apennine reliefs and filled their valleys with several
170 meter-thick covers of pyroclastic fall deposits, composed of pumice lapilli and ash layers separated
171 by paleosols (Pareschi et al., 2002; Bisson et al., 2007; Cinque and Robustelli, 2009; Gurioli et al.,
172 2010).
173 In terms of water drainage, the pyroclastic cover has peculiar geotechnical characteristics, such as a
174 positive correlation between grain-size and permeability, which enabled the development of lahars in
175 the area. In particular, coarser pumice layers are characterized by inter-clast void spaces that control
176 water accumulation, instead ash layers, soils and paleosols by a high water retention capacity
177 (Andosol-like soils), so that the differential behavior can regulate equilibrium among deposits
178 stability vs. remobilization (Fiorillo and Wilson, 2004).
179 Regarding the volcanic activity of Vesuvius in the last 2,000 years, the largest eruptions after the 79
180 CE Plinian one were two sub-Plinian eruptions, the 472 CE Pollena and 1631 ones, but several other
181 effusive and explosive events occurred in historical times. In the Campanian Plain, lahar deposits
182 related to these two eruptions are quite abundant due to past heavy rains (Fiorillo and Wilson, 2004;
183 Zanchetta et al., 2004b; Stanzione et al., 2023), also the sub-Plinian scenario is of interest for civil
184 protection purposes, which is why in the present work we focus on the 472 CE Pollena and 1631
185 eruptions. A particular attention is given to the distribution of the primary pyroclastic deposits and

186 related syn-eruptive lahars, which are mass flow events directly related to specific eruptions, even if
187 the condition is not necessarily that of an event contemporaneous to the eruption. Those deposits are
188 mainly composed of >90% fragments from the parental eruption, while the remaining fragments
189 pertain to other eruptions mixed by volcaniclastic colluvium (Sulpizio et al., 2006). The syn-eruptive
190 feature is thus related to the remobilization of pyroclastic deposits more than to the exact timing of
191 lahar emplacement, the latter being of the order of max a few years (before humification processes or
192 significant human activities can occur). Such a feature distinction is important because directly related
193 to volcanic hazard.
194

195 **3. Materials and methods**

196 **3.1. Evidence from historical sources**

197 We collected data from historical sources, maps, documents, and newspapers to supplement the
198 geological data, gathered directly or indirectly, for the definition of the areal distribution of the syn-
199 eruptive and post-eruptive lahar deposits at Vesuvius and in the surrounding region. Such collection
200 concerned the phenomena that took place starting from the sixteenth century CE to 2005. This time
201 span has been chosen depending on data availability, and to show the high recurrence of events over
202 time in the area. The data were collected and grouped not only by years but also by the municipal
203 areas existing at those times. It should be noted that the distribution of the data can be affected by the
204 different urbanization over time, and by the presence of damage to people, infrastructures and goods,
205 economic activities and settlements. In the absence of local weather data series over the analyzed
206 period, we assumed that the phenomena of remobilization of the pyroclastic deposits, and the
207 consequent generation of large flooding events and volcaniclastic mass flows, coincided with extreme
208 weather events often described and reported in the analyzed sources. We identified about 500
209 individual reports, covering events between the sixteenth century CE and 2005 that took place in 97
210 different municipalities. The data were organized in a geospatial database, so that it was possible to

211 define different areas affected by frequent syn-eruptive floods and lahars, concomitant/related with
212 the sub-Plinian eruption of 1631, to be used as benchmark for the main geological analyses. We could
213 not add the Pollena eruption to this historical data set, as there are no available sources for similar
214 occurrences other than documents deriving from archaeological excavations (see next sections).
215 The municipalities with the highest number of reports are: Sarno (43), Salerno (32), Siano (26), Vietri
216 sul Mare (22), Bracigliano (21), Nocera Inferiore (20), Maiori (19), Quindici (17) (Fig. 1). The events
217 of greatest intensity, which affected more than five municipal territories at the same time, are 19.
218 Some of these occurrences result closely connected with the volcanic events of Vesuvius, such as
219 those that occurred in 1631, 1823, 1910, 1949 and 1954, simultaneously or within months to a few
220 years after the Vesuvius eruptions of 1631, 1822, 1906 and 1944.

Eruption	Lahar/Intense Alluvial Event	Municipalities affected
December 1631	16/12/1631	Sant'Anastasia, San Giorgio a Cremano, Massa di Somma, Somma, Ottaviano, San Sebastiano, Trocchia, Torre del Greco, Portici, Pugliano, Madonna dell'Arco, Palma, Nola Arpaia, Arienzo, Cicciano, Marigliano, Benevento, Avellino
October 1822	24/01/1823	Amalfi, Bracigliano, Cava de' Tirreni, Cetara, Minori, Nocera Inferiore, Pagani, Salerno, Sant'Egidio del Monte Albino, Tramonti, Vietri sul Mare
	12/02/1823	Maiori
	12/04/1823	Sarno
	18/10/1823	Corbara, Praiano, Sant'Egidio del Monte Albino, Sarno, Siano
	15/11/1823	Salerno
April 1906	24/10/1910	Amalfi, Boscotrecase, Cercola, Cetara, Ercolano, Giffoni Valle Piana, Maiori, Marano di Napoli, Minori, Napoli, Pollena Trocchia, Torre del Greco, Vico Equense, Vietri sul Mare, Sant'Anastasia, San Giorgio a Cremano, Sarno, Scala, Pomigliano d'Arco, Portici, Ravello, Salerno
March 1944	02/10/1949	Lauro, Maiori, Minori Nocera Inferiore, Sarno, Vietri sul Mare
	25/10/1954	Cava de' Tirreni, Maiori, Minori, Nocera Inferiore, Salerno, Tramonti, Vietri sul Mare

221 Tab. 1. Historical archive of lahar and alluvial events related to the four most significant Vesuvius eruption in the last
222 four centuries, and municipalities affected by such events.

223 The absence of information in the Lauro and Avella-Baiano valleys is likely due to the absence of
224 detailed descriptions of alluvial events, or most likely to the position of the inhabited areas generally
225 located on the hills thus far from the lower part of the valleys. The investigated area was affected
226 many times by post-eruptive lahar events due to the presence of thick variably-weathered pyroclastic
227 deposits mantling the steep slopes of Somma-Vesuvius and Apennines. One of the most recent event
228 occurred on May 5th 1998, when a 16-hours prolonged heavy rainfall triggered a huge number of
229 Apennine slope failures toward the towns of Quindici, Bracigliano, Siano, Sarno and San Felice a
230 Cancello, all located near the Apennine ridges east-northeast of Somma-Vesuvius (Fig. 1). This
231 catastrophic event involved an extension area of around 60 km^2, and a volume of more than 2x10^6 m^3
232 (40% derived from materials eroded along the channels), causing 160 victims and severe damages to
233 the quoted towns (Di Vito et al., 2019 and references therein).

234

235 **3.2. Field and archaeological investigations**

236 We used a set of geological, stratigraphical, sedimentological, archaeological, and pedological
237 information for the reconstruction of the type of events, their emplacement mechanisms, timing, and
238 impact on pre-existing structures/environment. Such an approach enabled us to cross-check
239 geological and archaeological evidence allowing us to accurately fix the age of events. Conversely,
240 the presence of well-dated primary pyroclastic deposits can define the age of human traces otherwise
241 not easily datable. Furthermore, the identification of the "primary" (fallout and pyroclastic current,
242 along with the archeological findings) can give the absolute age (*ante* or *post quem*) of a given deposit.
243 The definition of isochronic paleosurfaces can also contribute to the reconstruction of the paleo-
244 environments affected by the deposition, and of the variations that occurred during depositional
245 processes. For this purpose, particular attention was paid to the basal contacts between the deposits.

In some areas like Nola (10-15 km from Apennine source valleys), the lahar deposits directly overlie the primary pyroclastic deposits (both for the 472 CE Pollena and 1631 eruption), while in other areas some pyroclastic units or the whole primary deposits are missing (eroded) or lacking. Only the correlation with the nearby areas permitted to define whether the emplacement of the lahars eroded partly or significantly the underlain primary deposits, vice versa the complete absence in the emplacement areas could also be due to the distribution of these latter. The analysis of the internal structure marked by sharp changes in grain sizes, color, presence of erosional unconformities, or interposition of lenses of coarser material also permitted the identification of one or more flow units within the same individual deposit package. The macroscopic characteristics of the sequences permitted some inferences on the transport and depositional mechanisms, while the grain-size and componentry analyses provided information on the source deposits that were remobilized. This brings to another important definition, that is syn-eruptive vs. post-eruptive lahars, according to the definition of Sulpizio et al. (2006) and Iverson and Vallance (2015), which applies during or soon after the eruption vs. several years to centuries after the eruption ended, respectively. The macroscopic analysis allowed us to distinguish between the syn-eruptive and post-eruptive deposits. The first ones are defined by the occurrence of pyroclastic components with a lithology similar to the one of the primary deposits. The second ones are characterized by some evidence of depositional stasis like humified paleosurfaces below the lahar deposits or of anthropogenic activities, or by the presence of humified material and/or fragments of older eruptions in the deposits. All these characteristics allowed the correlation between the various volcaniclastic units for the whole set of the studied sequences, marking the differences needed to hypothesize on the source and invasion areas.

We reviewed all the volcanological and archaeological data collected during the last 20 years from drill cores, outcrops, archaeological excavations, and from the existing literature, in collaboration with colleagues of the Archaeological Superintendence of Campania region. The preliminary collection and analysis of the existing data permitted to plan a hundred of new stratigraphic trenches

(Fig. 2), with the aim of collecting stratigraphic, sedimentological, lithological and chronological data on the primary pyroclastic and secondary (lahar) deposits. Particular attention was also paid to the geometric relations of these deposits with the paleotopography and preexisting anthropogenic structures.

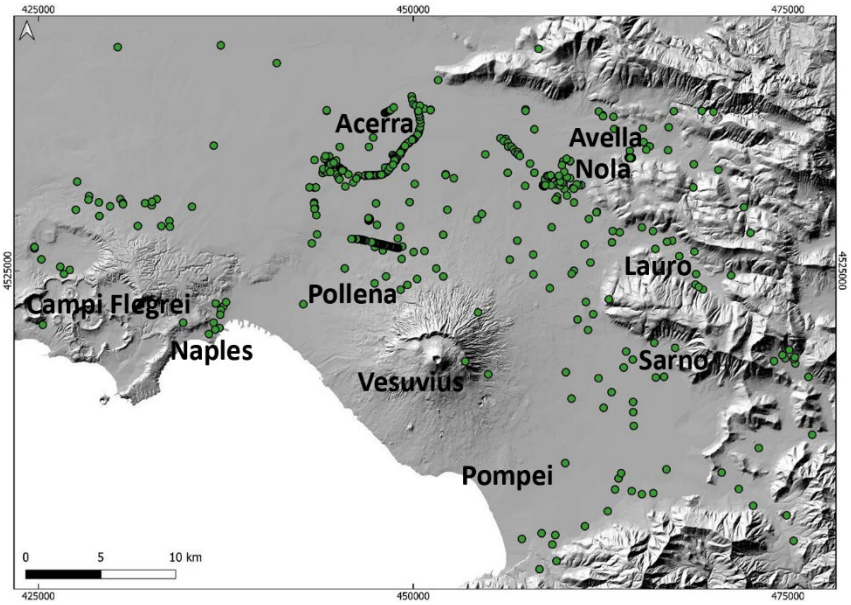

Fig. 2. Shaded relief of the studied area and location of all the sites where stratigraphic analyses were carried out.

The collected data were organized into a geospatial database (QGIS Platform), in which each point represents an investigated site linked to a series of information, such as the precise location, type of volcanic sequence, and stratigraphic features (primary and secondary units, thickness, type of deposit, etc…). The data were visualized using a Digital Elevation Model (DEM) of the Campanian Plain as reference topography and the UTM WGS 84 – Zone 33N reference projection.

3.3. Geomorphological analysis

This analysis is aimed at identifying the macro-basins that fed the lahars in the study area after the two sub-Plinian eruptions (Pollena and 1631). The analysis was carried out on the basis of the slopes distribution and the watersheds extracted from a Digital Elevation Model (DEM). The DEM was

290 derived from a LiDAR flight of 2012 (cell size of 10 m). In particular, six macro-basins characterized
291 by slopes > 20° were identified in the Somma-Vesuvius area, whereas fifteen macro-basins with
292 slopes > 25° were identified in the Apennines to the East of the volcano (Fig. 3). The different slopes
293 thresholds are defined starting from previous studies (Pareschi et al., 2000, 2002; see also Bisson et
294 al., 2013, 2014), and on the basis of a better analysis of the physical characteristics of the remobilized
295 material, in turns related to the various types of deposits. In fact, on the steep slopes and in the valleys
296 of Somma-Vesuvius the deposits are mainly ash-rich pyroclastic current deposits and subordinately
297 lapilli fallout deposits, while on the Apennines they are ash and lapilli fallout deposits. Each basin
298 was considered as a single feeding unit for the lahars generation, and this is an input for the modeling
299 of possible future lahars in the companion papers (de' Michieli Vitturi et al., this issue; Sandri et al.,
300 this issue).
301

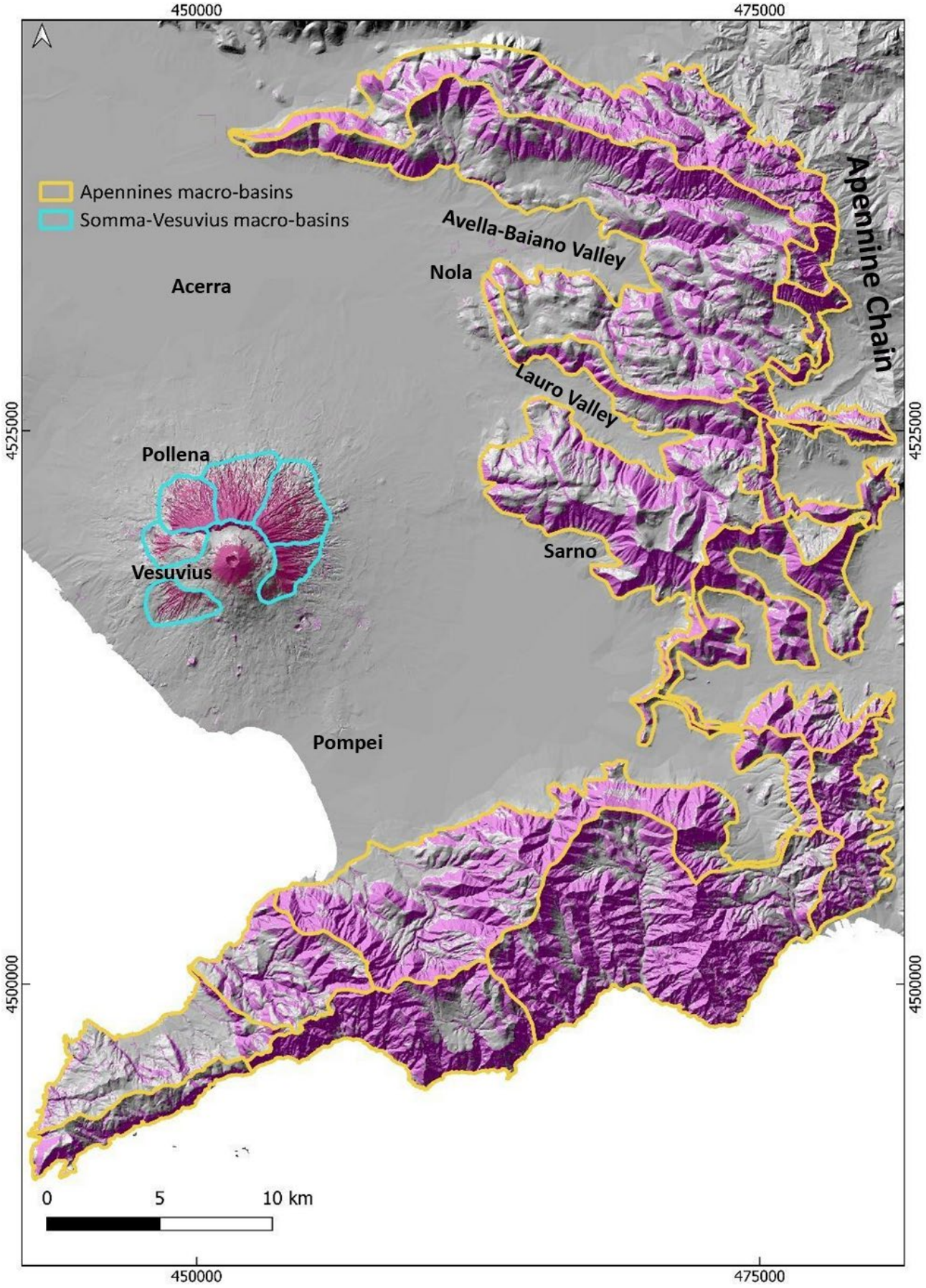
450000
475000
Apennines macro-basins
Somma-Vesuvius macro-basins
Avella-Baiano Valley
Nola
Acerra
Apennine Chain
Lauro Valley
4525000
Pollena
Vesuvius
Sarno
Pompei
4500000
0
5
10 km
450000
475000

302

303 Fig. 3. The macro-basins defined on the basis of their geomorphological features to study the areas of possible
304 accumulation and mobilization of deposits, which are used in modeling lahar generation of future events.

305

306 **3.4. Laboratory and analytical work**

307 **3.4.1. Grain-size**

308 In selected studied sites reported in Fig. 4, macroscopic analyses of the stratigraphic sequences were
309 carried out in the field to first identify any homogeneities or similarities between the juvenile fraction
310 of the primary and secondary deposits, and then recognize the various volcaniclastic units. This was
311 followed by sampling the deposits and carrying out the laboratory analyses.
312 In particular, the sampling was mostly made on the syn-eruptive lahar deposits, but also on the post-
313 eruptive and, in a few cases, on the primary pyroclastic deposits. All lab analyses were performed in
314 the laboratories of sedimentology and optical microscopy at the Istituto Nazionale di Geofisica e
315 Vulcanologia, Sezione di Napoli Osservatorio Vesuviano (INGV – OV). The material samples were
316 pre-heated at a temperature of 60-70 °C to eliminate any fraction of humidity, then were quartered
317 and sieved. To avoid any breaking of fragile clasts like pumices, the dry sieving of the grain-size
318 classes between -4 (a coarse limit variable depending on the sample) and 0 phi was made manually,
319 while for the classes between 0.5 and 5 phi a mechanical sieving apparatus was used.
320 In particular, the fine ash-rich deposit samples with a high degree of cohesion (with a significant
321 amount >0 phi) were diluted in distilled water, then boiled to remove all ash aggregates, before being
322 analyzed for grain-sizes following a wet procedure, and finally dried and weighted by classes. The
323 cumulative class >5 phi was further separated by interpolation modelling (de'Michieli Vitturi et al.,
324 this issue). In the post-processing of the data, the GRADISTAT excel package by Blott and Pye
325 (2001) was used to determine the main statistical parameters. On selected samples, a microscopic
326 componentry analysis was performed, consisting of recognizing and separating the various lithotypes
327 that compose the volcaniclastic deposits, that is juvenile, lithic and crystal clasts. The clasts

recognition was made manually for the coarser fractions, while for the finest fractions it was necessary the use of a reflected-light binocular microscope.

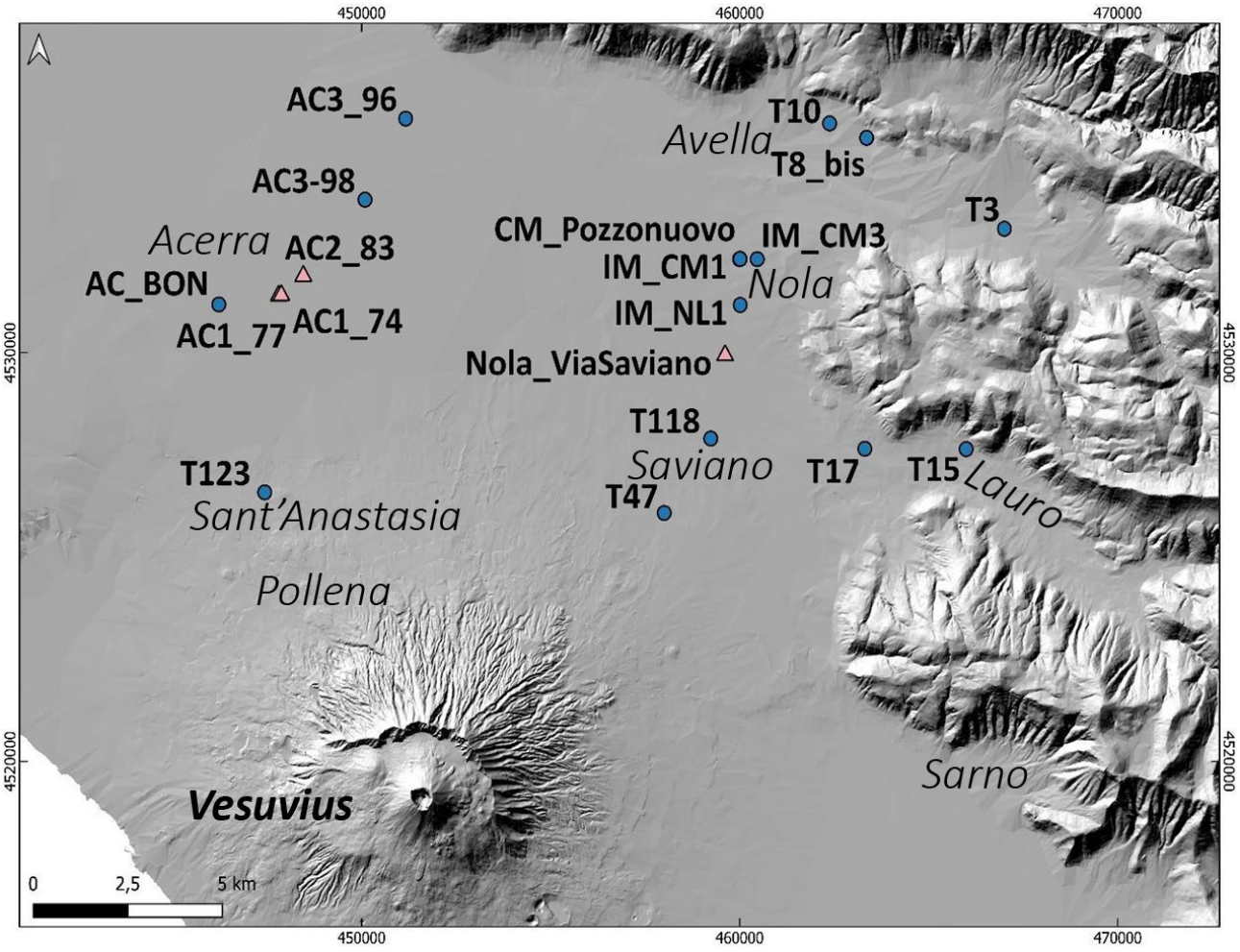

Fig. 4. Location of sites in which the sampling was carried out for sedimentological and paleomagnetic analyses. The pink triangles represent the sites for which a paleomagnetic study was carried out (AC1_74, AC1_77, AC2_83, and Nola_Via Saviano). In several sites, multiple samples were taken at different stratigraphic heights; samples labeled with US were taken at CM_Pozzonuovo site (see results).

3.4.2. Input for impact parameters

A significant number of large clasts and boulders was also found embedded in the lahar deposits at different locations. These clasts have dimensions from several centimeters to several tens of centimeters in diameter, and their nature is variable, that is limestone, ceramic, brick, tephra, lava, sandstone, iron (in order of abundance). Most of the clasts are fragments of artifacts from buildings, structures, and other archaeological finds of the Roman period, and their shape can be approximated in the field to ellipsoid. All these features suggest that they were entrained from substrate into the lahars to ultimately be deposited together with the main finer solid load of the lahars. In the dynamics of volcaniclastic mass flows like lahars and pyroclastic currents, the occurrence of boulder entrainment by flow dynamic pressure is recognized as a quite common feature (e.g., Zanchetta et al., 2004a; Pittari et al., 2007; Duller et al., 2008; Toyos et al., 2008; Cas et al., 2011; Carling, 2013; Doronzo, 2013; Jenkins et al., 2015; Roche, 2015; Martí et al., 2019; Guzman et al., 2020). The capability of a flow to entrain a clast is a function of flow properties (velocity, density) and clast properties (dimension, density, shape), and dynamic pressure well syntheses and quantifies such capability also in terms of flow hazard (Toyos et al., 2008; Zuccaro and De Gregorio, 2013; Jenkins et al., 2015). In Appendix A, a theoretical scheme is presented to invert these field features for calculation of the impact parameters at local scale.

3.4.3. Rock magnetism

The lahar deposits related to the Pollena eruption were analyzed by rock magnetism in the municipalities of Acerra (12 km from Somma-Vesuvius) and Nola (10-15 km from 10-15 km from Apennine source valleys) at four localities (Fig. 4), where the lahars interacted with anthropogenic structures. At each locality, we collected oriented samples, then measured about 200 specimens. We sampled both the deposit matrix and some potsherds embedded along three trenches (74, 77 and 83) and in the “Nola-Via Saviano” excavation. The purpose of the magnetic measurements was threefold: i) evaluating the magnetic fabric of the deposits to infer the local to regional flow directions of the

364 lahars and possibly their origin, whether from the Apennines or Vesuvius. The magnetic fabric in this
365 type of deposits records the main flow direction (local/regional) followed during the emplacement
366 processes; ii) estimating the deposition temperature (T_{dep}) of the deposits, to understand whether the
367 lahar was triggered soon after the eruption or at later times. The hypothesis is that the temperature is
368 higher in case of syn-eruptive lahars deriving from hot (pyroclastic current) deposits, and lower in all
369 other cases; iii) testing the relative sequence (contemporaneity) of the lahars emplacement with
370 respect to the Pollena eruption. All hand-samples were oriented *in-situ* with magnetic and solar
371 compasses and reduced to standard sizes at the CIMaN-ALP laboratory (Peveragno, Italy), where all
372 the magnetic measurements were made. In Appendix B, the adopted paleomagnetic techniques and
373 nomenclature are described.
374

375 **4. Results**

376 **4.1. Field stratigraphy and sedimentological features**

377 In this study, data of about 500 sites were collected, covering an area of >1000 km^2 from the plain
378 around the volcanic edifice to the Apennine valleys to the north and east (Fig. 2).
379

380 **4.1.1. Pyroclastic deposits: Pollena and 1631 eruptions**

381 The integration of the collected data with the existing ones (Rosi and Santacroce, 1983; Rosi et al.,
382 1993; Rolandi et al., 2004; Sulpizio et al., 2005; Perrotta et al., 2006; Bisson et al., 2007; Santacroce
383 et al., 2008; Gurioli et al., 2010; De Simone et al., 2011) allowed the reconstruction of the distribution
384 maps for both the fallout and pyroclastic current deposits. In particular, the spatial distribution
385 highlights that for both the Pollena and 1631 primary deposits, thick fine ash deposits are widely
386 distributed and cover the coarse fallout sequence or directly the ground, modifying the isopachs
387 reconstructed by previous authors (Sulpizio et al., 2006 and references therein; Figs. 5 and 6). This

388 enlargement of the area affected can have important implications on the hazard evaluation in terms
389 of possible damages on a densely inhabited territory.
390 The area covered by the comprehensive isopach maps (including both lapilli and ash fallout) turns
391 out to be wider than previously known, above all because we took into account for the ash fallout
392 occurred during the final phreatomagmatic stages of the eruptions (Rosi and Santacroce, 1983;
393 Sulpizio et al. 2005). The great availability and distribution of these ash deposits could explain the
394 wide generation and distribution of the syn-eruptive lahars in the area. This has important implications
395 on the evaluation of the source area and material available for the lahars accompanying and following
396 these eruptions. Interestingly, there is an increase of the areas covered by pyroclastic deposits. The
397 QGIS recalculated 10-cm isopach area covered by the fallout deposits is of 837 km^2 (Pollena eruption)
398 and 528 km^2 (1631 eruption), which compared to the lower values of 569 km^2 (Pollena eruption) and
399 158 km^2 (1631 eruption) after Sulpizio et al. (2006) give an extra surface of about 47% and 230%,
400 respectively. Geotechnically, another implication is that the wide presence of fine and cohesive ash,
401 not only on top of the coarse fallout sequences but also on the ground, preventing water infiltration,
402 favoring surficial runoff and creating sliding surfaces (Baumann et al., 2020).
403

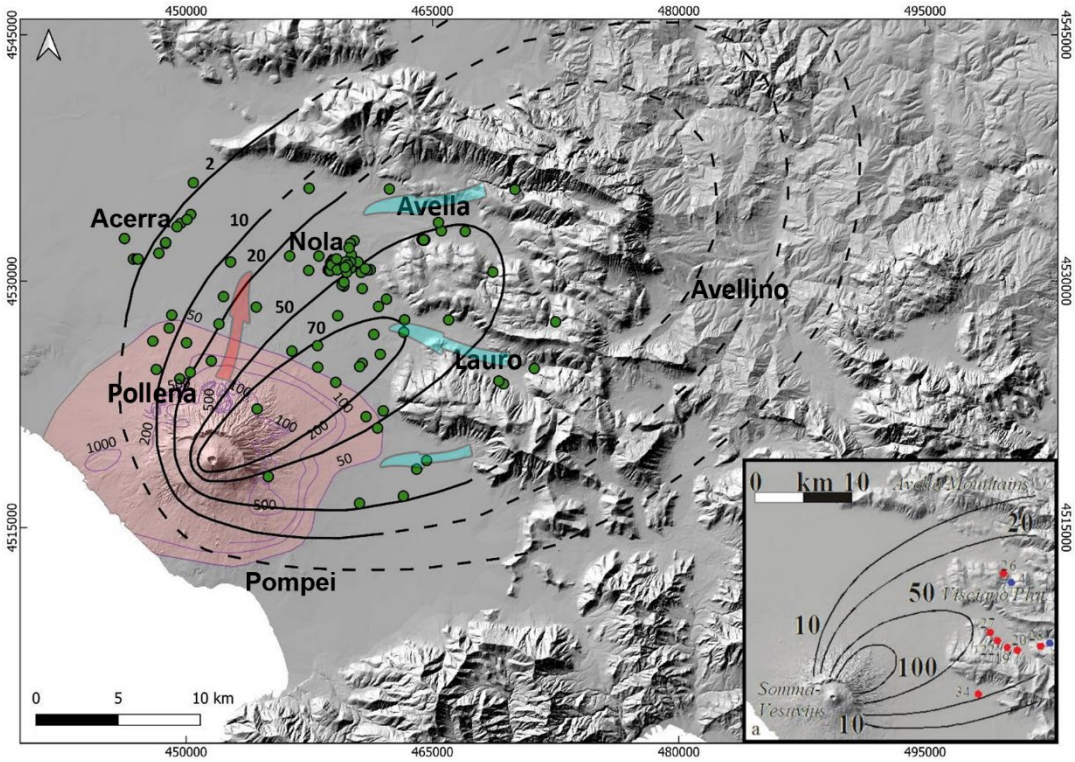

Fig. 5. Pollena eruption: the black lines represent the isopachs (in cm) of the fallout deposits modified after Sulpizio et al. (2006) (in the inset) on the basis of the new collected data (green dots), while in pink is colored the area affected by the pyroclastic current deposits (isopachs in cm, purple lines) modified after Gurioli et al. (2010). The dotted isopachs are extrapolated. The light blue arrows represent the general remobilization of the pyroclastic fallout deposits and lahar propagation from the Apennine slopes, while the pink one represents the combined remobilization of the pyroclastic current and fallout deposits and lahar propagation from Somma-Vesuvius.

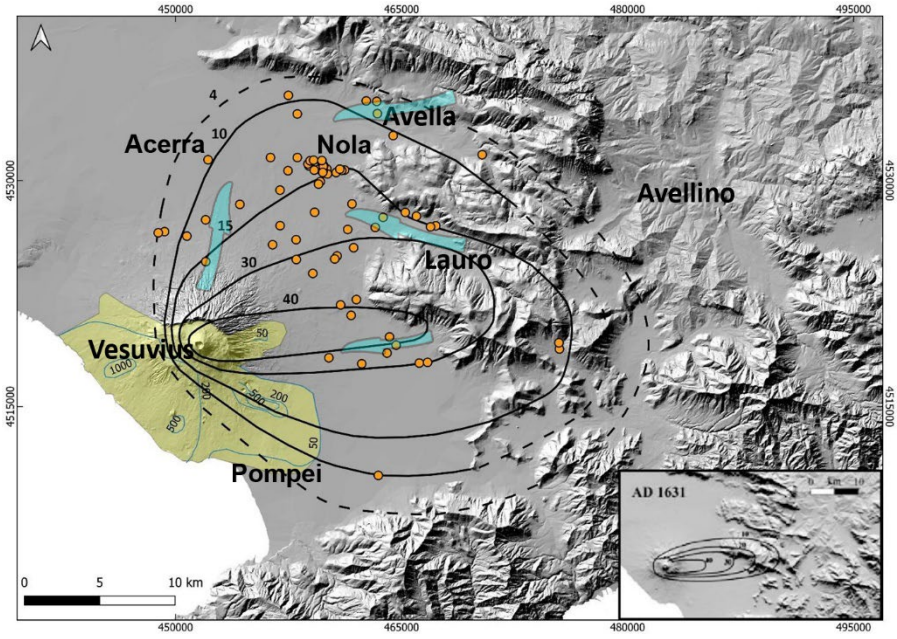

Fig. 6. 1631 eruption: the black lines represent the isopachs (in cm) of the fallout deposits modified after Santacroce et al. (2008) (in the inset) on the basis of the new collected data (orange dots), while in yellow is colored the area affected by pyroclastic current deposits (isopachs in cm, light blue lines). The light blue lines represent the inferred distribution on the basis of an integration between field data and chronicles modified after Gurioli et al. (2010). The dotted isopachs are extrapolated. The light blue arrows represent the general remobilization of the pyroclastic fallout deposits and lahar propagation from the Apennine slopes and Somma-Vesuvius.

The area affected by accumulation of the 1631 eruption tephra-fallout deposits is wider than previously known, particularly toward the north, which follows the inclusion of the final ash deposits into the new isopachs. Interestingly, such widening of the area agrees with the occurrence of lahars in the plain north of Vesuvius, as documented in the historical sources (Rolandi et al., 1993; Rosi et al., 1993, and references therein), and as follows.

4.1.2. Lahar deposits

The lithological and sedimentological analyses carried out in the field allowed the macroscopic definition of the primary pyroclastic deposits affected by the remobilization, and of the lahar deposits.

In many cases, the archaeological findings permitted to define the local paleoenvironment and related land use, then permitted to constrain the age and timing of the deposition.

We grouped all deposit descriptions into representative lithofacies to more directly characterize both the primary pyroclastic and lahar deposits (Tab. 2 and Fig. 7). Given the amount of data and description of the studied areas, we used these lithofacies to characterize a number of macro-areas between the Somma-Vesuvius sector and the nearby Apennine valleys (Appendix C).

Symbol	Lithofacies
P	Paleosol and humified surface, massive and composed of fine sand and silt from brown to dark brown, with several percentages of clay and organic matter. It indicates a stasis in the depositional processes.
mL	Alternation of massive lapilli layers. Pyroclastic fall deposit composed of pumice and scoria lapilli with sparse accidental lithics.
mA	Massive ash. Pyroclastic fall deposit composed of fine to coarse ash with sparse pumice fragments, scoriae and accidental lithics.
Gms	Massive gravel and sand deposit, matrix-supported and poorly-sorted. The matrix is composed of fine to coarse sand, while the gravel clasts comprise scoria and pumice clasts from the pyroclastic fall deposits. The massive feature of the single layers suggests a rapid emplacement from a highly-concentrated lahar.
mM	Massive mud deposit composed of fine sand, silt and clay, sometimes with sparse pumice and lithic clasts. It is generated from a mud-dominated lahar.
Sh	Horizontal lamination and bedding features in sands. The deposit is composed of an alternation of fine to coarse sand and gravel, which can be gradual or sharp. It comes from a hyper-concentrated lahar (less dense than the Gms one).
Ss	Scour and fill structures composed of fine to coarse sand, generally with a normal grading. A single structure consists of an erosive, concave upwards basal surface and a planar/convex top.
fM	Fine mud deposit composed of fine sand, silt and clay. It is generated when the lahar loses its energy and the fine grains settle gently.

Tab. 2. Symbol and description of the recognized lithofacies, and photos representative of each of them.

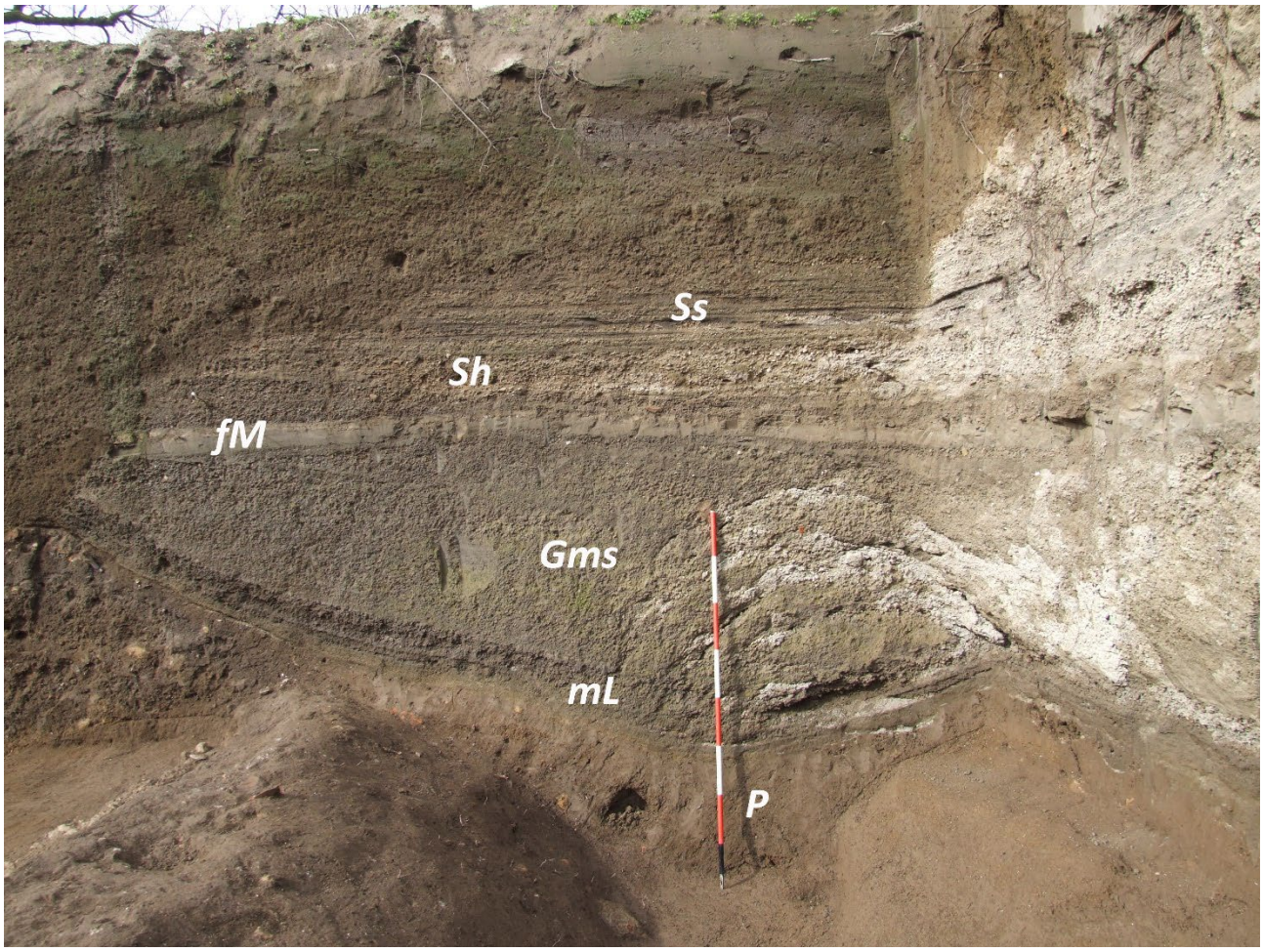

a)

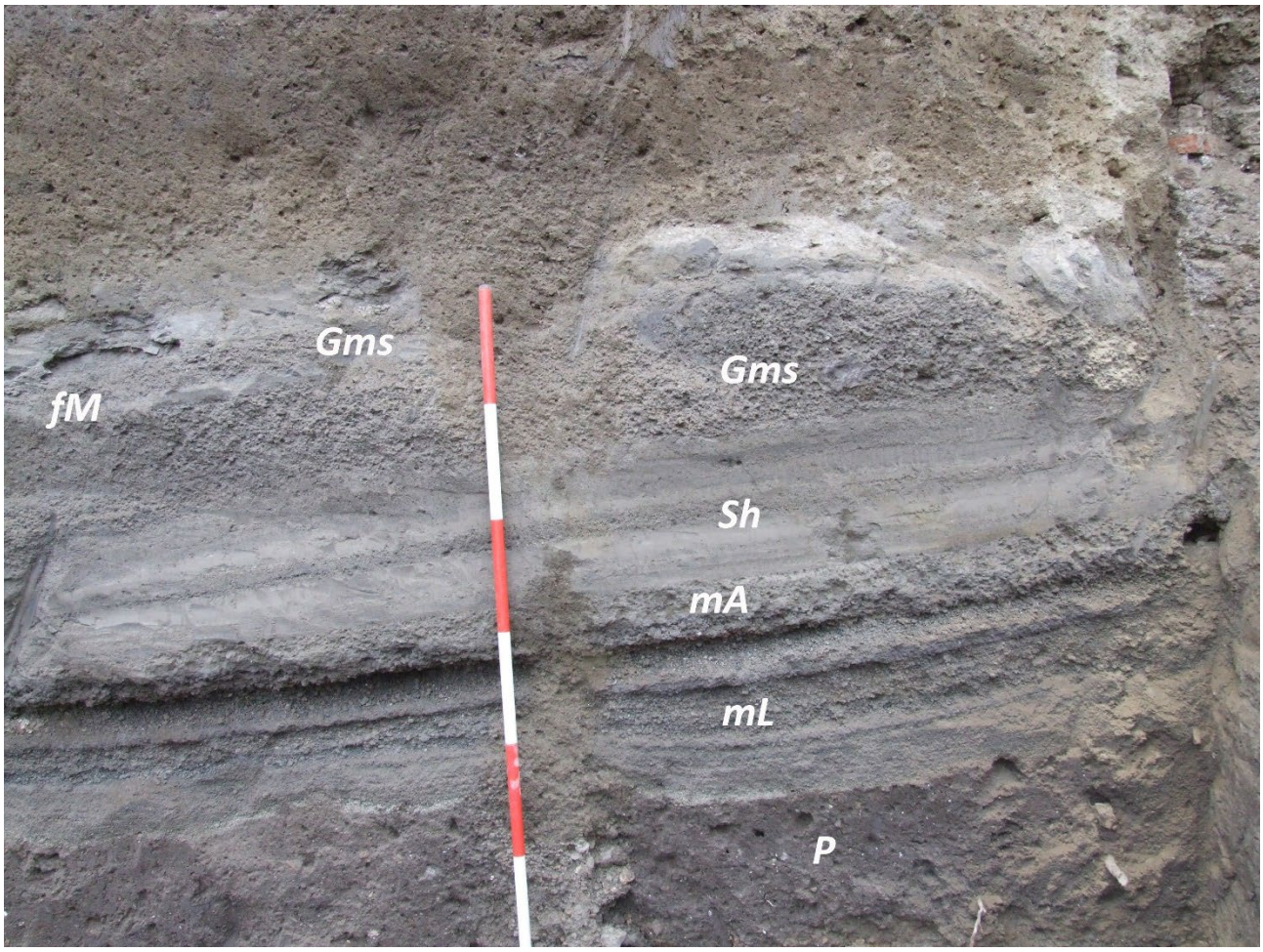

b)

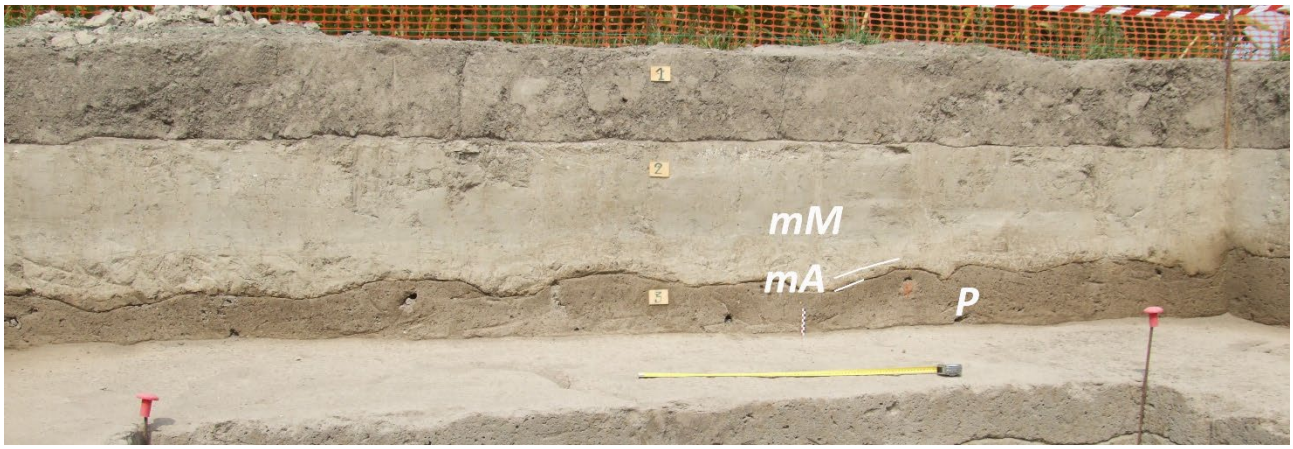

c)

Fig. 7. In these three photos of archaeological excavations (a-b, Nola at 10-15 km from Apennine source valleys; c, Acerra at 12 km from Somma-Vesuvius), the main lithofacies recognized in the field are shown, including paleosols, pyroclastic deposits, and lahar deposits; the corresponding lithofacies descriptions are reported in Tab. 2.

448 Usually, the syn-eruptive lahar deposits directly overlie the primary pyroclastic deposits, sometimes
449 eroding them. They have a matrix-supported texture and are composed of fine to very fine cohesive
450 ash, and contain more or less abundant cm-sized pumice and lithic fragments. In general, these
451 deposits consist of multiple depositional flow units, each one resulting from single-pulse “en masse”
452 emplacement, the piling of which resulting from rapid progressive aggradation through multiple flow
453 pulses, in analogy with dense pyroclastic currents (Sulpizio et al., 2006; Doronzo, 2012; Roche, 2012,
454 2015; Breard and Lube, 2017; Smith et al., 2018; Guzman et al., 2020; see Sulpizio et al., 2014, p.
455 56). Consequently, the studied lahars were modelled using a shallow layer approach (de’Michieli
456 Vitturi et al., this issue). The different depositional flow units in the same deposit are distinguishable
457 (still in continuity) from each other based on vertical granulometric changes, sparse pumice
458 alignments, deposit layering and/or unconformities. For example, compared to channelized
459 pyroclastic currents, dense water flows and floods, such depositional units (layers) could have been
460 repeatedly emplaced, from bottom to top, under accumulation rates of a few tens to hundreds kg/m^2s
461 (Lowe, 1988; Russell and Knudsen, 1999; Whipple et al., 2000; Girolami et al., 2010; Roche, 2015;
462 Marti et al., 2019; Guzman et al., 2020). In various areas, such rapid sequential emplacement is
463 suggested by the presence of water escape structures through the whole deposit by crossing the
464 sequence of several units. These are vertical structures consisting of small “pipes” filled with fine
465 mud transported by the escaping water, and formed soon after the emplacement of the lahar units.
466 The textural characteristics are variable even within the same site, but in general the deposits are
467 massive and contain vesicles, from circular to flattened, coated by fine ash that adhered into the voids
468 after water loss. For the syn-eruptive lahar deposits, the pumice fragments are those of the primary
469 deposits. On the other hand, in the upper parts of the sequences it is not uncommon to find units that
470 contain pumice fragments related to previous eruptions (9.0 ka B.P. "Mercato" and 3.9 ka B.P.
471 "Avellino" Plinian eruptions), recognizable based on pumice texture and crystal content (Santacroce
472 et al., 2008). In this second case, the lahar deposits are considered as post-eruptive, meaning that the
473 pyroclastic deposits older than the two studied sub-Plinian eruptions were progressively involved in

474 an advanced erosion of the slopes and valleys. The presence of slightly humified surfaces below the
475 lahar deposits or the trace of human artifacts, such as for example excavations, ploughing, etc…, are
476 considered as evidence of a long period without deposition; also in this case, the lahars are considered
477 as post-eruptive. In other words, the similar componentry of the lahar and pyroclastic deposits, and
478 the evidence of short-term exposure between these two, are strong indicators of the syn-eruptive
479 occurrence of the lahar events. Instead, the absence of such features is more indicative of a post-
480 eruptive origin, i.e. lahars events more spaced in time from the corresponding eruption.
481 In Appendix C, a description is reported for some of the most representative sequences, which were
482 sampled in different areas throughout the plain (Figs. 2 and 4).

483

484 **4.1.3. Distribution maps of the lahar deposits**

485 Here we present distribution maps for the lahar deposits of the Pollena and 1631 eruptions (Figs. 8-
486 11). The maps show the distribution of all thicknesses detected in the studied sites. In particular, the
487 syn-eruptive Pollena lahar deposits are distributed in the NW quadrants of the volcano and in the
488 Avella, Lauro and Sarno valleys (see Fig. 1), with a thickness exceeding 1 m in the Vesuvius apron
489 and in the plain between Nola and Cimitile at about 10-15 km from Apennine source valleys (see
490 Figs. 1 and 8). A volume estimation of the remobilized deposits is of the order of 7×10^7 m^3 for the
491 northern Vesuvius area, and 4×10^7 m^3 for the Lauro Valley. Such volumes are referred to the
492 depositional areas, and not to the detachment ones; for the latter see de'Michieli Vitturi et al. (this
493 issue) and Sandri et al. (this issue). The provenance of the material in each site was inferred by
494 sedimentological recognition and magnetic reconstruction. Then, the covered areas were subdivided
495 into polygons in the geospatial database, in order to weight the local deposit thicknesses and estimate
496 the volumes with a lower approximation.

497

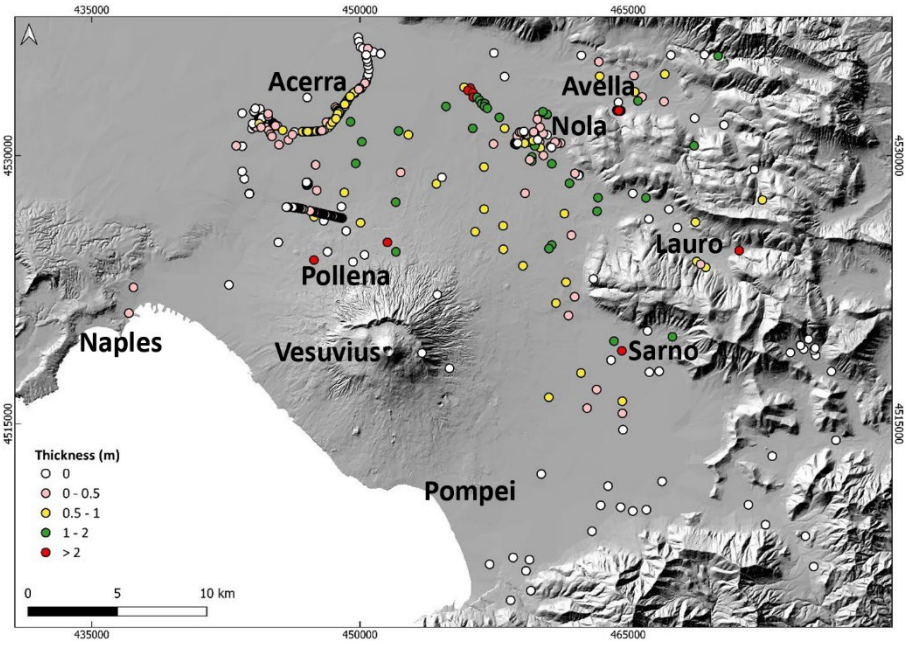

Fig. 8. Distribution of the syn-eruptive lahar deposits related to the Pollena eruption. The 0 m points represent the studied sites where the lahar deposits were absent, and in some cases even the primary pyroclastic deposits below were absent; they are reported anyway, as their absence might have not necessarily occurred by no deposition (local erosion).

The post-eruptive lahar deposits of the Pollena eruption are more distributed in the Avella and Lauro valleys, and in the plain north of the volcano close to the apron area (low-angle edifice outer slopes) (Figs. 1 and 9). Their deposits contain both fragments from the Pollena eruption and from preceding eruptions, suggesting that pyroclastic deposits of the older sequences were progressively eroded and involved in remobilization processes over time. As an example, on Fig. C1 it is to remark that whitish pumice fragments from the Pomici di Avellino and Mercato eruptions were identified on top of the Pollena lahar deposits.

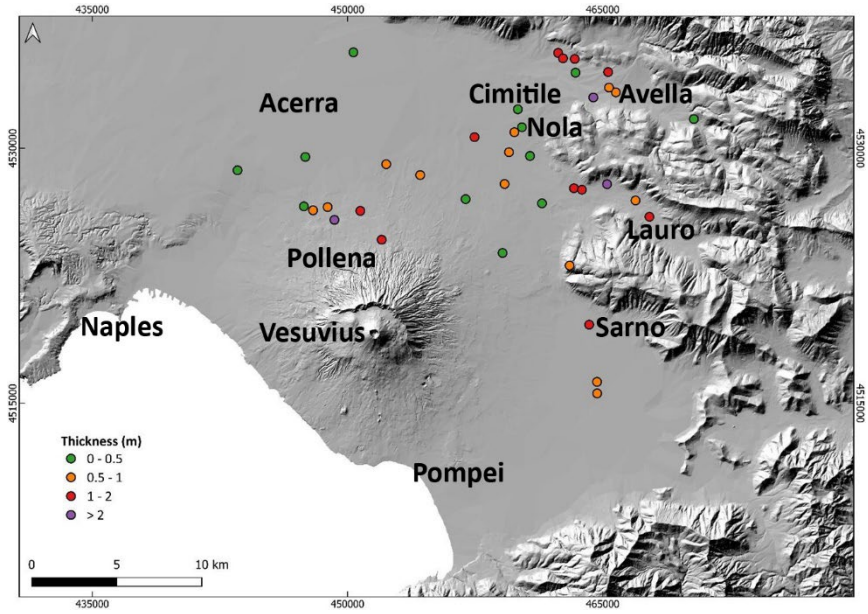

Fig. 9. Distribution of the post-eruptive lahar deposits related to the Pollena eruption.

The distribution of the syn- and post-eruptive Pollena lahar deposits is related to the primary pyroclasts deposition: the dense distribution of the lahar deposits north of Somma-Vesuvius depends on the presence of thick pyroclastic current deposits that were remobilized from the northern slopes of the volcano, while the distribution in the Apennine valleys is related to the fallout deposits that are thicker along the major Pollena dispersal axis (Fig. 5).

Above the Pollena pyroclastic and lahar deposits (both syn- and post-eruptive), the studied sequences in almost all the sites show the presence of a well-developed soil bed with many traces of cultivation, as well as of inhabited areas and buildings (Figs. C1-4). These traces and the presence of the soil bed are evidence of a progressive geomorphological stabilization of the territory. The occurrence of the 1631 sub-Plinian event determined a new phase of marked geomorphological instability for a large territory surrounding the volcano. In Fig. 10, it is shown the distribution of the syn-eruptive lahar deposits for the 1631 eruption in all the studied areas, having a variable thickness, generally <50 cm. Such distribution affected mostly the areas of Acerra-Nola, Sarno, the Vesuvius apron and the Apennine valleys (Figs. 1 and 10). Rosi et al. (1993) and Sulpizio et al. (2006) reported that floods and lahars heavily impacted (also with injuries and victims) the N and NE quadrants of Somma-

Vesuvius soon after the eruption with a timescale of days (Rosi et al., 1993; see also the historical chronicles of Braccini, 1632), corroborating the syn-eruptive behavior of such lahars. Some lahar deposits are intercalated within the primary pyroclastic deposits, but in general they directly stand on top of the pyroclastic deposits (Rosi et al., 1993); both cases unequivocally constrain the syn-eruptive behavior of the 1631 eruption lahars.

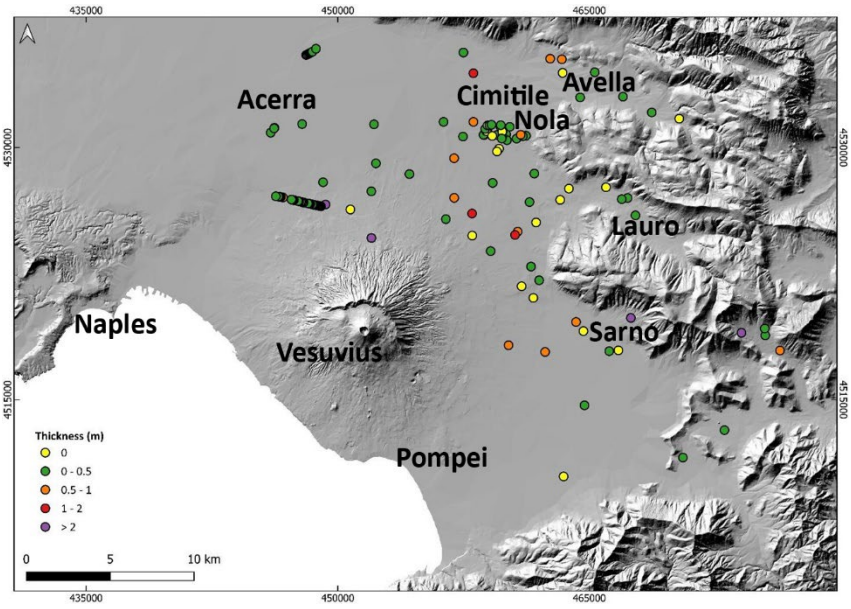

Fig. 10. Distribution of the syn-eruptive lahar deposits related to the 1631 eruption. The 0 m points represent the studied sites where the lahar deposits were absent, and in some cases even the primary pyroclastic deposits below were absent; they are reported anyway, as their absence might have not necessarily occurred by no deposition (local erosion).

In Fig. 11, minor post-eruptive lahar deposits of the 1631 eruption are reported, with a preferential distribution to the E quadrants of the volcano from N to S, both in the plain and the valleys. These deposits are still significant, with a thickness of around half a meter to a meter or more in a few points.

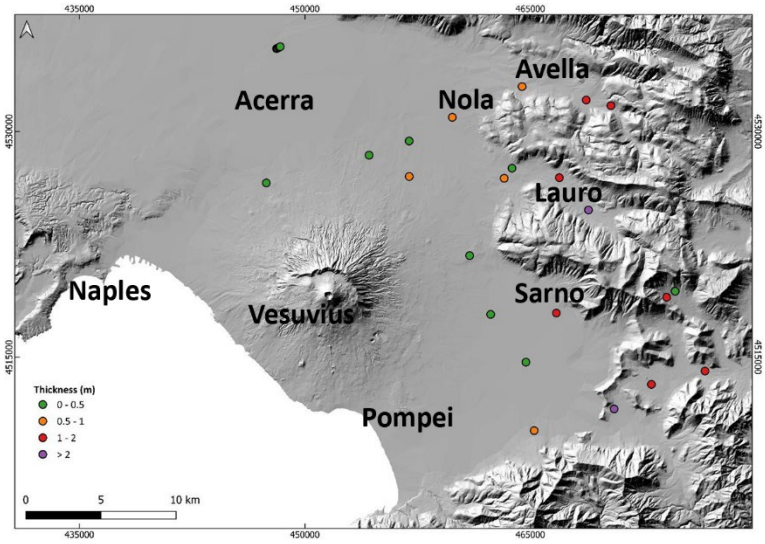

Fig. 11. Distribution of the post-eruptive lahar deposits related to the 1631 eruption.

The distribution of the syn- and post-eruptive 1631 lahar deposits mainly reflects the major dispersal axis affecting the fallout deposits distribution, while the pyroclastic current deposits were minorly remobilized as exposed on the gentler slopes of southwestern Vesuvius (Fig. 6).

4.1.4. Sedimentological characteristics of the Pollena lahar deposits

The field analysis was carried out in about 500 different sites for the construction of the database and maps, while the laboratory analysis was carried out on 30 samples representative of the different areas. The results of the grain-size analyses (cumulative curves and statistical parameters) are presented in Fig. 12 and Tab. 1.

Petrological analysis on the syn-eruptive lahar deposits have not been performed because the lithology (colour, texture, mineral content) of the components is the same as the juvenile material of the primary deposits described in Sulpizio et al. (2005). The loose crystals consist of sanidine, leucite, biotite and pyroxene fragments. Based on the results of the grain-size analyses, the coarser classes are defined from -4 to -1 phi, the medium ones from -0.5 to 2.5 phi, and the finest one from 3 phi. The juvenile pumice clasts are an ubiquitous component of the lahar deposits (both syn- and post-eruptive), but they decrease with distance for the finer grain-size classes, while the crystal content

563 increases with the same progression. The lithic clasts are abundant for the coarser classes, they
564 decrease with distance for the medium classes, and increase again for the finer classes.

565

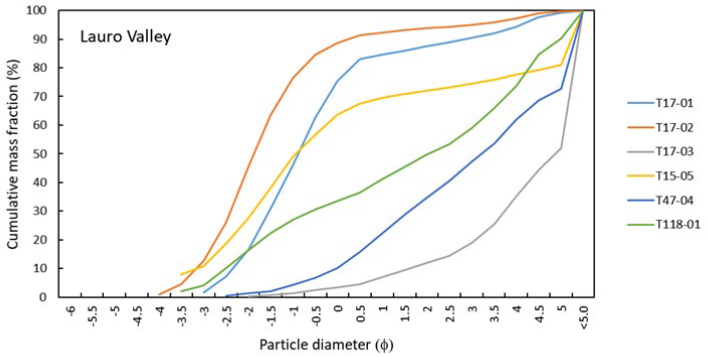

566

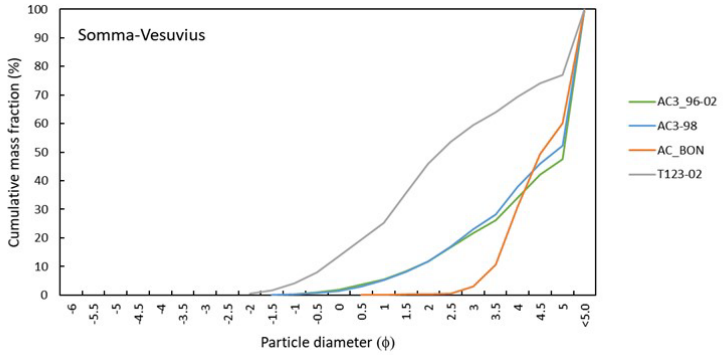

567

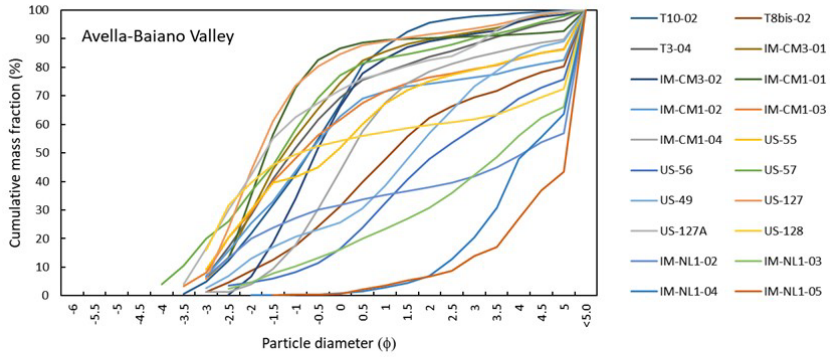

568

569 Fig. 12. Cumulative curves of the grain-size analysis on the samples taken at the locations reported in Fig. 4, and

570 subdivided in three sectors: Lauro Valley (top), Somma-Vesuvius (middle), and Avella-Baiano Valley (bottom).

571

572

573

Sample	Mean (ϕ)	Sorting (ϕ)	Lithofacies
Lauro Valley			
T17-01	-0.93	1.41	Gms
T17-02	-1.83	1.23	Gms
T17-03	2.42	1.46	Sh
T15-05	-1.39	1.74	Gms
T47-04	1.67	1.61	Mm
T118-01	1.13	2.7	Gms
Avella–Baiano Valley			
T10-02	-0.78	1.47	Sh
T8bis-02	0.31	1.83	Sh
T3-04	-0.95	1.83	Gms
IM-CM3-01	-1.13	1.54	Gms
IM-CM3-02	-0.48	1.35	Gms
IM-CM1-01	-1.66	0.86	Gms
IM-CM1-02	-1.17	1.62	Gms
IM-CM1-03	-1.13	1.83	Gms
IM-CM1-04	0.06	1.39	Fm

US-55	-0.84	1.97	Gms
US-56	1.17	1.8	Sh
US-57	-1.51	1.86	Gms
US-49	0.69	2.16	Gms
US-127	-1.66	1.39	Gms
US-127A	-1.02	2.23	Gms
US-128	-1.72	1.91	Gms
IM-NL1-02	-0.5	2.49	Gms
IM-NL1-03	1.25	2.1	Gms
IM-NL1-04	2.99	0.89	fM
IM-NL1-05	2.64	1.20	fM
Somma-Vesuvius			
AC3_96-02	2.37	1.26	mM
AC3-98	2.48	1.2	mM
AC_BON	3.52	0.38	mM
T123-02	1.37	1.5	mM

Tab. 3. Statistical parameters (mean and sorting) extracted from the grain-size analyses, and reference lithofacies (see Tab. 2 for descriptions).

Field observations and grain-size analyses, highlight significant differences between the sectors of Lauro Valley, Avella-Baiano Valley, and Somma-Vesuvius. A common feature between the three sectors is that the lahar deposit samples are mostly massive, poorly-sorted and polymodal; only a few samples are moderately-sorted and unimodal (sorting <1.5 phi). On the other hand, the grain-size modes found show some interesting differences (in Fig. 12 the cumulative curves are shown). The coarse modes for Lauro Valley and Avella-Baiano Valley span from fine/medium lapilli to coarse ash, while for Somma-Vesuvius span from coarse to fine ash. The medium modes for Lauro Valley and Avella-Baiano Valley span from coarse to medium ash, while for Somma-Vesuvius span from medium to fine ash. The fine modes for Lauro Valley and Avella-Baiano Valley, and for Somma-Vesuvius span from medium to fine ash. All these differences basically depend on the origin of the primary pyroclastic deposits, fallout vs. pyroclastic currents, which were remobilized from different sectors, Apennines and Somma-Vesuvius. The grain-size analysis is used as an input information for

590 the lahar transport model (de' Michieli Vitturi et al., this issue) aimed at assessing the related hazard
591 (Sandri et al., this issue).
592
593 **4.2. Magnetic results**
594 Both Acerra (12 km from Somma-Vesuvius) and Nola (10-15 km from Apennine source valleys)
595 localities show a well-defined magnetic fabric for the Pollena syn-eruptive lahar deposits. Principal
596 susceptibility axes ($K_1 \geq K_2 \geq K_3$) are clustered. Magnetic lineation (K_1) and magnetic foliation (K_3,
597 pole of the plane) are mostly sub-horizontal or gently embricated. The anisotropy degree P (K_1/K_3)
598 is mostly lower than 1.060, but can reach high values like 1.200. At Acerra, the magnetic foliation is
599 always dominant, and the fabric is oblate. The Pj is linearly correlated to the mean susceptibility (k_m).
600 In Appendix B, the full nomenclature is defined for completeness. The magnetic fabric has a
601 horizontal magnetic foliation and a clustered magnetic lineation, whose mean direction is NE-SW.
602 Considering the chaotic nature of the lahar deposits, the high Pj and the clustered susceptibility axes
603 can highlight a channelized flow (Fig. 13). At Nola instead, the fabric is both prolate/oblate, and Pj
604 is lower than 1.040. The susceptibility axes are more dispersed than at Acerra, but mean magnetic
605 lineation clearly shows a NW-SE direction. If one considers the oblate specimens only, the magnetic
606 foliation is sub-horizontal, on the contrary, the magnetic foliation of the prolate specimens is steeply
607 dipping (65°) toward SE. At Nola, the flow direction inferred by AMS is consistent and parallel to
608 the invasion basin.

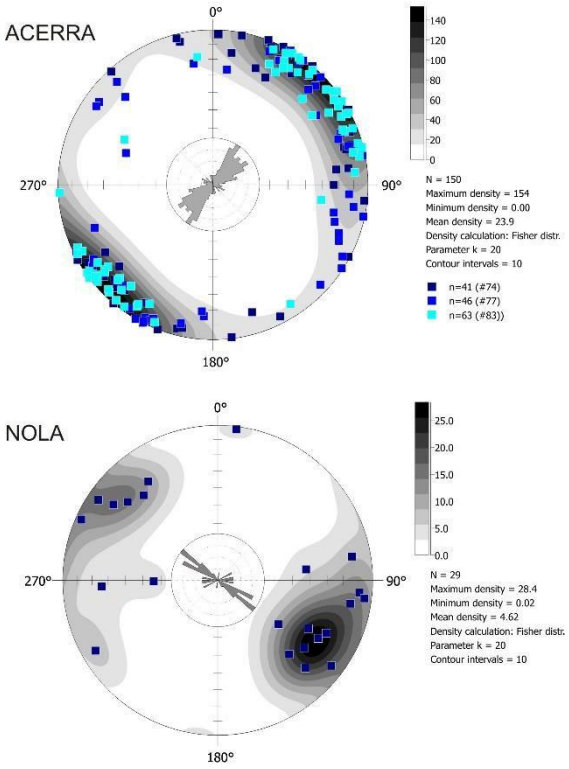

609

610 Fig. 13. Equal area projection and Rose diagram of the K_1 directions at Acerra (12 km from Somma-Vesuvius) and Nola
611 (10-15 km from Apennine source valleys).

612

613 At Acerra, the T_{dep} interval is 120-140 °C, while for Nola T_{dep} is lower than 120 °C (Fig. 14). In the
614 Nola case, a low temperature magnetization component lower than 120 °C cannot be directly
615 considered as a TRM. In fact, the low T_b Earth's field component of magnetization can also be
616 produced by a viscous remanent magnetization (VRM), acquired during exposure to weak fields
617 (Bardot and McClelland, 2000). The acquisition of the VRM depends on the duration of the exposure.
618 For age around that of the Pollena eruption, the minimum T_{dep} which can be distinguished is ca. 120
619 °C. For this reason, we considered the Nola lahar to be emplaced at low temperature.

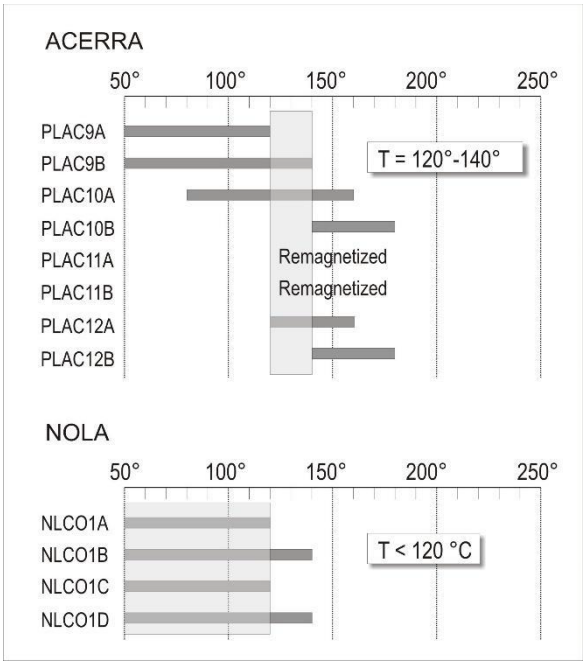

Fig. 14. Deposition temperature at Acerra and Nola. The site T_{dep} is estimated from the overlapping reheating temperature ranges for all lithic clasts sampled.

The mean paleomagnetic direction for each locality, calculated using Fisher's statistics, is well-defined, and its directional value and confidence limits do not overlap (Fig. 15). Thus, the two directions are statistically distinguishable at the 95% confidence limits. Since a paleomagnetic direction is a record of the Earth's magnetic field acting during the emplacement, it follows that the lahar deposits at the two localities are not synchronous.

Overall, all magnetic measurements just discussed show distinctly different characters between Acerra and Nola, clearly indicating two distinct events of emplacement.

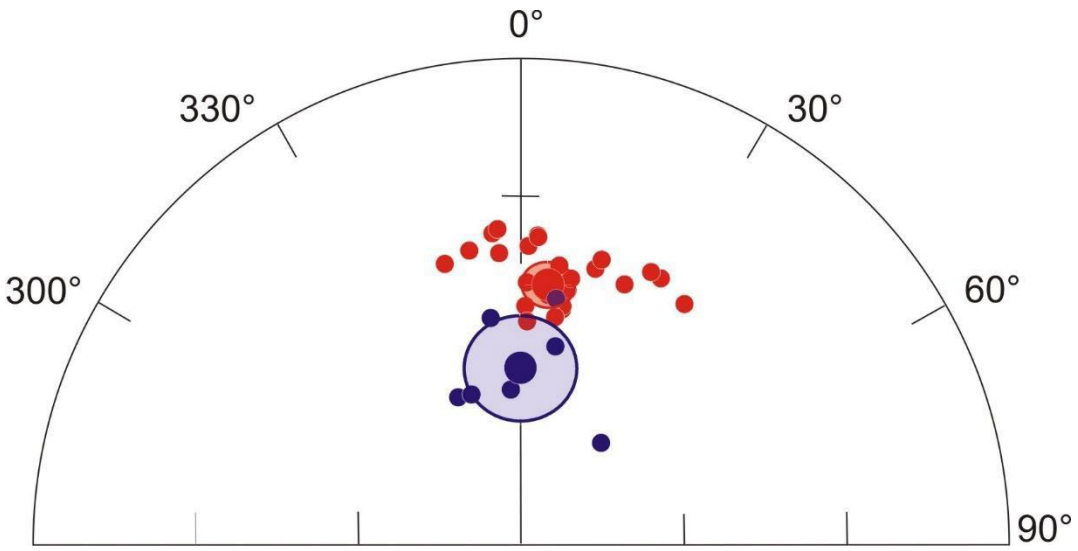

Fig. 15. Equal-area projection of the characteristic remanent magnetization directions, and their mean value with associated confidence limit, from Acerra (red dots, mean value: n=26 D=7.5°, I=43.4°, alpha95=3.5°), and Nola (blue dots, mean value: n=7, D=0.8°, I=60.2°, alpha95=9.0°).

4.3. Lahar dynamics

By inverting the field evidence and data, it is possible to reconstruct the macroscopic flow dynamics that occurred in the lahar invasion, which are particularly interesting to understand the impact that those lahars had on the Vesuvius territory. As already described, the lahar deposits show thicknesses that are variable from several centimeters to a few meters, and this can depend on multiple local factors: i) topography; ii) distance from source; iii) erosion; iv) source area and type of remobilized sediment (variably sized fallout vs. flow deposits). In particular, thicker deposits are found near the mouth of the valleys and in the flat alluvial plain, as shown in the deposit distribution maps. On the other hand, the deposits show a general tabular-like shape (Fig. 7), with an average thickness of the order of 0.5-1 m recurrent for several studied sites, which is the first evidence of the lahars impact and mass flow emplacement in the area. In terms of runout distance, the lahars travelled for 10 to 15 km from sources (Somma-Vesuvius and Apennine detachment areas), based on the geospatial database that includes all studied sites. It was possible to infer the source areas based on the common sedimentological features of the lahar deposits between nearby sites. On the other hand, distant sites

with sedimentologically different deposits were fed from different source areas. These important constraints are used to validate and inform lahar numerical models (de' Michieli Vitturi et al., this issue) and simulations (Sandri et al., this issue) using a shallow layer approach for hazard assessment. We cannot rule out that lahar pulses from different source areas (Somma-Vesuvius vs. Apennines) might have overlapped and further aggraded in the open plain.

At several locations, we found erosional unconformities (Fig. 16a) between the lower and upper flow units (Fig. 16b), as well as between the pyroclastic and lahar deposits. Erosion is an important factor for the entrainment of pre-existing materials and objects, which include large-size clasts external to the remobilized pyroclastic material. Size and density of the largest clasts embedded in the deposits can give an idea of the carrying capacity of the lahars.

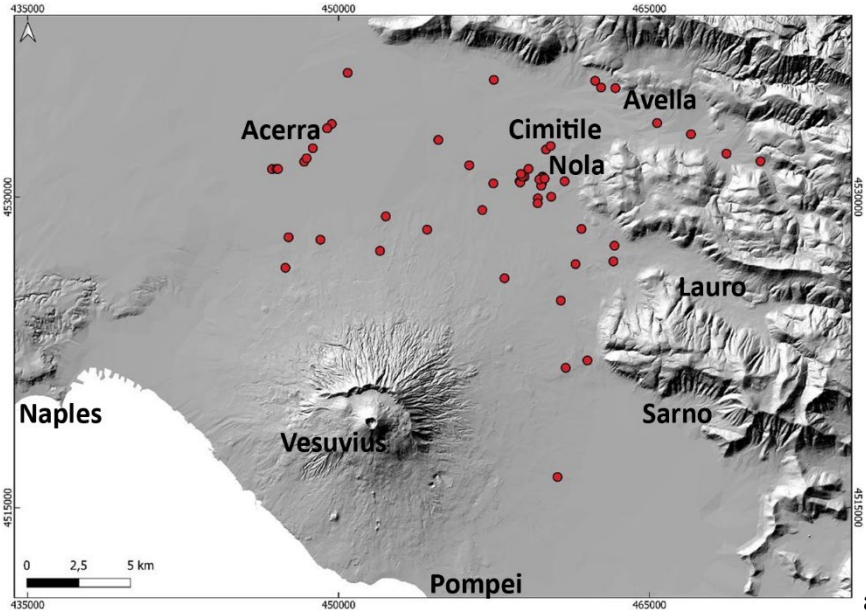

a)

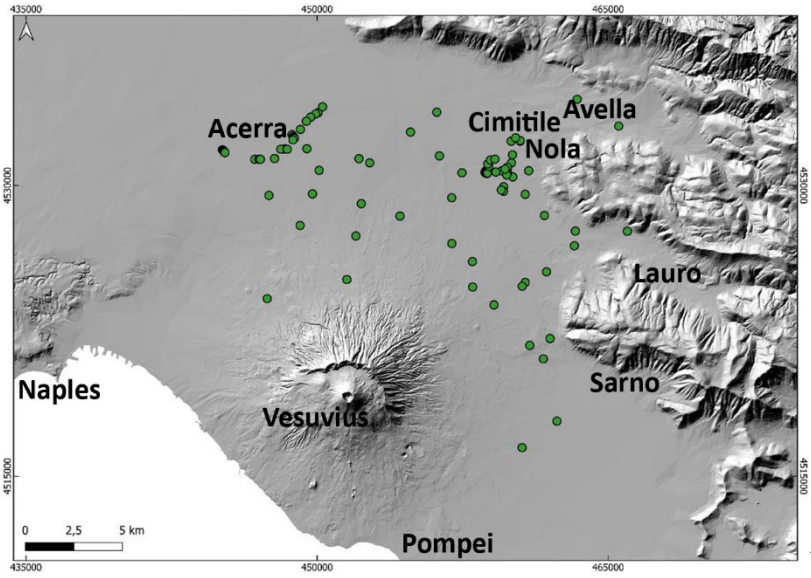

b)

Fig. 16. a) Sites with evident erosion traces at the base of the lahar units; b) Sites in which multiple depositional flow units are vertically identified. Both evidences corroborate the interpretation of the depositional mechanisms, as well as constrain the choice of the shallow layer approach for the lahar models and simulations (de'Michieli Vitturi et al., this issue; Sandri et al., this issue).

Occurrences of large clasts and boulders are reported in the area invaded both by the syn- and post-eruptive lahars, with a distribution that follows the one of the lahar deposits, in particular both are found at the mouth of the valleys and in the alluvial plain. The presence of the erosional features (Fig. 16a), and the fact that the deposits are mostly composed of massive and relatively thick units (Fig. 16b), suggest that high sediment transport and deposition both occurred in the same area (Doronzo and Dellino, 2013; Roche, 2015). Such occurrences of erosion and accumulation of multiple units were useful to inform the lahar modelling of de'Michieli Vitturi et al. (this issue).

We calculated local velocities of the syn- and post-eruptive Pollena lahars based on the biggest clasts that are found in the deposits at various stratigraphic heights, with boulder dimensions from several centimeters to a meter, and for flow density ≥ water density (Appendix A). The faster the lahar the higher the capability of its flow to entrain bigger external clasts. This occurred at locations where such clasts were freely available on the substrate, or where the lahars impacted and damaged anthropogenic structures.

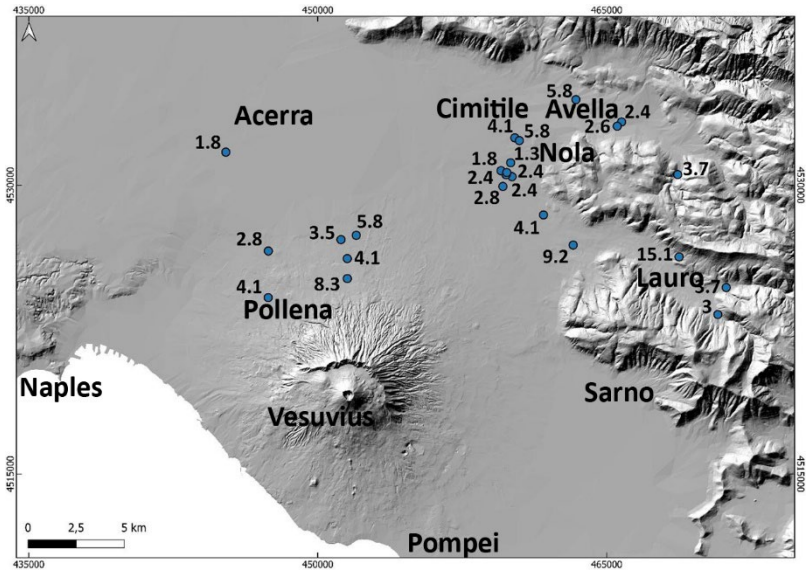

Fig. 17. Average lahar velocities (in m/s) estimated with a point-by-point reverse engineering approach.

Then, we used the flow velocities (Fig. 17) to calculate local dynamic pressures of the lahars (Fig. 18) as a function of the clast properties (size, density and shape). The obtained estimations are used by Sandri et al. (this issue) to validate the probabilistic hazard assessment of lahars from Vesuvius eruptions.

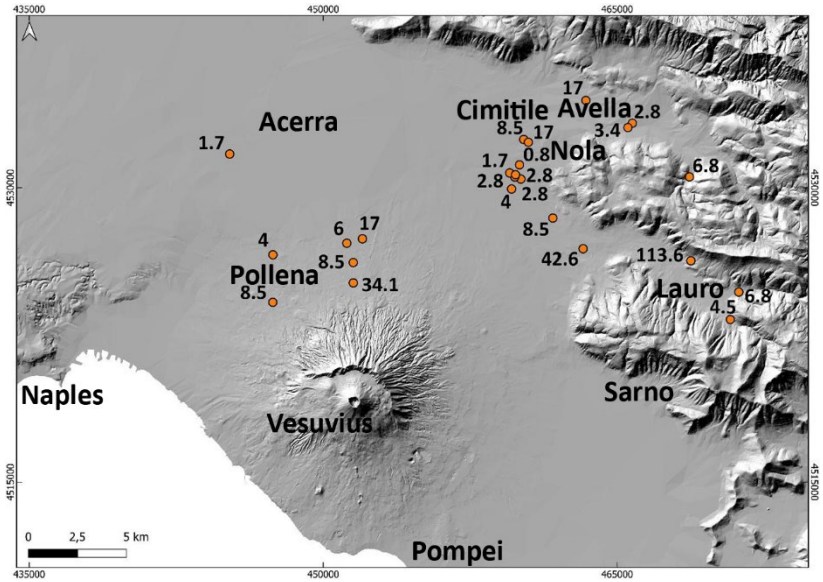

Fig. 18. Average lahar dynamic pressures (in kPa) estimated with a point-by-point reverse engineering approach.

695 The data presented in Figs. 17 and 18 represent minimum local values of the flow velocity and
696 dynamic pressure, respectively, useful to assess some minimum impact of the lahars in the alluvial
697 plain. An approximation of this point-by-point approach is that the values were calculated for the
698 finding locations of the clasts in the deposits, meaning that the values are overestimated for those
699 exact locations, while they should more properly be referred to the immediate surroundings upstream.
700 We did a parametric test to quantify the sensitivity for different physical states of the multiphase flow
701 depending on initial fluidization and flow density, and considering two end members, from a non-
702 fluidized case to an initially fluidized and non-expanded case (see Appendix A; Roche et al., 2013).
703 From the performed analysis, we found that the most typical values are referred to the initially
704 fluidized and slightly expanded case (that is a few % more expanded than the non-expanded case),
705 with most of the points falling in the range of velocity of 2-4 m/s, and dynamic pressure of 4-8 kPa.
706 Lastly, in eight locations we found the lahar deposits emplaced against meter-sized obstacles, from
707 which we estimated, by comparison, local flow heights of the order of 1-1.5 m, and particle volumetric
708 concentrations of ~30% or more, i.e. the deposit thickness is ~1/3 of the lahar thickness (cf. Capra et
709 al., 2018).

710

711 **5. Discussion**

712 The historical sources used as benchmark for lahars around Somma-Vesuvius and in the Apennine
713 valleys remark the frequent and broad impact that explosive eruptions of Vesuvius had in historical
714 times. Some of the eruptions in the last four centuries (e.g., 1631, 1822, 1906 and 1944) impacted on
715 a number of municipalities, particularly during the sub-Plinian eruption of 1631. Heavy rain events
716 caused remobilization of the primary pyroclastic deposits, triggering multiple lahars during or
717 immediately after the eruption up to a few years (syn-eruptive lahars; Sulpizio et al., 2006); post-
718 eruptive lahars were triggered on the longer term.

719 On the other hand, the Pollena eruption had an even wider impact, both in terms of primary pyroclastic
720 deposition and secondary (lahar) impact. For this event, the historical sources are scarce to absent.
721 The analysis of – and realization of a database with – more than 500 stratigraphic sections were done,
722 which also includes the sedimentological features of the lahars deposits relative to the two sub-Plinian
723 Vesuvius eruption case-studies, Pollena and 1631. The detailed reconstruction and mapping of the
724 primary deposits allowed to update the area affected by pyroclasts dispersal, and it was found that
725 both eruptions had an impact larger than previously known. In particular, the stratigraphic and
726 sedimentological reconstruction of the deposits was done not only in the countryside but also close
727 to urban areas, and this is important in terms of local impact of the lahars in the environment.
728 Specifically, such impact investigation was done in urban areas including archaeological findings
729 (e.g., urban structures, walls, etc…).
730 These findings include not only new data from the Somma-Vesuvius plain, but also more distal data
731 from Lauro Valley and Avella-Baiano Valley (Apennines), which were subjected to heavy
732 remobilization of the primary deposits including the widely-dispersed fine ash deposits formed in the
733 late stage of the eruptions. Indeed, the accumulation areas that were reconstructed reveal an
734 enlargement and extra 47% (Pollena eruption) and 230% (1631 eruption) coverage that was not
735 previously known, and this should be considered in the hazard and impact evaluation in the
736 Campanian plain and on the nearby Apennine reliefs. The full database allows a more precise
737 reconstruction of the new isopachs, both for the Pollena and 1631 eruptions, which is possible given
738 the high number of data points in the study area.
739 With particular reference to the lahar deposits, the syn-eruptive ones occurred by relatively short-
740 term (during or immediately after the eruption) events, and were directly emplaced on the primary
741 pyroclastic deposits, both for the Pollena and 1631 eruptions. Also, there are not any significant
742 erosion surfaces nor humification traces in the sequences due to prolonged exposure of the primary
743 deposits, testifying that the secondary emplacement was quite immediate (max a few years; Sulpizio
744 et al., 2006) after or even during the eruption. The syn-eruptive features are also testified by the

745 absence of anthropogenic traces or humified surfaces at the base of or interbedded in the lahar
746 deposits, as further evidence of a very short-term time span between the eruptions and the lahar
747 events. Another interesting feature is the presence of multiple depositional flow units, as evidenced
748 by grain-size changes, some clast alignments and concave erosion surfaces in the lahar deposits. Such
749 depositional units were formed by en-masse emplacement (with reference to single flow pulse), while
750 the whole lahar deposits were formed by rapid progressive aggradation of the various flow units
751 (Vallance and Scott, 1997; Doronzo, 2012; Roche, 2012; Smith et al., 2018; Martí et al., 2019;
752 Guzman et al., 2020; see also Sulpizio et al., 2014, p. 56), which does not contradict the principle of
753 superposition. This can be argued by the generally massive facies of each flow unit in the deposits,
754 and by the presence of water escape structures that cross vertically the entire deposits sequences. The
755 latter evidence testifies a rapid water loss through vertical escaping "pipes" during or soon after the
756 aggradation of the sequences. In other words, the various flow units (layers) must decouple from the
757 transport system, and such decoupling occurs unit-by-unit and not particle-by-particle (Sulpizio et
758 al., 2006, 2014; Roche, 2012; Doronzo and Dellino, 2013; Breard and Lube, 2017; Smith et al., 2018),
759 through a massive accumulation rate (Duller et al., 2008; Doronzo et al., 2012; Martí et al., 2019).

760 The analysis of the Pollena lahar lithofacies allowed the identification of two main deposit categories.
761 The first one occurs on an area that extends for more than 10 km north of Mount Somma, and the
762 second one occurs on an area that extends west of the Apennines. For the latter, we can recognize two
763 significant sub-categories of deposits, corresponding to the main valleys in northwest-southeast
764 direction, Avella-Baiano Valley and Lauro Valley. The difference between the first and the second
765 deposit categories seems to reflect the type of primary deposits that were remobilized (fine ash vs.
766 ash and lapilli). In the area north of Mount Somma, which also comprises the municipalities of Acerra
767 and Afragola (about 12 km from Somma-Vesuvius), the primary lapilli fallout deposits are absent. In
768 this part of the plain, the thin layer of phreatomagmatic ash is widely present, while thick fine-grained
769 pyroclastic current deposits are present in the Mount Somma valleys that fed some of the lahars. In

770 Avella-Baiano Valley and Lauro Valley, which also comprise the municipalities around Nola at 10-
771 15 km from Apennine source valleys(Fig. 1 and Appendix C), the lahar deposits are generally coarser,
772 and consist of multiple depositional units with different lithofacies (Tab. 3). In this case, both grain-
773 size and componentry indicate that lahar deposits resulted from the remobilization of the fallout
774 deposits. Such considerations also derive from the full compilation of the geospatial database. A
775 volume estimation of the remobilized syn-eruptive deposits, based on a QGIS calculation, is of 7×10^7
776 m^3 for the northern Vesuvius area, and 4×10^7 m^3 for the Lauro Valley.

777 Referring to the 1631 eruption, previous maps have shown the distribution of the 1631 lahar deposits
778 toward east, basically following the distribution of the primary pyroclastic fall deposits (Sulpizio et
779 al., 2006), while in Figs. 10 and 11 we show a significantly larger distribution area particularly toward
780 the north (Somma-Vesuvius ramps and plain) and east (Apennines valleys), and less toward the
781 southeast. In particular, this distribution is well explained by the wide distribution of the ash fallout
782 deposit toward both north and northeast (Fig. 6), remobilized during the lahar generation both from
783 the Mount Somma and Apennine slopes. On the other hand, looking at the average deposit
784 thicknesses, they reach half a meter in the north and northeast, while reach a couple of meters in some
785 locations in the northeast (aligned with the dispersion axis of the primary fallout deposits and out of
786 the Apennine valleys).

787 The sedimentological analyses carried out on a number of samples from the different studied sectors
788 (Somma-Vesuvius, Lauro Valley, Avella-Baiano Valley) are useful for discriminating the various
789 factors that contributed to the initiation of the lahars and emplacement of their deposits. The samples
790 from Lauro Valley and Avella-Baiano Valley are coarser (but have a significant finer tail) than the
791 ones for Somma-Vesuvius, and this can depend on three factors: i) genetic types of the primary
792 pyroclastic deposits (fall vs. flow); ii) interaction between lahars and morphology (valley vs. plain);
793 iii) major remobilization in Lauro Valley and Avella-Baiano Valley of the distal phreatomagmatic
794 fine ash deposits formed in the late eruption stages. In other words, the primary grain sizes involved

795 in the remobilization (finer and higher-water retention for Somma-Vesuvius), as well as the general
796 topography (gentler but longer ramp for Somma-Vesuvius) likely acted as the main factors directly
797 impacting the distribution of the lahar deposits, and the decay of the flow velocities and dynamic
798 pressures in the area.

799 Interestingly, an emplacement temperature of ~120 °C of the lahar deposits was calculated for those
800 generated along the Somma-Vesuvius slopes, indicating a relatively hot provenance after
801 remobilization of the pyroclastic current deposits. Instead, the remobilization from the Apennines
802 sectors involved only cold fallout deposits. The companion paper of de'Michieli Vitturi et al. (this
803 issue) investigates also the nexus between water temperature, flow viscosity, and their consequential
804 impact on fluid dynamics. Specifically, when the dominance of frictional forces is attributable to the
805 yield slope term, the initial divergence between high- and low-temperature scenarios appears
806 negligible. However, discernible dissimilarity appears over time for the inundation area of the colder
807 flow case (i.e., 27 °C) with respect to the warmer counterpart (i.e., 100 °C), the latter case being close
808 to the 120 °C one reported from paleomagnetism. Remarkably, the temperature-induced variations
809 assume a pivotal role in shaping the dynamic characteristics of the hotter flow. The diminished
810 viscosity associated with elevated temperatures not only amplifies fluid mobility but also prompts a
811 notable acceleration in sediment settling velocity. This, in turn, initiates a debulking mechanism,
812 thereby intensifying overall flow mobility. Consequently, this intricate interplay contributes to a
813 reduced footprint of deposited material from the flow, altering the spatial distribution of sediments.
814 However, the overall impact on the inundation area is typically quite reduced, being typically less
815 than 10-20% even considering a thickness threshold of 1 mm (see de'Michieli Vitturi et al., this issue).
816 The sampled clasts might have been incorporated multiple times by the flows, and the heating/cooling
817 processes that we interpret as indicating T_{dep} in the diagrams are the last to have occurred and affected
818 the samples. Besides, a third heating component is clearly observed for some of them. The
819 paleomagnetic directions are statistically distinguishable, supporting that the lahar emplacement at

820 Nola (10-15 km from Apennine source valleys) and Acerra (12 km from Somma-Vesuvius) was not
821 synchronous, as further evidence of the different timing hence likely different detachment areas
822 involved during the pyroclasts remobilization. However, the comparison with the paleosecular
823 variation curves of the Earth's magnetic field does not allow to better constrain the entity of the time
824 span between the two lahar events. The parental lahars acted as mass flows capable of entraining
825 outsized clasts (where available) from substrate under the action of shallow-layer flow velocity and
826 dynamic pressure (de'Michieli Vitturi et al., this issue), then emplaced massive flow units with
827 uplifted external clasts set into the much finer matrix (see Roche, 2015). In some lahar units, various
828 clasts have been found, showing some alignment that depends on the mechanisms of entrainment and
829 uplift (with respect to substrate) within the flow.

830 In terms of local impact in the Pollena case study (the largest one), while most of the calculated points
831 (44) fall in the range of lahar velocity of 2-4 m/s and dynamic pressure of 4-8 kPa, a few peak values
832 of velocity of 13-15 m/s and dynamic pressure of 90-115 kPa are also calculated, which are directly
833 related to meter-sized clasts entrained into the lahars on the steep slopes, then deposited downstream
834 of alluvial fans. Such values of the velocity and dynamic pressure are well comparable with those
835 calculated for lahars that occurred recently at Ruapehu in 2007 (Lube et al., 2012) and Merapi in 2011
836 (Jenkins et al., 2015), and in historical times at El Misti (Thouret et al., 2022). In particular, the
837 estimated velocities and pressure agree with those of Lube et al. (2012) and Jenkins et al. (2015).
838 Moreover, multiplying velocity and density gives a power per unit surface, so those most
839 representative values correspond to a flow power per unit surface of $8 \cdot 10^3$ - $3.2 \cdot 10^4$ W/m^2, with peak
840 values of $1.17 \cdot 10^6$ - $1.72 \cdot 10^6$ W/m^2, in agreement with typical values reported for floods and
841 megafloods (Russell and Knudsen, 1999; Whipple et al., 2000; Carling, 2013).
842

843 **6. Conclusions**

844 The integration of the historical, stratigraphic, sedimentological, laboratory, and impact parameter
845 analyses carried out in the Vesuvius area allow us updating on the lahar invasion related to the Pollena
846 and 1631 eruptions. In general, the physical characteristics of the analyzed deposits indicate that syn-
847 eruptive lahars are related to the rapid remobilization of large volumes of pyroclastic material, which
848 is mainly fine-grained and almost exclusively derived from the accumulation of products related to a
849 single eruption. The analysis also shows that tardive (post-eruptive) mass flows are common, and
850 involve multiple and variably altered deposits, and that their energy and frequency are progressively
851 lower over time, after the last eruption has occurred. In particular, a higher impact both from primary
852 and secondary phenomena is something that should be accounted in the Vesuvius area and that:

853 i) The new isopach maps of the Pollena and 1631 eruptions allow us to infer a larger impact
854 than previously known for these two sub-Plinian events of the Vesuvius. Thus, it is worth
855 reconsidering the territorial impact that sub-Plinian eruptions can have in the Vesuvius
856 (but not only) area. In particular, the ash deposits can have a high impact in relation to
857 their high density and low permeability.
858 ii) The primary impact from fallout and pyroclastic current processes in the Vesuvius area
859 was - and may be in the future – followed by the secondary impact from lahars generated
860 during or immediately after the eruption events. Both impacts can have a wide distribution,
861 because they are directly controlled by the primary deposits distributions, both around
862 Somma-Vesuvius and in the Apennines valleys.
863 iii) The runouts of such lahars were significant both for the Pollena and 1631 eruptions, by
864 reaching distances of 10 to 15 km from the sources, and their deposits geometry is tabular-
865 like with average thicknesses of 0.5 to 1 m.
866 iv) The paleotemperature data highlight a relatively hot dynamics (~120 °C) for those lahar
867 flow pulses that traveled down the Somma-Vesuvius slopes because of pyroclastic current

deposit remobilization. This did not occur from the Apennines sectors, where pyroclastic currents did not get to, and only cold fallout deposits were remobilized.

v) A reverse engineering approach allowed to calculate the local lahar velocities (2-4 m/s, with peaks of 13-15 m/s), dynamic pressures (4-8 kPa, with peaks of 90-115 kPa), and solid volumetric concentration (~30%, implying a 1:3 ratio between deposit and flow thickness), on the basis of the external clast properties entrained into the flows then emplaced into the ash matrix, and on the presence of the lahar deposits in proximity of obstacles and archaeological findings.

As a general conclusion, we have demonstrated that the areal impact of both primary deposits and lahars, in case of sub-Plinian events at Somma-Vesuvius, involves a territory wider than previously known and for several years, with possible decreasing damages over time.

Appendix A. Calculation of lahar velocities and dynamic pressures

A theoretical scheme is presented to quantify local velocities and dynamic pressures of the lahars, by inverting the field features at selected locations. The final goal is to map the values of velocity and dynamic pressure to assessing the hazard from lahars in the study area. Flow dynamic pressure, P_{dyn}, results from a combination of flow density, ρ_f, and flow velocity, v, and is defined as follows

$$P_{dyn} = 0.5\rho_f v^2 \quad \text{(A1)}$$

In the study area, the original flow was a multiphase flow of water + pyroclastic sediment, which during remobilization evolved into a flow of water + pyroclastic sediment + external clasts. Generically, flow density results from a combination of particle density, ρ_p, and water density, ρ_w, through particle volume concentration, C, and is defined as follows

$$\rho_f = \rho_p C + \rho_w (1 - C) \quad \text{(A2)}$$

In order to define flow velocity, we take into account stratigraphic and sedimentological

892 characteristics of the lahar flow units: i) they are ubiquitously massive, and result from remobilization
893 of the primary pyroclastic deposits then emplacement from mass flows; ii) they contain big external
894 clasts entrained (by dynamic pressure) and uplifted (also by pore pressure) from substrate into the
895 flows. With these field characteristics, flow velocity can be expressed as a combination of entrained
896 clast properties and flow density, and is defined as follows (modified after Roche, 2015)

$$v = \sqrt{\frac{X\psi(\rho_c - \rho_w)g}{\gamma\rho_f}} \quad \text{(A3)}$$

897

898 where X is clast small axis, Ψ is clast shape factor, ρ_c is clast density, g is gravity acceleration and γ
899 is an empirical constant. Eq. 3 allows quantifying the incipient motion of the big clasts, and gives
900 minimum values of flow velocity required to entrain and uplift the clasts from substrate, probably
901 more than once, before being emplaced into the lahar deposits by flow velocity drop. Such equation
902 has been originally derived in laboratory experiments for a multiphase flow of air + sediment, and is
903 highly performing at $\rho_f \sim 1000$ kg/m^3 (hindered settling) for dense pyroclastic currents controlled by
904 topography then opened to alluvial plain (Martí et al., 2019), which is a case similar to the lahars in
905 the study area. Substituting Eq. 3 into Eq. 1 and simplifying gives

$$P_{dyn} = 0.5\frac{X\psi(\rho_c - \rho_w)g}{\gamma} \quad \text{(A4)}$$

906

907 For given clast properties, flow dynamic pressure has a unique value, while flow velocity is a function
908 of flow density. Indeed, the present scheme is a spot model that basically depends on, and is limited
909 to, the finding of big clasts and boulders within the lahar deposits. An approximation is that velocity
910 and dynamic pressure are calculated for the locations where the clasts are found in the deposits,
911 meaning that the calculated values are overestimated for those exact locations, while they are more
912 properly referred to the immediate surroundings upstream.
913 At the selected locations in the study area, we collected the dimensions of the biggest clasts found in
914 the lahar deposits, and we characterized lithologically the clasts in the field, to calculate flow dynamic
915 pressures using Eq. 4. We used the following values for the various parameters in the calculations: Ψ

916 (ellipsoid) = 0.66; ρ_c (limestone) = 2500 kg/m^3; ρ_c (ceramic) = 2000 kg/m^3; ρ_c (brick) = 2000 kg/m^3;
917 ρ_c (tephra) = 1500 kg/m^3; ρ_c (lava) = 2500 kg/m^3; ρ_c (iron) = 8000 kg/m^3; ρ_w = 1000 kg/m^3; g = 9.81
918 m/s^2; γ = 0.031 – 0.071. Also, we calculated flow velocities using Eq. 3, in the following range of
919 flow density: $\rho_w \leq \rho_f \leq \rho_p$, where ρ_w = 1000 kg/m^3 and ρ_p = 2000 kg/m^3. In this way, flow density
920 spans from two extreme cases: i) $\rho_f = \rho_w$, negligible pyroclastic sediment and external clasts, so water
921 flow only; ii) $\rho_f = \rho_p$, negligible water and dominant pyroclastic sediment, so ash flow only. For the
922 empirical constant in Eq. 3, we used three different values to test the sensitivity with respect to
923 different physical states of the multiphase flow: γ (non-fluidized) = 0.031; γ (initially fluidized and
924 slightly expanded) = 0.057; γ (initially fluidized and non-expanded) = 0.071 (see Roche et al., 2013;
925 Fig. A1).
926 Regarding flow velocity, after calculation we can rewrite Eq. 3 in a simpler form (to more directly
927 relate velocity to density) as follows

928 $$v = \frac{a}{\sqrt{\rho_f}} \qquad \text{(A5)}$$

929 where $a > 0$ depends on clast properties, and its square has dimension of pressure. On the other hand,
930 it is not straightforward to constrain local flow velocities with unique values of flow densities, mostly
931 because small variations of velocity correspond to large variations of density, and this is particularly
932 valid for volcaniclastic mass flows (Carling, 2013; Jenkins et al., 2015; Roche, 2015; Martí et al.,
933 2019; Guzman et al., 2020; Thouret et al., 2022).

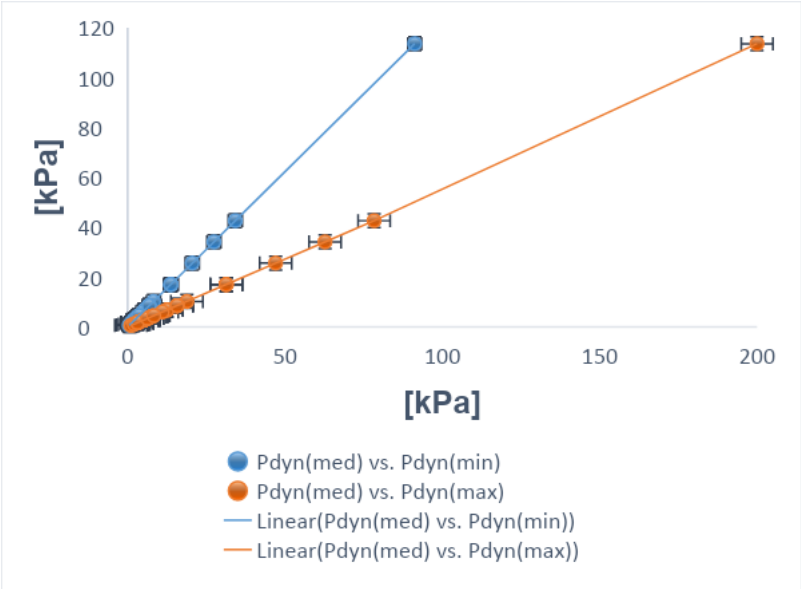

934 **A**

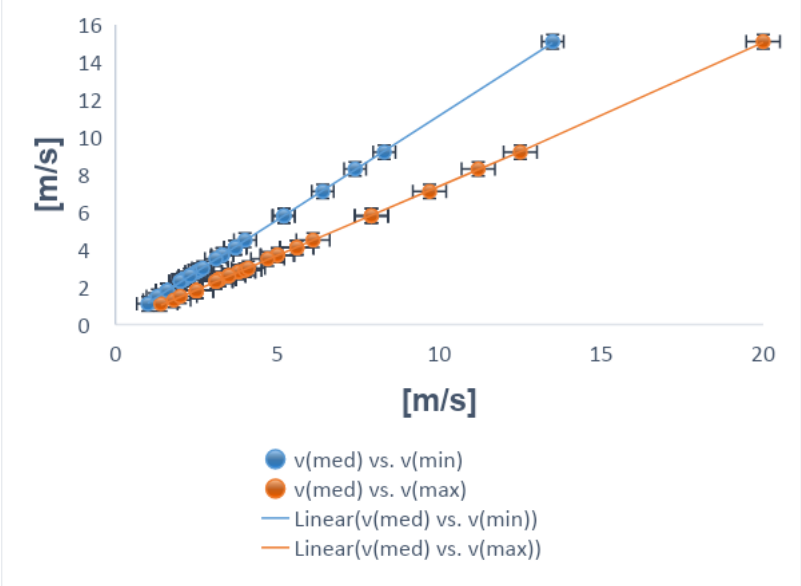

935 **B**

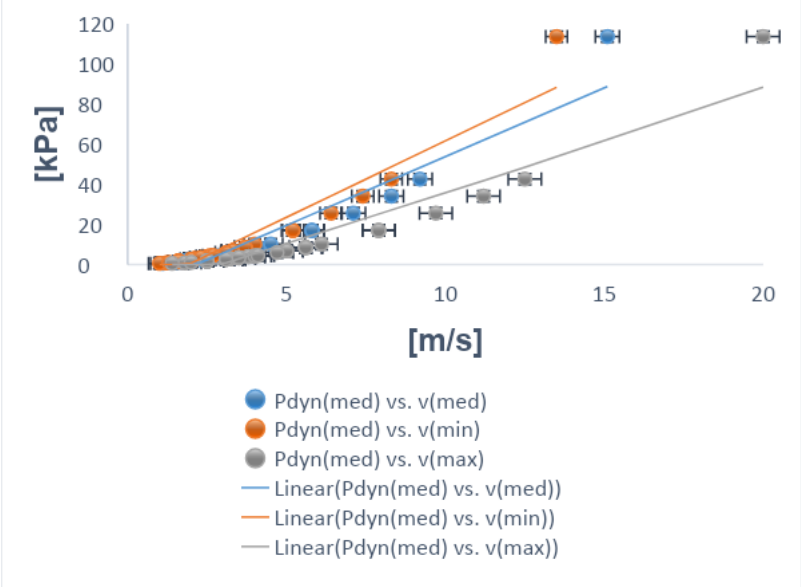

936 **C**

Fig. A1. Local dynamic pressures and velocities for the syn- and post-eruptive Pollena lahars calculated with the reverse engineering approach. **A**, dynamic pressure for the initially-fluidized and slightly expanded case vs. dynamic pressure for the initially-fluidized and non-expanded (blue) and non-fluidized (orange) cases; **B**, velocity for the initially-fluidized and slightly expanded case vs. velocity for the initially-fluidized and non-expanded (blue) and non-fluidized (orange) cases; **C**, dynamic pressure for the initially-fluidized and slightly expanded case vs. velocity for the initially-fluidized and slightly expanded (blue), vs. velocity for the initially-fluidized and non-expanded (orange), vs. velocity for the non-fluidized (grey) cases.

At some locations in the study area, we found lahar deposits against meter-scale manufacturing obstacles (Di Vito et al., 2009). The peculiarity is that the deposits in proximity of the obstacles are thicker than the correlated ones in the free field, but never reach the top of the obstacles themselves. This means that the lahars were not much expanded, so unable to overcome the obstacles as stratified flows would have done (cf. Spence et al., 2004; Gurioli et al., 2005; Doronzo, 2013; Breard et al., 2015). With this field evidence, we can assume that local flow height, H, was similar to deposit thickness against the obstacle, h_o, as follows

$$H \approx h_o \tag{A6}$$

In order to estimate flow density using Eq. 2, we focus on particle volumetric concentration. For well-sorted deposits, such concentration can be defined with an average value over flow height as follows (modified after Doronzo and Dellino, 2013; see also Eq. 30 in de' Michieli Vitturi et al., this issue)

$$C = \frac{h_f}{H} \tag{A7}$$

where h_f is deposit thickness in the free field. Substituting Eq. 6 into Eq. 7 gives

$$C \approx \frac{h_f}{h_o} \tag{A8}$$

In particular, h_f refers to those lahar deposits relatively close to the obstacles, but which were not affected by them during emplacement, i.e. close but not so much. We assessed that correlation taking

into account the stratigraphic and sedimentological characteristics of the lahar deposits, and the fact that Eq. 7 performs better with layers emplaced after remobilization of primary pyroclastic fallout or dominantly ash flow deposits.

Lastly, we macroscopically assessed erosion in the field, by characterizing the unconformities present both on the primary pyroclastic and lahar deposits. In particular, the syn-eruptive lahar deposits consist of more than one flow unit, so it is important to understand how the different flow pulses interacted with each other during emplacement. The main unconformities that are found in the field are referred to the partial absence of a flow unit, and the loss of lateral continuity despite some flat geometry of the deposits. On the other hand, at some locations we were not able to assess if erosion occurred or not due to multiple open issues: i) possible absence of the primary pyroclastic deposits; ii) possible exclusive presence of the post-eruptive lahar deposits; iii) impossibility to get to some outcropping deposit base and possible unconformities.

Appendix B. Paleo-temperature and paleo-direction determinations

The magnetic fabric of a deposit was investigated by measurements of the magnetic susceptibility and its anisotropy (AMS). AMS was measured with a Kappabridge KLY-3 (AGICO), and data were elaborated by the software Anisoft5 (AGICO). AMS depends on the type, concentration, and distribution of all the minerals within the specimen. It is geometrically described by a triaxial ellipsoid, whose axes coincide with the maximum (k_1), intermediate (k_2) and minimum (k_3) susceptibility directions. The magnetic fabric of a specimen is then described by the direction of the k_1 axis, the magnetic lineation (L) and that of the k_3 axis, which is parallel to the pole of the magnetic foliation plane (F). Besides, the modulus of the susceptibility axes provides some magnetic parameters useful to express the intensity of the anisotropy (P_j) and the oblate/prolate fabric occurrence (T) (Jelinek, 1981). Generally, sedimentary vs. pyroclastic deposits fabric, here considered as the proxy of the lahar fabric, is oblate with a horizontal to gently imbricated (less than

986 20°) magnetic foliation. The magnetic lineation is normally clustered along the foliation plunge. In
987 this case, both the F imbrication and the L direction can provide the local flow direction. Other times,
988 L is orthogonal to the F plunge or F is statistically horizontal, and it is not possible to infer the flow
989 direction.
990 For T_{dep} estimation, pottery sherds were subjected to progressive thermal demagnetization (PTD),
991 with heating steps of 40 °C, up to the Curie Temperature (T_C), using the Schonstedt furnace and the
992 spinner magnetometer JR6 (AGICO). The rationale of the method has been described in detail in
993 several papers (McClelland and Druitt, 1989; Bardot, 2000, Porreca, 2007; Paterson et al., 2010; Lesti
994 et al., 2011), many of them dedicated to PDCs of the Vesuvius area (Cioni et al., 2004; Di Vito et al.,
995 2009; Giordano et al., 2018; Zanella et al., 2007; 2018; 2015). Typically, measurements are made on
996 accidental lava lithics that were entrained during pyroclastic or lahar flows. In this case, we had the
997 opportunity to estimate the T_{dep} by measuring ancient pottery artifacts. Briefly, pottery is
998 characterized by a thermal remanent magnetization (TRM) acquired during its manufacture and its
999 subsequent history of daily use. Whenever it is heated, part of its TRM, the one associated with
1000 blocking temperatures (T_b) below the heating one (T_h), is overwritten. Without alteration phenomena,
1001 the heating/cooling is a reversible process, except for the magnetic directions. The original TRM
1002 shows a random paleomagnetic direction, due to the transport during emplacement. Subsequent
1003 TRMs show directions parallel to the Earth's magnetic field during their cooling. This is clearly
1004 illustrated in the Zijderveld diagrams. The composition of the different magnetization components
1005 reveals thermal intervals characteristic of the heating history of the potsherd. Of course, this
1006 explanation is simplified, but the method is well-established and has been shown to work well with
1007 heated artifacts, such in the case of tiles and pottery embedded in the PDC deposits at Pompeii
1008 (Gurioli et al., 2005; Zanella et al.,2007), Afragola (Di Vito et al., 2009) and Santorini (Tema et al.,
1009 2015). In case of lahar, we expect low T_{dep} or cold deposits. This can be a major concern because of
1010 the difficulties to distinguish between the TRM secondary components, and the chemical (CRM) and
1011 viscous (VRM) remanent magnetization. The CRM may develop due to mineralogical changes during

1012 reheating (McClelland, 1996). Instead, VRM is typical of ferromagnetic grains with low T_b and often
1013 occurs in most rocks. Following Bardot and McClelland (2000) relationship for time intervals in the
1014 10^2–10^6 year range, T_b=75+15 log (acquisition time in years), and using the Pollena eruption date
1015 (472 CE), e obtain a lower limit of the T_b around 123 °C. This means that this temperature helps us
1016 in discriminating between "hot" (T_b > 120 °C) or "cold" lahar (Tb < 120 °C).
1017 Finally, routine magnetic measurements on the lahar matrix were done on the lahar matrix to
1018 determine the Characteristic Remanent Magnetization (ChRM) by Thermal and Alternating Field
1019 demagnetizations. The direction of the Earth's Magnetic Field during the Pollena eruption is well-
1020 known (Zanella et al., 2008). If the sampled lahars were emplaced shortly after the eruption, both the
1021 secondary TRMs and the matrix of the lahars should show a remanent magnetization direction similar
1022 to the Pollena ones. ChRMs can also test if the two lahars (Acerra at 12 km from Somma-Vesuvius,
1023 and Nola at 10-15 km from Apennine source valleys) are coeval.
1024

1025 **Appendix C. Description of the studied areas**

1026 *Area 1 – Nola*

1027 In the area surrounding Nola (10-15 km from Apennine source valleys), it is possible to recognize
1028 the complete fallout sequence of the Pollena eruption (a in Fig. C1 and C2), which usually covers
1029 ploughed soils (p in Fig C1) and late Roman archaeological remains. The sequence is composed of
1030 an alternation of coarse pumice and thin ash fallout layers. Its top is always made of a fine ash bed
1031 related to the phreatomagmatic phase of the eruption (b in Fig. C1 and C2), with a thickness ranging
1032 from 1 to 14 cm due to erosion. They are almost always overlain by lahar deposits composed of
1033 several flow units (c in Fig. C1 and C2) with a large thickness variability due to channeling and
1034 presence of barriers and buildings. They sometimes include blocks, tiles, and other archaeological
1035 remains.

In Fig. C1, above the primary deposit, there is an example of a well-exposed sequence composed of at least five units (c in Fig. C1). The first one is a massive and matrix-supported deposit composed of fine and not vesiculated ash (lithofacies Gms), with fragments of greenish to blackish scoriae and minor fragments of pumices, lavas and limestones. The fragments are cm-sized and are both angular and rounded. The second flow unit is similar to the one below, but is darker and contains less coarse fragments. Its matrix is composed of an alternation of fine to medium ash layers. It follows a plane-parallel sequence of well-sorted fine sand and silt layers characterized by the lithofacies fM. A massive deposit follows upward, it is progressively humified and contains abundant reworked and rounded pumice clasts from the Avellino eruption. The top humified surface is almost always eroded by anthropogenic activity and is generally ploughed (p1 in Fig. C2). It is overlain by the primary deposits of the 1631 eruption (d in Fig. C2). It is few cm thick and is composed of a basal layer of dark coarse ash (small pumice fragments), overlain by a massive ash bed, containing abundant accretionary lapilli. The following deposit thickens in the ploughing furrows and depressions, and is composed of massive fine-ash beds, vesiculated and cohesive, and is interpreted as a lahar deposit (lithofacies mM) (e in Fig. C2). This deposit (e in Fig. C3) overlies the foundations of Palazzo Orsini (blocks in Fig. C3), now seat of the Court of Nola and built in the second half of the XV century (Fig. C3). The top is always eroded by the modern anthropogenic activity, and locally by deposits of recent eruptions of Vesuvius (e.g., 1822, 1906).

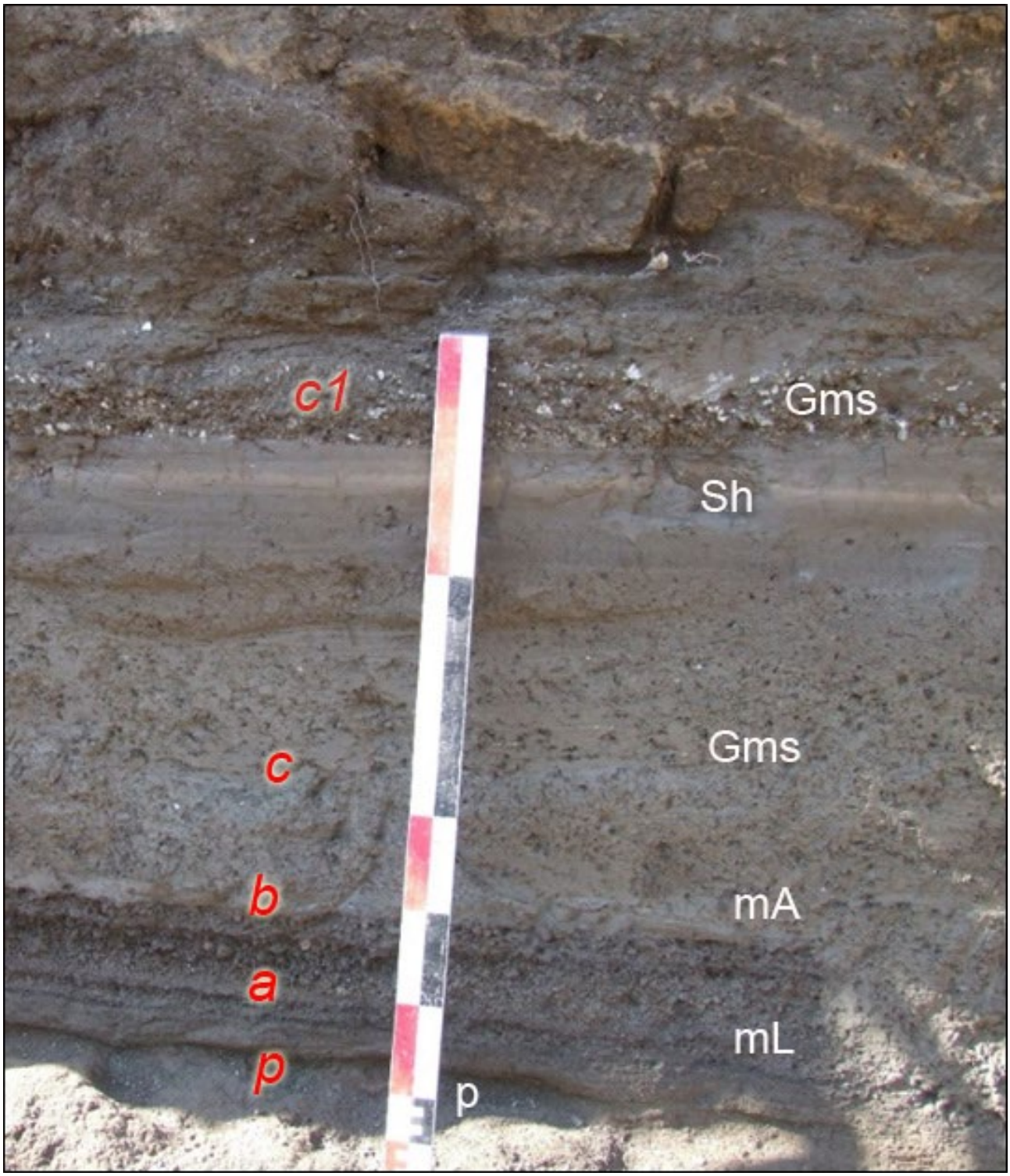

Fig. C1. Nola (10-15 km from Apennine source valleys), Pollena fallout deposits overlain by at least five lahar units. In particular: p = paleosol; a = alternation of coarse and fine fallout sequence of the Pollena eruption; b = final ash fallout of the eruption; c = sequence of syn-eruptive lahars; c1 = post-eruptive lahar containing white pumice fragments of the Pomici di Avellino eruption. For the description of lithofacies see Tab. 2.

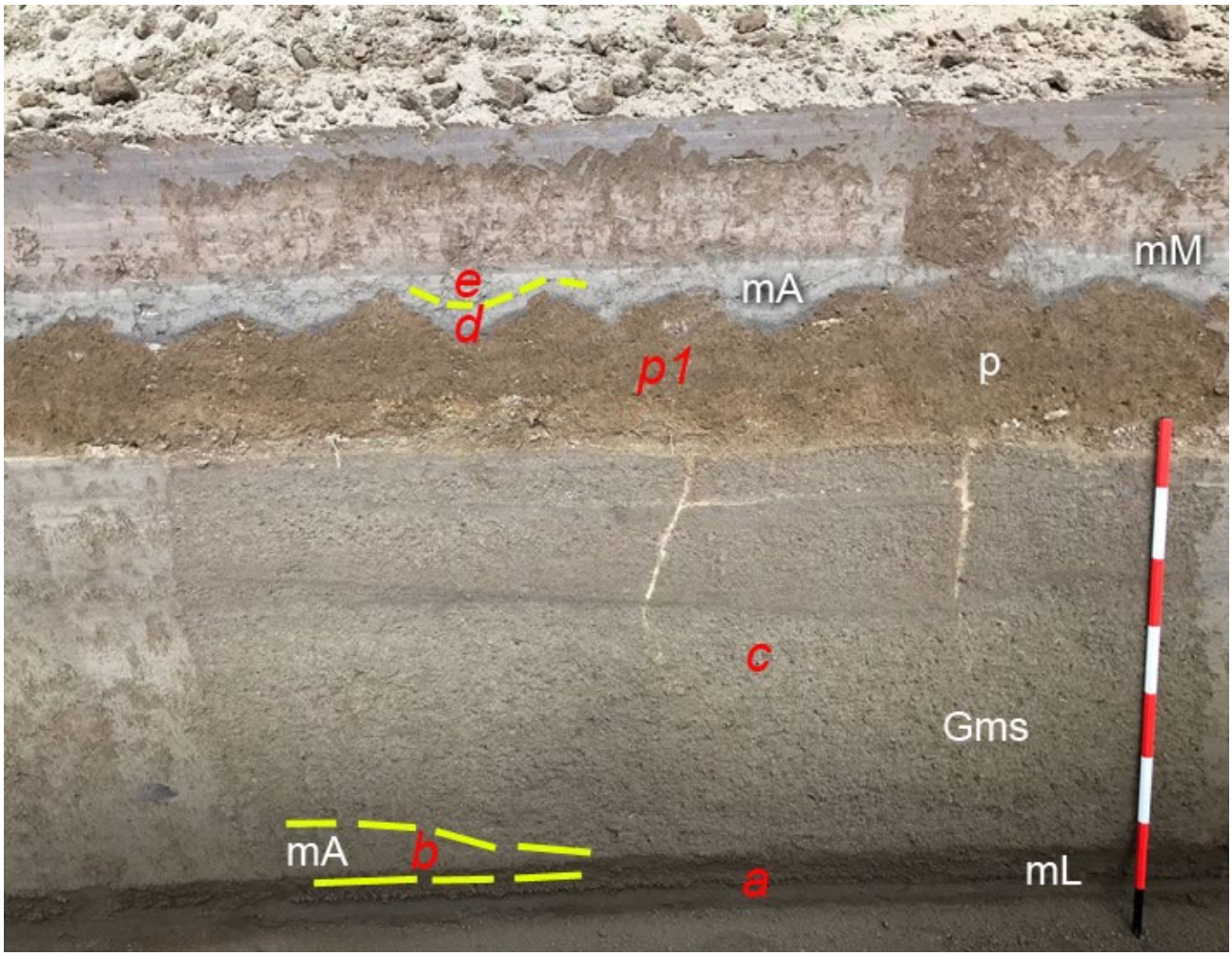

Fig. C2. Nola, Pollena lahar deposits overlain by a cultivated paleosol, and by the 1631 ash fallout and lahars. In particular: a = alternation of coarse and fine fallout sequence of the Pollena eruption; b = final ash fallout of the eruption, partially eroded; c = sequence of three lahar units; p1 = ploughed paleosol; d = 1631 ash fallout deposit mantling the undulated paleosol; e = lahar deposit composed of a massive ash layer. For the description of lithofacies see Tab. 2.

Fig. C3. Palazzo Orsini, Nola (1631 fallout and lahars). In particular: d = 1631 ash fallout deposit overlying the foundations of the building (in the inset); e = syn-eruptive lahar deposit. For the description of lithofacies see Tab. 2.

In Nola and in the nearby Cimitile (about 10-15 km from Apennine source valleys), the effects on the territory of the lahar emplacement related to the Pollena eruption are testified by numerous archaeological remains. The Nola and Cimitile areas are covered by thick sequences of fallout and lahar deposits. In fact, the previous ground level was at least 2-3 m below the present one. This effect is well visible in the Amphitheater Laterizio, which was completely filled by the primary and

1078 secondary deposits, and the same in Cimitile, where in the archaeological site of the Early Christian
1079 basilicas the present ground level is about two meters higher than the one before the eruption. It is
1080 worth noting that in Cimitile the flows were able to carry limestone blocks of 50 cm in diameter,
1081 likely along the main flow direction of the lahars (Fig. C4).
1082

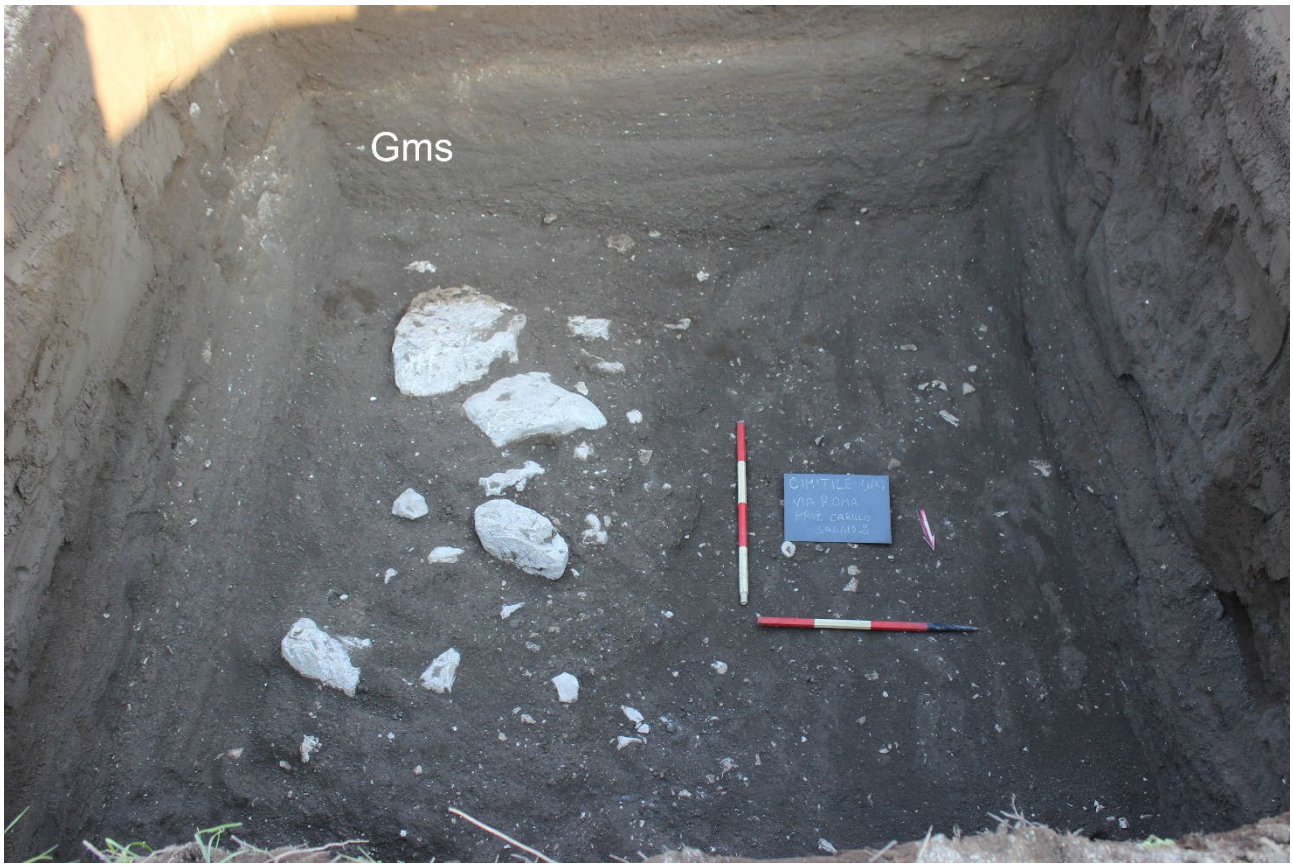

1083
1084 Fig. C4. Cimitile, sequence of three m-thick syn-eruptive lahar units with the evidence of transport of calcareous block
1085 (up to 50 cm). The largest are in the lower unit. The base of the lahar sequence and the underlying fallout deposit of the
1086 Pollena eruption are not visible in the photo. For the description of lithofacies see Tab. 2.
1087
1088 *Area 2 – Acerra-Afragola*
1089 The Acerra and Afragola territories (about 12 km from Somma-Vesuvius) are located north and north-
1090 west of Vesuvius, and are almost flat areas crossed by the Clanis river. Both the coarse fallout deposits
1091 of the Pollena and 1631 eruptions are absent in this area. Here, only a thin, centimetric ash bed
1092 overlies the Late Roman paleosol. This fine ash bed, which we correlate with the final

phreatomagmatic phases of the Pollena eruption, is homogeneous, cohesive and mantles the ground without any significant lateral variation. The overlying deposit is characterized by high thickness variations, it is generally massive and contains vesicles from circular to flattened and coated by fine ash. It has a matrix-supported texture and is composed of fine to very fine, very cohesive ash, and contains scattered and more or less abundant pumice and lithic fragments (lithofacies mM) and remains of vegetation (Barone et al., 2023). From one to three depositional units have been recognized, marked by unconformities, and differences in grain-size or color. The uppermost unit always contains white pumice fragments of the Avellino eruption. Very common are drying out structures and water escape structures, which are vertical structures (Fig. C5) looking like fractures a few cm large, filled by finer material transported by the escaping water, formed soon after the emplacement of the sequence of the syn-eruptive lahars (Fig. C5). The maximum thickness recorded in this area is about 90 cm.

Fig. C5. Acerra (12 km from Somma-Vesuvius), lahar deposit (unit 2) overlaying a cultivated paleosol (unit 3). The index finger indicates a water escape structure crossing the sequence of lahars. For the description of lithofacies see Tab. 2.

The top is almost always horizontal due to the erosion related to the modern anthropogenic activity, and only in a few exposures it is capped by a paleosol, with traces of human presence of the Medieval times and of the deposits of the 1631 eruption as well. The base of this latter deposit is a cm-thick fine-ash bed with an internal plane-parallel layering emplaced by fallout. It underlies a massive deposit with high thickness variations (max 20 cm) at the outcrop scale. It is composed of fine ash, cohesive and vesiculated and contains scattered small pumice fragments (lithofacies mM). The pumice fragments are vesicular, dark gray to blackish, highly porphyritic with leucite, pyroxene and feldspar crystals. The stratigraphic position and lithology confirm their attribution to the 1631 primary and secondary (lahars) deposits.

Area 3 – Pomigliano-Marigliano

This area is located along the northern outer part of the Vesuvius apron (Santacroce et al., 2003). The studied sequences start from the paleosol developed on top of the ash deposits of the AD 79 eruption. The paleosol is mature and contains pottery fragments till the II century AD. Its top is undulated with traces of ploughing spaced about 50 cm (a in Fig. C6). Representative sequences of the area include a basal ash layer with a thickness ranging from 1 to 4 cm (b in Fig. C7), thickening in the depressions, cohesive and locally vesiculated. It is here interpreted as co-ignimbritic ash emplaced by fallout during the phreatomagmatic final phases of the Pollena eruption. Upwardly, the sequence includes several lahar units from massive to slightly stratified, composed of fine and very cohesive ash, and containing scattered greenish pumice fragments (lithofacies mM) (b1 in Fig. C7). Locally this deposit, also in the case of multiple units, is cut by vertical drying cracks. The sequence is overlain by a 25-30 cm thick mature paleosol, containing cultivation traces and majolica fragments (c in Figs. C6 and C7).

The top of this paleosol is undulated and covered by the primary deposit of the 1631 eruption (d in Fig. C7). This latter is represented by a discontinuous medium-to-fine ash layer, slightly laminated for contrasting grain-size, up to 5 cm thick, with a gray to violet color, and containing dark pumice fragments and loose crystals of leucite, pyroxene and biotite (Fig. C7). Its thickness variation is due both to slight internal variations (thickening in correspondence of depressions) and erosion by the following lahars. These latter are composed of one to three flow units (d1 in Fig. C7), with a cumulative total thickness varying from 10 to 45 cm. They are composed of massive fine and very cohesive ash, and contain rare scattered dark pumice fragments similar to those of the 1631 eruption (lithofacies mM). These sequences are overlain by recent, cultivated soil. Locally, thin ash beds of the recent Vesuvius activity (like 1822, 1906) overlie the 1631 deposits.

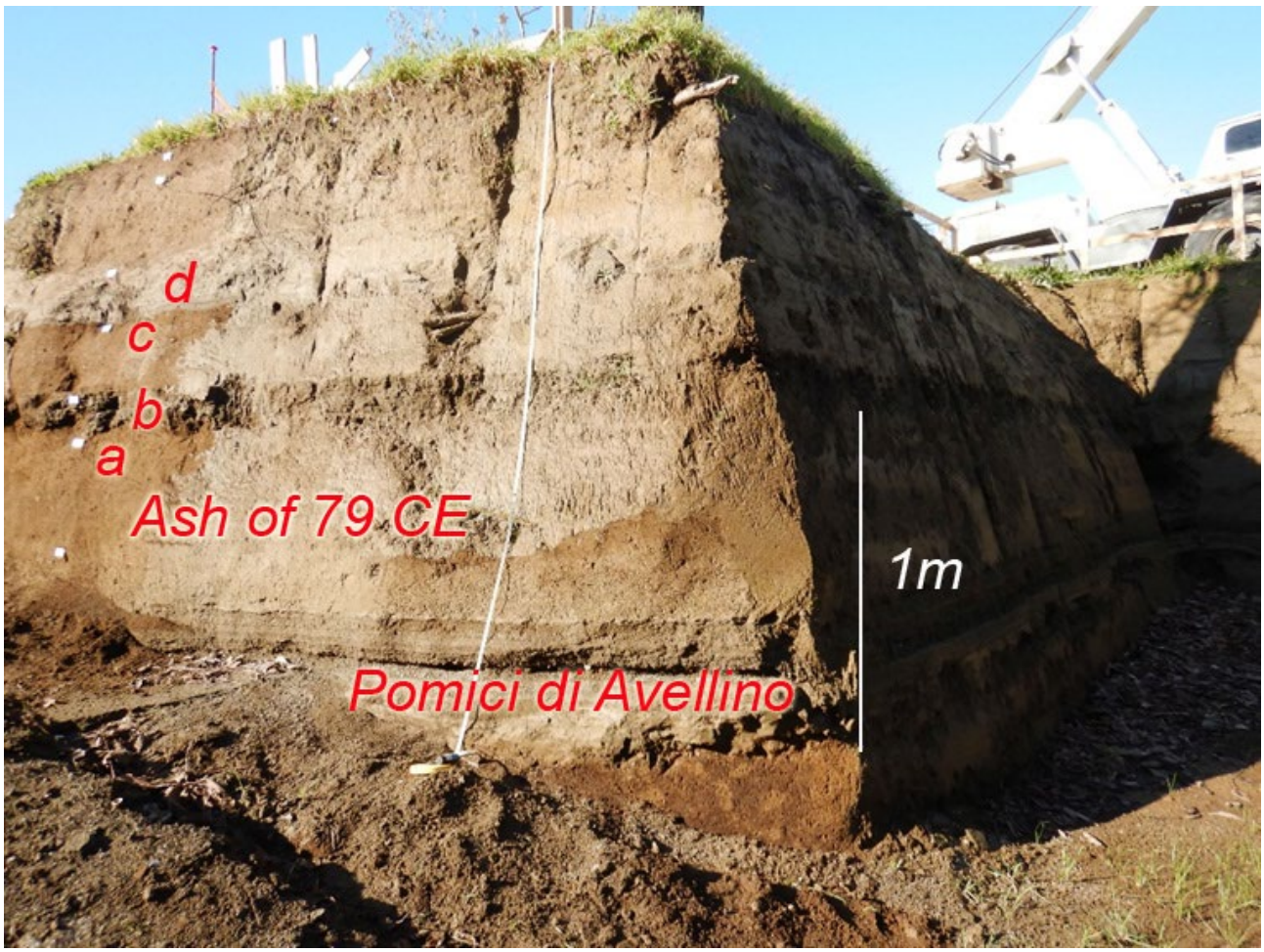

Fig. C6. Pomigliano, sequence of deposits including bottom to top: Bronze Age paleosol, Pomici di Avellino (unit EU 5 of Di Vito et al., 2009), paleosol developed on top of Pomici di Avellino and buried by the Pollena eruption deposits. In the central part, fine ash deposits of the 79 CE eruption are visible. The top of the paleosol is undulated and ploughed. In particular: a = paleosol of Roman Age; b = primary and secondary deposits of the Pollena eruption; c = paleosol between Pollena and 1631 deposits; d = 1631 primary and secondary deposits. Further details in Fig. C7.

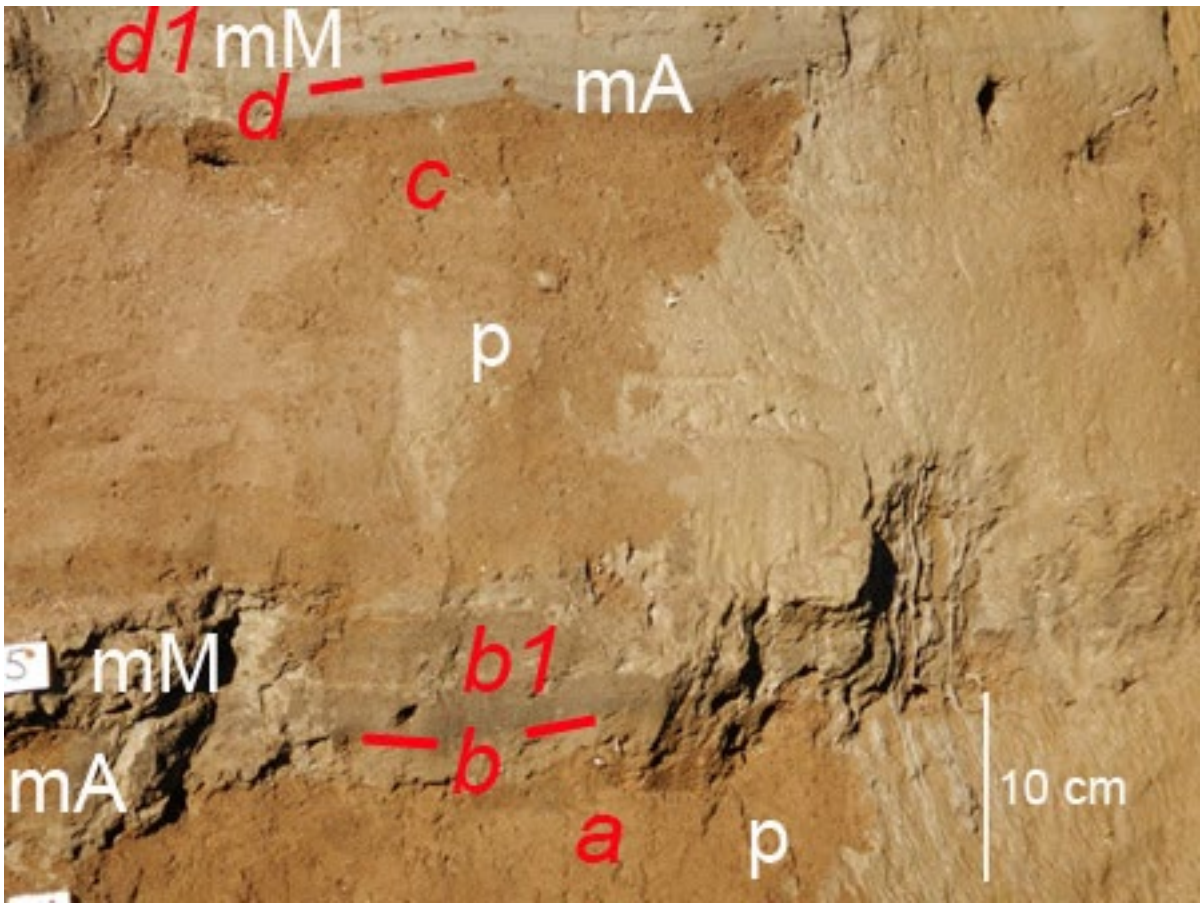

Fig. C7. Pomigliano, particular of Fig. C6: a = paleosol containing potteries of the II Cent. AD; b = ash deposit of the Pollena eruption; b1 = syn-eruptive lahars of the Pollena eruption; c = paleosol between Pollena and 1631; d = primary deposits of the 1631 eruption overlain by syn-eruptive lahars (d1). For the description of lithofacies see Tab. 2.

Area 4 – Avella-Baiano Valley

We have analyzed several sequences along the *Avella-Baiano* Valley, both exposed and excavated for the present work. Here the sequences of primary deposits are often affected by deep erosion, in

fact, in some places the Pollena primary deposits are completely lacking and only the syn-eruptive lahar deposits are present on top of the late Roman paleosol. Where preserved, the paleosol has often an undulated surface due to cultivation (ploughing and hoeing). The Pollena eruption sequence consists of an alternation of coarse pumice and fine ash layers emplaced by fallout (a in Fig. C8). It is up to 50 cm thick and ends with a cohesive yellowish ash layer (b in Fig. C8), overlain by the lahar deposits, generally composed of 2-3 flow units (c in Fig. C8). The total thickness of the lahars is largely variable with maxima at the base of the slopes where it can reach 2-3 m. In some excavations we did not reach the base of the deposit, deeper than 3.5 m. In Fig. C8, it is possible to observe a complete sequence of the Pollena deposits overlying a late Roman paleosol. The sequence includes the fallout layers and thick lahar deposits. These latter are always massive, matrix-supported, and contain abundant scattered pumice and lithic fragments (lithofacies Gms). In some cases, the lower part contains several limestone fragments up to 10 cm in diameter. The described deposit has been also found in the Roman Amphitheatre of Avella, where it has a variable thickness (order of decimetric). Here, it has been almost all excavated and only remnants are presently exposed.

Generally, the upper part of the sequences is composed of an alternation of plane-parallel to cross-layered sands and gravels, with abundant rounded limestone fragments, emplaced by several alluvial episodes (post-eruptive) (lithofacies Sh-Ss). In these post-eruptive deposits, it is not uncommon to find terracotta fragments from the Imperial Roman age.

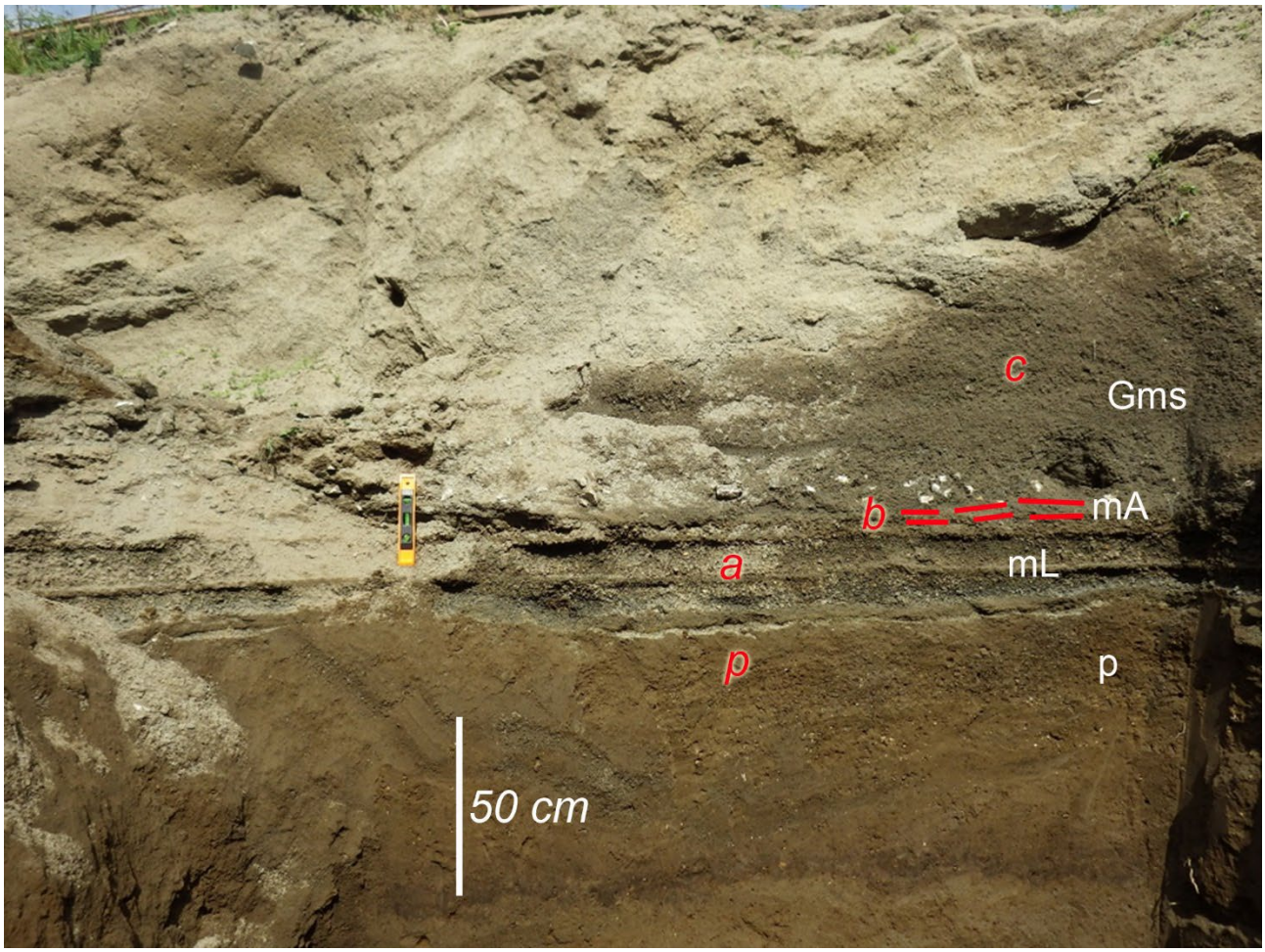

Fig. C8. Avella-Baiano Valley, the Pollena primary deposit (a,b) lies on a ploughed soil (p), and is covered by at least three flow units of lahars (c). For the description of lithofacies see Tab. 2.

The Pollena primary and secondary sequences are overlain by a mature paleosol with frequent evidence of cultivation (ploughing, p in Fig. C9) and locally by the 1631 eruption deposits. The primary deposit related to the 1631 eruption is not always present. It is up to 2 cm (a in Fig. C9) thick ash layer, gray-violet in color deposited by fallout deposit and overlaying a ploughed paleosol (p in Fig. C9). It is overlain by lahar deposits (b in Fig. C9) composed of several units and characterized by contrasting grain-sizes. The deposits are composed of medium ash, are massive and matrix-supported, and contain abundant scattered mm- to cm-sized pumice fragments (all with the same lithology of the primary deposits) and sometimes vegetal remain traces (lithofacies Gms).

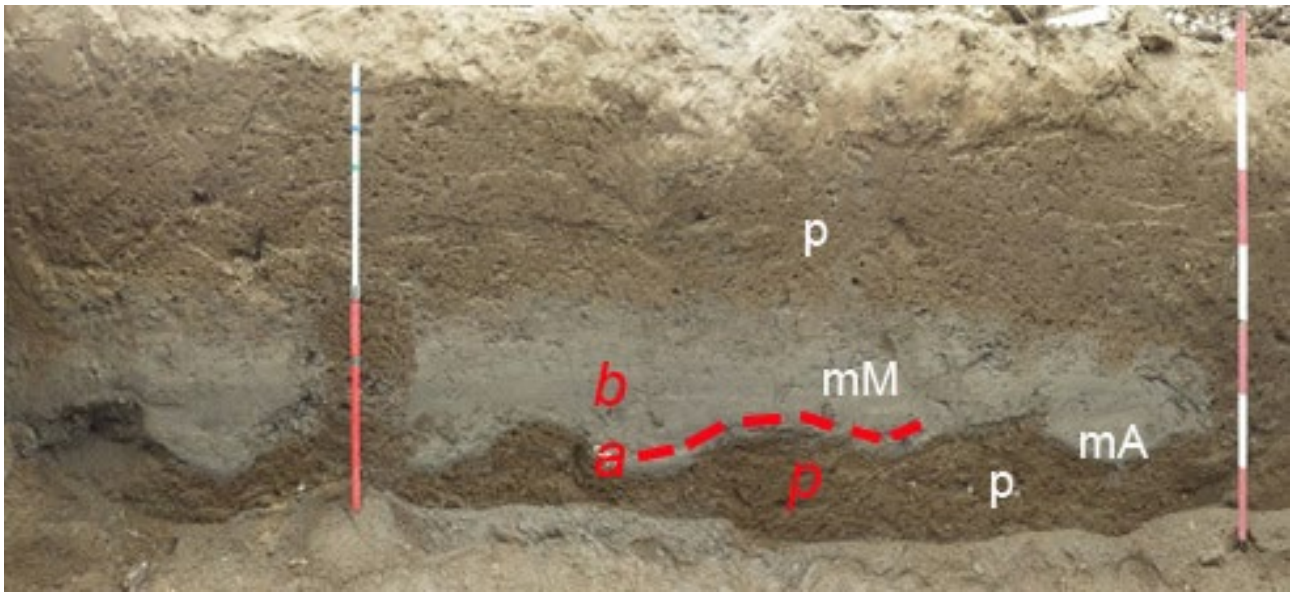

Fig. C9. Avella-Baiano Valley, particular of the 1631 primary (a) and secondary deposits (b, syn-eruptive lahars) in a trench at Cicciano locality. For the description of lithofacies see Tab. 2.

Area 5 – Lauro Valley

Lauro Valley has characteristics similar to the Avella-Baiano Valley, but the primary deposits of Pollena and 1631 eruptions are thicker (Figs. 5 and 6) and coarser. In this valley, also the sequences are locally deeply eroded. In fact, the deposits of the Pollena eruption (normally 50-70 cm thick) (Fig. C10) are sometimes missing. They overlie a mature paleosol with abundant traces of cultivation. Overall, the characteristics of the deposits are very similar to the ones of the Nola area (10-15 km from Apennine source valleys). The overlying lahar deposits are always massive, matrix-supported, and composed of fine and very cohesive ash with abundant scattered pumices and lithic fragments (similar in lithology to those of the primary deposits) (lithofacies Gms). These deposits have a high variable thickness, with a measured maximum of 2 m, but sometimes reduced by erosion. In some trenches the base of the sequences was deeper than the investigated depth (>3.5 m).

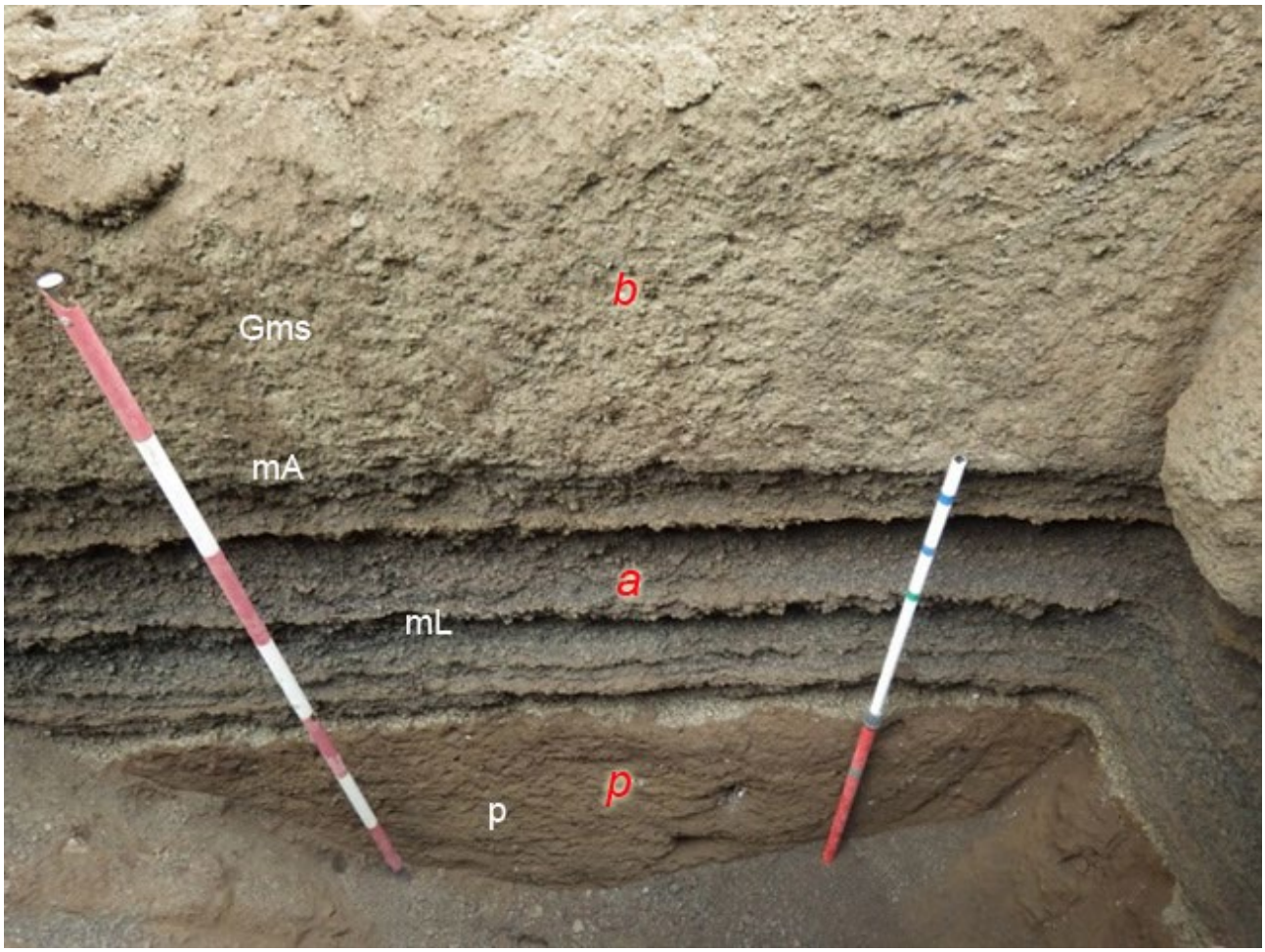

Fig. C10. Lauro Valley, Pago del Vallo, in particular: a = sequence of the Pollena fallout deposits overlain by syn-eruptive lahars (b); p = late Roman paleosol at the base. For the description of lithofacies see Tab. 2.

It is possible to evaluate the effects of the lahars on building in the Roman Villa di Lauro, at Taurano, where a 70 cm thick fallout is overlain, without paleosol, by syn-eruptive lahars which engulfed and transported pieces of walls, bricks and potteries. The lahar deposits are matrix supported and composed of fine to coarse ash and contain abundant pumice lapilli (all similar to the Pollena fallout deposits). They are massive, cohesive and have a thickness up to about 1 m, thickening in depressions and near barriers (Fig. C11).

The sequence related to the eruption of 1631 is not always present, but it is possible to find its primary deposit, composed of a basal layer of stratified fine and medium thin ash beds, and minor dark pumice and lithic fragments overlain by a thin, very fine and cohesive accretionary lapilli-rich ash bed. The

maximum measured thickness is 30 cm. The overlying lahar deposits are massive and matrix-supported, composed of fine to coarse ash and contain abundant pumice fragments of the primary deposit.

Fig. C11. Taurano (Villa Lauro), baulk showing a thick sequence of the Pollena syn-eruptive lahar units filling the Roman Villa. Some units engulf and transport pieces of walls and large blocks. The fallout sequence is not exposed in the Villa, likely due to the presence of a roof. The deposit below the damaged walls is composed of multiple lahar units represented by the Gms lithofacies (see Tab. 2).

Author contribution

MDV: conceptualization, investigation, methodology, writing - original draft preparation, writing - review & editing, funding acquisition; IR: data curation, investigation, writing - original draft preparation; SdV: investigation, writing - original draft preparation, writing - review & editing; DMD: investigation, methodology, data curation, writing - original draft preparation, writing - review &

editing; MB: data curation, methodology, writing - original draft preparation; MdMV: writing - review & editing; MR: conceptualization, writing - review & editing; LS: writing - review & editing; GZ: investigation, writing - review & editing; EZ: investigation, methodology, writing - original draft preparation; AC: conceptualization, writing - review & editing, funding acquisition.

Acknowledgements

This work benefited of the agreement between Istituto Nazionale di Geofisica e Vulcanologia and the Italian Presidenza del Consiglio dei Ministri, Dipartimento della Protezione Civile (DPC), Convenzione INGV-DPC All. B2. The work was also supported by the INGV project Pianeta Dinamico—Working Earth (CUP 1466 D53J19000170001—"Fondo finalizzato al rilancio degli investimenti delle 1467 amministrazioni centrali dello Stato e allo sviluppo del Paese", legge 145/2018)—Task V3 (MDV).The paper does not necessarily represent DPC official opinion and policies. We thank very much Ulrich Kueppers, Lucia Capra, an anonymous reviewer and the editor Andrea Di Muro for their help in improving this manuscript in the revision process.

References

Acocella V and Funiciello R (2006) Transverse systems along the extensional Tyrrhenian margin of Central Italy and their influence on volcanism. Tectonics 25,1-24.

Arguden AT and Rodolfo KS (1990) Sedimentologic and dynamic differences between hot and cold laharic debris flows of Mayon Volcano, Philippines. Geological Society of America Bulletin 102, 865-876.

Bardot L (2000) Emplacement temperature determinations of proximal pyroclastic deposits on Santorini, Greece, and their implications. Bulletin of Volcanology 61, 450-467.

1259 Bardot L, McClelland E (2000) The reliability of emplacement temperature estimates using
1260 paleomagnetic methods: a case study from Santorini, Greece. Geophysical Journal International 143,
1261 39-51.

1262 Bartole R (1984) Tectonic Structure of the Latian-Campanian Shelf (Tyrrhenian Sea). Bollettino di
1263 Oceanologia Teorica Applicata 2, 197-230.

1264 Baumann V, Bonadonna C, Cuomo S, Moscariello M (2020) Modelling of erosion processes
1265 associated with rainfall-triggered lahars following the 2011 Cordon Caulle eruption (Chile). Journal
1266 of Volcanology and Geothermal Research 390, 106727.

1267 Bisson M, Pareschi MT, Zanchetta G, Sulpizio R, Santacroce R (2007) Volcaniclastic debris-flow
1268 occurrences in the Campania region (Southern Italy) and their relation to Holocene–Late Pleistocene
1269 pyroclastic fall deposits: implications for large-scale hazard mapping. Bulletin of Volcanology 70,
1270 157-167.

1271 Bisson M, Spinetti C, Sulpizio R (2014) Volcaniclastic flow hazard zonation in the Sub-Apennine
1272 Vesuvian area using GIS and remote sensing. Geosphere 10, 1419-1431.

1273 Bisson M, Zanchetta G, Sulpizio R, Demi F (2013) A map for volcaniclastic debris flow hazards in
1274 Apennine areas surrounding the Vesuvius volcano (Italy). Journal of Maps 9, 230-238.

1275 Blott SJ and Pye K (2001) Gradistat: A Grain Size Distribution and Statistics Package for the Analysis
1276 of Unconsolidated Sediments. Earth Surface Processes and Landforms 26, 1237-1248.

1277 Braccini GC (1632) Dell'Incendio Fattosi nel Vesuvio a XVI di Dicembre MDCXXXI. Secondino
1278 Roncagliolo, 104 pp.

1279 Brancaccio L, Cinque A, Romano P, Rosskopf C, Russo F, Santangelo N, Santo A (1991)
1280 Geomorphology and neotectonic evolution of a sector of the Tyrrhenian flank of the Southern
1281 Apennines (Region of Naples, Italy). Zeitschrift für Geomorphologie Supplement Bd. 82, 47-58.

1282 Breard ECP, Lube G, Cronin SJ, Valentine GA (2015) Transport and deposition processes of the
1283 hydrothermal blast of the 6 August 2012 Te Maari eruption, Mt. Tongariro. Bulletin of Volcanology
1284 77, 100.

1285 Breard ECP, Lube G (2017) Inside pyroclastic density currents – uncovering the enigmatic flow
1286 structure and transport behaviour in large-scale experiments. Earth and Planetary Science Letters 458,
1287 22-36.

1288 Brocchini D, Principe C, Castradori D, Laurenzi MA, Gorla L (2001) Quaternary evolution of the
1289 southern sector of the Campanian Plain and early Somma-Vesuvius activity: insights from the Trecase
1290 1 well. Mineralogy and Petrology 73, 67-91.

1291 Capra L, Sulpizio R, Marquez-Ramirez VH, Coviello V, Doronzo DM, Arambula-Mendoza R, Cruz
1292 S (2018) The anatomy of a pyroclastic density current: the 10 July 2015 event at Volcan de Colima
1293 (Mexico). Bulletin of Volcanology 80, 34.

1294 Carling PA (2013) Freshwater megaflood sedimentation: What can we learn about generic processes?
1295 Earth-Science Reviews 125, 87-113.

1296 Carrara E, Iacobucci F, Pinna E, Rapolla A (1973) Gravity and magnetic survey of the Campanian
1297 volcanic area, S. Italy. Bollettino di Geofisica Teorica e Applicata 15, 39-51.

1298 Cas RAF, Wright HMN, Folkes CB, Lesti C, Porreca M, Giordano G, Viramonte JG (2011) The flow
1299 dynamics of an extremely large volume pyroclastic flow, the 2.08-Ma Cerro Galán Ignimbrite, NW
1300 Argentina, and comparison with other flow types. Bulletin of Volcanology 73, 1583-1609.

1301 Cinque A and Robustelli G (2009) Alluvial and coastal hazards caused by long-range effects of
1302 Plinian eruptions: The case of the Lattari Mts. After the AD 79 eruption of Vesuvius. Geological
1303 Society London Special Publications 322, 155-171.

1304 Cioni R, Santacroce R, Sbrana A (1999) Pyroclastic deposits as a guide for reconstructing the multi-
1305 stage evolution of the Somma-Vesuvius Caldera. Bulletin of Volcanology 60, 207-222.

1306 Cioni R, Gurioli L, Lanza R, Zanella, E (2004) Temperatures of A.D. 79 pyroclastic density current
1307 deposits (Vesuvius, Italy). Journal of Geophysical Research 109, B02207.

1308 Costa JE (1997) Hydraulic modeling for lahar hazards at Cascades volcanoes. Environmental
1309 Engineering Geoscience 3, 21-30.

1310 D'Argenio B, Pescatore TS, Scandone P (1973) Schema geologico dell'Appennino meridionale
1311 (Campania e Lucania). In: Moderne vedute sulla geologia dell'Appennino. Convegno (Roma, 16-18
1312 Febbraio 1972). Accademia Nazionale dei Lincei, Problemi Attuali di Scienza e Cultura, Quaderni
1313 183, 49-72.

1314 de' Michieli Vitturi M, Costa A, Di Vito MA, Sandri L, Doronzo DM (this issue). Lahar events in the
1315 last 2,000 years from Vesuvius eruptions. Part 2: Formulation and validation of a computational
1316 model based on a shallow layer approach.

1317 De Simone GF, Perrotta A, Scarpati C (2011) L'eruzione del 472 d.C. ed il suo impatto su alcuni siti
1318 alle falde del Vesuvio. Rivista Studi Pompeiani 22, 61.71.

1319 De Vivo B, Rolandi G, Gans PB, Calvert A, Bohrson WA, Spera FJ, Belkin HE (2001) New
1320 constraints on the pyroclastic eruptive history of the Campanian volcanic Plain (Italy). Mineralogy
1321 and Petrology 73, 47-65.

1322 Di Crescenzo G and Santo A (2005) Nuovo contributo sul ruolo svolto dai livelli pomicei nelle aree
1323 di distacco delle frane di colata rapida dei massicci carbonatici campani. Convegno Nazionale La
1324 mitigazione del rischio da colate di fango a Sarno e negli altri Comuni colpiti dagli eventi del maggio
1325 1998. Napoli, 2 e 3 maggio 2005 - Sarno 4 e 5 maggio 2005.

1326 Di Vito MA, Castaldo N, de Vita S, Bishop J, Vecchio G (2013) Human colonization and volcanic

activity in the eastern Campania Plain (Italy) between the Eneolithic and Late Roman periods. Quaternary International 303, 132-141

Di Vito M.A., Calcaterra D., Petrosino P., Zanchetta G., De Vita S., Marotta E., Cesarano M. , De Simone A., Sansivero F., Rucco I. (2019) Landslides, volcanism and volcano-tectonics: the fragility of the Neapolitan territory. Geol. F. Trips Maps, Volume 11 (1.1)/2019. https://doi.org/10.3301/GFT.2019.01 - pp 1-53.

Di Vito MA, Sulpizio R., Zanchetta G (1998). I depositi ghiaiosi della valle dei torrenti Clanio e Acqualonga (Campania centro-orientale): significato stratigrafico e ricostruzione paleoambientale. Il Quaternario Italian Journal of Quaternary Sciences 11, 273-286.

Di Vito MA, Talamo P, de Vita S, Rucco I, Zanchetta G, Cesarano M (2019) Dynamics and effects of the Vesuvius Pomici di Avellino Plinian eruption and related phenomena on the Bronze Age landscape of Campania region (Southern Italy). Quaternary International 499, 231-244.

Di Vito M, Zanella E, Gurioli L, Lanza R, Sulpizio R, Bishop J, Tema E, Boenzi G, Laforgia E (2009) The Afragola settlement near Vesuvius, Italy: The destruction and abandonment of a Bronze Age village revealed by archeology, volcanology and rock-magnetism. Earth and Planetary Science Letters 277, 408-421.

Doronzo DM (2012) Two new end members of pyroclastic density currents: Forced-convection dominated and inertia-dominated. Journal of Volcanology and Geothermal Research 219-220, 87-91.

Doronzo DM, Martí J, Sulpizio R, Dellino P (2012) Aerodynamics of stratovolcanoes during multiphase processes. Journal of Geophysical Research 117, B01207.

Doronzo DM, Dellino P (2013) Hydraulics of subaqueous ash flows as deduced from their deposits: 2. Water entrainment, sedimentation, and deposition, with implications on pyroclastic density current deposit emplacement. Journal of Volcanology and Geothermal Research 258, 176-186.

1350 Doronzo DM (2013) Aeromechanic analysis of pyroclastic density currents past a building. Bulletin
1351 of Volcanology 75, 684.

1352 Duller RA, Mountney NP, Russell AJ, Cassidy NC (2008) Architectural analysis of a volcaniclastic
1353 jökulhlaup deposit, southern Iceland: sedimentary evidence for supercritical flow. Sedimentology 55,
1354 939-964.

1355 Faccenna C, Funiciello R, Bruni A, Mattei M, Sagnotti L (1994) Evolution of a transfer related basin:
1356 the Ardea basin (Latium, Central Italy). Basin Resources 5, 1-11.

1357 Fedi M and Rapolla A (1987) The Campanian Volcanic Area: analysis of the magnetic and
1358 gravimetric anomalies. Bollettino della Società Geologica Italiana 106, 793-805.

1359 Finetti I and Morelli C (1974) Esplorazione di sismica a riflessione nei Golfi di Napoli e Pozzuoli.
1360 Bollettino di Geofisica Teorica e Applicata 16, 62-63.

1361 Fiorillo F and Wilson RC (2004) Rainfall induced debris flows in pyroclastic deposits, Campania
1362 (southern Italy). Engineering Geology 75, 263-289.

1363 Giordano G, Zanella E, Trolese M, Baffioni C, Vona A, Caricchi C, De Benedetti AA, Corrado S,
1364 Romano C, Sulpizio R, Geshi N (2018) Thermal interactions of the AD79 Vesuvius pyroclastic
1365 density currents and their deposits at Villa dei Papiri (Herculaneum archaeological site, Italy). Earth
1366 and Planetary Science Letters 490, 180-192.

1367 Girolami L, Roche O, Druitt T, Corpetti T (2010) Velocity fields and depositional processes in
1368 laboratory ash flows, with implications for the dynamics of dense pyroclastic flows. Bulletin of
1369 Volcanology 72, 747-759.

1370 Gurioli L, Pareschi MT, Zanella E, Lanza R, Deluca E, Bisson M (2005) Interaction of pyroclastic
1371 density currents with human settlements: Evidence from ancient Pompeii. Geology 33, 441-444.

1372 Gurioli L, Sulpizio R, Cioni R, Sbrana A, Santacroce R, Luperini W, Andronico D (2010) Pyroclastic
1373 flow hazard assessment at Somma-Vesuvius based on the geological record. Bulletin of Volcanology
1374 72, 1021-1038.

1375 Guzman S, Doronzo DM, Martí J, Seggiaro R (2020). Characteristics and emplacement mechanisms
1376 of the Coranzulí ignimbrites (Central Andes). Sedimentary Geology 405, 105699.

1377 Ippolito F, Ortolani F, Russo M (1973) Struttura marginale tirrenica dell'Appennino campano:
1378 reinterpretazioni di dati di antiche ricerche di idrocarburi. Memorie della Società Geologica Italiana
1379 12, 227–250.

1380 Iverson RM, Denlinger RP, LaHusen RG, Logan M, (2000) Two-phase debris-flow across 3-D
1381 terrain: Model predictions, *in* Wieczorek GF and Naeser ND, eds., Debris-Flow Hazard Mitigation,
1382 Mechanics, Prediction, and Assessment: Taipei, Taiwan, 16-18 August 2000: Rotterdam, Balkema,
1383 521-529.

1384 Jenkins SF, Phillips JC, Price R, Feloy K, Baxter PJ, Sri Hadmoko D, de Bélizal E (2015) Developing
1385 building-damage scales for lahars: application to Merapi volcano Indonesia. Bulletin of Volcanology
1386 77, 1-17.

1387 Lesti C, Porreca M, Giordano G, Mattei M, Cas R, Wright H, Viramonte J (2011) High temperature
1388 emplacement of the Cerro Galán and Toconquis Group ignimbrites (Puna plateau, NW Argentina)
1389 determined by TRM analyses. Bulletin of Volcanology 73, 1535-1565.

1390 Lowe DR, Williams SN, Leigh H, Connort CB, Gemmell JB, Stoiber RE (1986) Lahars initiated by
1391 the 13 November 1985 eruption of Nevado del Ruiz, Colombia. Nature 324, 51-53.

1392 Lowe DR (1988) Suspended-load fallout rate as an independent variable in the analysis of current
1393 structures. Sedimentology 35, 765–776.

1394 Lube G, Cronin S, Manville V, Procter J, Cole S, Freundt A (2012) Energy growth in laharic mass
1395 flows. Geology 40, 475-478.

1396 Macedonio G and Pareschi MT (1992) Numerical simulation of some lahars from Mount St. Helens.
1397 Journal of Volcanology and Geothermal Research 54, 65-80.

1398 Manville V, Nemeth K, Kano K (2009) Source to sink: A review of three decades of progress in the
1399 understanding of volcaniclastic processes, deposits, and hazards. Sedimentary Geology 220, 136-161.

1400 Mariani M and Prato R (1988) I bacini neogenici costieri del margine tirrenico: approccio sismico-
1401 stratigrafico. Memorie della Società Geologica Italiana 41, 519-531.

1402 Marotta E., Berrino G., de Vita S., Di Vito M.A., Camacho A.G., 2022. Structural setting of the Ischia
1403 resurgent caldera (Southern Tyrrhenian Sea, Italy) by integrated 3D gravity inversion and geological
1404 models. In: Marotta, E., D'Auria, L., Zaniboni, F. and Nave, R. (eds) Volcanic Island: from Hazard
1405 Assessment to Risk Mitigation. Geological Society, London, Special Publications, 519.

1406 Martí J, Doronzo DM, Pedrazzi D, Colombo F (2019) Topographical controls on small-volume
1407 pyroclastic flows. Sedimentology 66, 2297-2317.

1408 McClelland E, Druitt TH (1989) Paleomagnetic estimates of emplacement temperatures of
1409 pyroclastic deposits on Santorini, Greece. Bulletin of Volcanology 51, 16-27.

1410 McClelland E (1996) Theory of CRM acquired by grain growth, and its implications for TRM
1411 discrimination and paleointensity determination in igneous rocks. Geophysical Journal International
1412 126, 271-280.

1413 Newhall CG and Punongbayan R (Eds.) (1996) Fire and mud: eruptions and lahars of Mount
1414 Pinatubo, Philippines. Quezon City: Philippine Institute of Volcanology and Seismology, 1126 pp.

1415 Orsi G, de Vita S, Di Vito MA (1996) The restless, resurgent Campi Flegrei Nested Caldera Italy.:
1416 constraints on its evolution and configuration. Journal of Volcanology and Geothermal Research 74,
1417 179-214.

1418 Pareschi MT, Favalli M, Giannini F, Sulpizio R, Zanchetta G, Santacroce R (2000) May 5, 1998,
1419 Debris flows in circumvesuvian areas (Southern Italy), insights for hazard assessment. Geology 28,
1420 639-642.

1421 Pareschi MT, Santacroce R, Sulpizio R, Zanchetta G (2002) The volcaniclastic mass flow hazard
1422 related to the remobilization of fallout deposits in southern Campania, Italy. Explosive volcanism in
1423 subduction zones, Mount Pelée, Martinique, 12-16 May 2002, abstract volume.

1424 Patacca E and Scandone P (2007) Geology of the Southern Apennines. Bollettino della Società
1425 Geologica Italiana Special Issue 7, 75-119.

1426 Paterson, GA, Muxwhorty AR, Roberts AP, MacNiocaill C (2010). Paleomagnetic determination of
1427 emplacement temperatures of pyroclastic deposits: un under-utilized tool. Bulletin of Volcanology,
1428 72, 309-330.

1429 Peccerillo A (2003) Plio-Quaternary magmatism in Italy. Episodes 26, 222-226.

1430 Perrotta A, Scarpati C, Luongo G, Aoyagi M (2006) Burial of Emperor Augustus' villa at Somma
1431 Vesuviana (Italy) by post-79 AD Vesuvius eruptions and reworked (lahars and stream flow) deposits.
1432 Journal of Volcanology and Geothermal Research 158, 445-466.

1433 Pierson TC (1985) Initiation and flow behavior of the 1980 Pine Creek and Muddy River lahars, Mt.
1434 St. Helens, Washington. Geological Society of America Bulletin 96, 1056-1069.

1435 Piochi M, Pappalardo L, De Astis G (2004) Geo-chemical and isotopical variations within the
1436 Campanian Comagmatic Province: implications on magma source composition, Annals of
1437 Geophysics 47, 1485-1499.

1438 Pittari A, Cas RAF, Monaghan JJ, Martí J (2007) Instantaneous dynamic pressure effects on the
1439 behaviour of lithic boulders in pyroclastic flows: the Abrigo Ignimbrite, Tenerife, Canary Island.
1440 Bulletin of Volcanology 69, 265-279.

1441 Porreca M, Mattei M, Mac Niocaill C, Giordano G, McClelland E, Funiciello R (2007) Paleomagnetic
1442 evidence for low-temperature emplacement of the phreatomagmatic Peperino Albano ignimbrite
1443 (Colli Albani volcano, Central Italy). Bulletin of Volcanology 70, 877-893.

1444 Roche O (2012) Depositional processes and gas pore pressure in pyroclastic flows: an experimental
1445 perspective. Bulletin of Volcanology 74, 1807-1820.

1446 Roche O, Niño Y, Mangeney A, Brand B, Pollock N, Valentine GA (2013) Dynamic pore-pressure
1447 variations induce substrate erosion by pyroclastic flows. Geology 41, 1107-1110.

1448 Roche O (2015) Nature and velocity of pyroclastic density currents inferred from models of
1449 entrainment of substrate lithic clasts. Earth and Planetary Science Letters 418, 115-125.

1450 Rodolfo KS (2000) The hazard from lahars and jökulhlaups. In: Encyclopedia of Volcanoes:
1451 Academic Press, Philadelphia, 973-995.

1452 Rodolfo KS and Arguden AT (1991) Rain-lahar generation and sediment-delivery systems at Mayon
1453 Volcano, Philippines: Sedimentation in Volcanic Settings, SEPM Special Publication 45, 71-87.

1454 Rodríguez-Sedano LA, Sarocchi D, Caballero L, Borselli L, Ortiz-Rodríguez AJ, Cerca-Ruiz MF,
1455 Moreno-Chávez G, Franco Ramos O (2022) Post-eruptive lahars related to the 1913 eruption in La
1456 Lumbre Ravine, Volcán de Colima, Mexico: The influence of ravine morphometry on flow dynamics.
1457 Journal of Volcanology and Geothermal Research 421, 107423.

1458 Rolandi G, Barrella AM, Borrelli A (1993) The 1631 eruption of Vesuvius. Journal of Volcanology
1459 and Geothermal Research 58, 183-201.

1460 Rolandi G, Munno R, Postiglione I (2004) The A.D. 472 eruption of the Somma volcano. Journal of
1461 Volcanology and Geothermal Research 129, 291-319.

1462 Rosi M, Principe C, Vecci R (1993) The 1631 Vesuvius eruption. A reconstruction based on historical
1463 and stratigraphical data. Journal of Volcanology and Geothermal Research 58, 151-182.

1464 Rosi M and Santacroce R (1983) The A.D. 472 "Pollena" eruption: volcanological and petrological
1465 data for this poorly-known, Plinian-type event at Vesuvius. Journal of Volcanology and Geothermal
1466 Research 17, 249-271.

1467 Russell AJ, Knudsen O (1999) An ice-contact rhythmite (turbidite) succession deposited during the
1468 November 1996 catastrophic outburst flood (jökulhlaup), Skeidarárjökull, Iceland. Sedimentary
1469 Geology 127, 1-10.

1470 Sandri L, de' Michieli Vitturi M, Costa A, Di Vito MA, Rucco I, Doronzo DM, Bisson M, Gianardi
1471 R, de Vita S, Sulpizio R (this issue) Lahar events in the last 2,000 years from Vesuvius eruptions.
1472 Part 3: Hazard assessment over the Campanian Plain.

1473 Santacroce R, Cioni R, Marianelli P, Sbrana A, Sulpizio R, Zanchetta G, Donahue DJ, Joron JL
1474 (2008) Age and whole rock-glass compositions of proximal pyroclastics from the major explosive
1475 eruptions of Somma-Vesuvius: A review as a tool for distal tephrostratigraphy. Journal of
1476 Volcanology and Geothermal Research 177, 1-18.

1477 Santacroce R., Sbrana A., Andronico D., Cioni R., Di Vito M., Marianelli P., Sulpizio R., Zanchetta
1478 G., Arrighi S., Benvenuti E., Gurioli L., Leoni F.M., Luperini W., 2003. Carta Geologica del Vesuvio
1479 in scala 1:15.000, Santacroce R., Sbrana A., eds. Cartografia derivata dai rilievi geologici in scala
1480 1:10.000 Regione Campania e dai rilievi in scala 1:25.000 del Progetto CARG., S.EL.C.A., Firenze.

1481 Santangelo N, Romano P, Ascione A, Russo Ermolli E (2017) Quaternary evolution of the Southern
1482 Apennines coastal plains: A review. Geologica Carpathica 68, 43-56.

1483 Scott KM (1989) Magnitude and frequency of lahars and lahar-runout flows in the Toutle-Cowlitz
1484 River System. U. S. Geological Survey Professional Paper 1447-B, 1–33.

1485 Scott KM, Vallance JW, Pringle PT (1995) Sedimentology, behavior, and hazard of debris flows at
1486 Mount Rainer, Washington. U. S. Geological Survey Professional Paper 1547, 1-56.

1487 Scott KM, Macìas JL, Naranjo JA, Rodriguez S, McGeehin JP (2001) Catastrophic debris flows
1488 transformed from landslide in volcanic terrains: mobility, hazard assessment and mitigation
1489 strategies. US Geol Surv Prof Pap. 1630, 1-59.

1490 Sheridan MF, Bonnard C, Carrero C, Siebe C, Strauch W, Navarro M, Calero JC, Trujillo NB (1999)
1491 Report of the 30 October 1998 rock fall/avalanche and breakout flow of Casita Volcano, Nicaragua,
1492 triggered by Hurracane Mitch. Landslide News 12, 2-4.

1493 Siebe C, Schaaf P, Urrutia-Fucugauchi J (1999) Mammoth bones embedded in a late Pleistocene lahar
1494 from Popocatépetl volcano, near Tocuila, central Mexico. Geological Society of America Bulletin
1495 111, 1550-1567.

1496 Smith G, Williams R, Rowley PJ, Parsons DR (2018) Investigation of variable aeration of
1497 monodisperse mixtures: implications for pyroclastic density currents. Bulletin of Volcanology 80, 67.

1498 Spence RJS, Zuccaro G, Petrazzuoli S, Baxter PJ (2004) Resistance of buildings to pyroclastic flows:
1499 analytical and experimental studies and their application to Vesuvius. Natural Hazards Review 5, 48-
1500 59.

1501 Stanzione M, Di Vito MA, Aurino P, Lumaga MRB (2023) Sacred plant impressions from Somma-
1502 Vesuvius volcanic ash deposits: A medicinal garden in Late Antique Acerra (Naples, Campania,
1503 Italy)? Journal of Archaeological Science: Reports 47, 103802.

1504 Sulpizio R, Mele D, Dellino P, La Volpe L (2005) A complex, Subplinian-type eruption from low-
1505 viscosity, phonolitic to tephri-phonolitic magma: the AD 472 (Pollena) eruption of Somma-Vesuvius,
1506 Italy. Bulletin of Volcanology 67, 743-767.

1507 Sulpizio R, Zanchetta G, Demi F, Di Vito MA, Pareschi MT, Santacroce R (2006) The Holocene
1508 syneruptive volcaniclastic debris flows in the Vesuvian area: Geological data as a guide for hazard
1509 assessment. Geological Society of America Special Paper 402, 203-221.

1510 Sulpizio R, Dellino P, Doronzo DM, Sarocchi D (2014) Pyroclastic density currents: state of the art
1511 and perspectives. Journal of Volcanology and Geothermal Research 283, 36-65.

1512 Tema E, Zanella E, Pavón-Carrasco FJ, Kondopoulo D, Pavlides S (2015) Palaeomagnetic analysis
1513 on pottery as indicator for the pyroclastic flows deposit temperature: New data and statistical
1514 interpretation from the Minoan eruption of Santorini, Greece. Geophysical International Journal 203,
1515 33-47.

1516 Thouret JC, Arapa E, Charbonnier S, Guerrero A, Kelfoun K, Cordoba G, Rodriguez D, Santoni O
1517 (2022) Modeling tephra fall and sediment-water flows to assess their impact on a vulnerable building
1518 stock in the City of Arequipa, Peru. Frontiers in Earth Science 10, 865989.

1519 Toyos G, Gunasekera R, Zanchetta G, Oppenheimer C, Sulpizio R, Favalli M, Pareschi MT (2008)
1520 GIS-assisted modelling for debris flow hazard assessment based on the events of May 1998 in the
1521 area of Sarno, Southern Italy: II. Velocity and dynamic pressure. Earth Surface Processes and
1522 Landforms 33, 1693-1708.

1523 Vallance JW and Iverson R (2015) Lahars and their deposits. In: Sigurdsson, H., Houghton, B.F.,
1524 McNutt, S.R., Rymer, H., Stix, J. (Eds.), Encyclopedia of Volcanoes. Academic Press, London, 649-
1525 664.

1526 Vallance JW and Scott KM (1997) The Osceola mudflow from Mount Rainer: Sedimentology and
1527 hazards implications of a huge clay-rich debris flow. Geological Society of America Bulletin 109,
1528 143-163.

1529 Vitale S and Ciarcia S (2018) Tectono-stratigraphic setting of the Campania region (southern Italy),
1530 Journal of Maps 14, 9-21.

1531 Voight B (1990) The 1985 Nevado del Ruiz volcano catastrophe: anatomy and retrospection. Journal
1532 of Volcanology and Geothermal Research 42, 151-188.

1533 Waitt RB Jr, TC Pierson TC, MacLeod NS, Janda RJ, Voight B, Holcomb RT (1983) Eruption-
1534 triggered avalanche, flood, and lahar at Mount St. Helens - Effects of winter snowpack. Science 221,
1535 1394-1397.

1536 Walsh B, Coviello V, Capra L, Procter J, Marquez-Ramirez V (2020) Insights into the internal
1537 dynamics of natural lahars from analysis of 3-component broadband seismic signals at Volcan de
1538 Colima, Mexico.

1539 Whipple KX, Hancock GS, Anderson RS (2000) River incision into bedrock: Mechanics and relative
1540 efficacy of plucking, abrasion, and cavitation. Geological Society of America Bulletin 112, 490-503.

1541 White S, García-Ruiz JM, Martí-Bono C, Valero B, Errea MP, Gómez-Villar A (1997) The 1996
1542 Biescas campsite disaster in the Central Spanish Pyrenees and its spatial and temporal context.
1543 Hydrological Processes 11, 1797-1812.

1544 Zanchetta G, Sulpizio R, Pareschi MT, Leoni FM, Santacroce R (2004a) Characteristics of May 5-6,
1545 1998 volcaniclastic debris flows in the Sarno area (Campania, southern Italy): relationships to
1546 structural damage and hazard zonation. Journal of Volcanology and Geothermal Research 133, 377-
1547 393.

1548 Zanchetta G, Sulpizio R, Di Vito MA (2004b). The role of volcanic activity and climate in alluvial
1549 fan growth at volcanic areas: an example from southern Campania (Italy). Sedimentary Geology 168,
1550 249-280.

1551 Zanella E, Gurioli L, Pareschi MT, Lanza R (2007). Influences of urban fabric on pyroclastic density
1552 currents at Pompeii (Italy): 2. Temperature of the deposits and hazard implications. Journal of
1553 Geophysical Research 112, B05214.

1554 Zanella E, Gurioli L, Lanza R, Sulpizio R, Bontempi M (2008). Deposition temperature of the AD
1555 472 Pollena pyroclastic density current deposits, Somma-Vesuvius, Italy. Bulletin of Volcanology
1556 70, 1237-1248.

1557 Zanella E, Sulpizio R, Gurioli L, Lanza R (2015). Temperatures of the pyroclastic density currents
1558 deposits emplaced in the last 22 kyr at Somma-Vesuvius (Italy). Geological Society, London, Special
1559 Publication, The Use of Palaeomagnetism and Rock Magnetism to Understand Volcanic Processes
1560 396.

1561 Zaragoza G, Caballero-Garcia L, Capra L, Nieto-Torres A (2020) Lahares secundarios en el volcan
1562 Popocatepetl: El lahar Nexpayantla del 4 de febrero, 2010. Revista Mexicana de Ciencias Geologicas
1563 37, 121-134.

1564 Zuccaro G, De Gregorio D (2013) Time and space dependency in impact damage evaluation of a sub-
1565 Plinian eruption at Mount Vesuvius. Natural Hazards 68, 1399-1423.